Springer Theses
Recognizing Outstanding Ph.D. Research

Nishu Goyal

In silico Modeling and Experimental Validation for Improving Methanogenesis from CO_2 via *M. maripaludis*

Springer

Springer Theses

Recognizing Outstanding Ph.D. Research

Aims and Scope

The series "Springer Theses" brings together a selection of the very best Ph.D. theses from around the world and across the physical sciences. Nominated and endorsed by two recognized specialists, each published volume has been selected for its scientific excellence and the high impact of its contents for the pertinent field of research. For greater accessibility to non-specialists, the published versions include an extended introduction, as well as a foreword by the student's supervisor explaining the special relevance of the work for the field. As a whole, the series will provide a valuable resource both for newcomers to the research fields described, and for other scientists seeking detailed background information on special questions. Finally, it provides an accredited documentation of the valuable contributions made by today's younger generation of scientists.

Theses are accepted into the series by invited nomination only and must fulfill all of the following criteria

- They must be written in good English.
- The topic should fall within the confines of Chemistry, Physics, Earth Sciences, Engineering and related interdisciplinary fields such as Materials, Nanoscience, Chemical Engineering, Complex Systems and Biophysics.
- The work reported in the thesis must represent a significant scientific advance.
- If the thesis includes previously published material, permission to reproduce this must be gained from the respective copyright holder.
- They must have been examined and passed during the 12 months prior to nomination.
- Each thesis should include a foreword by the supervisor outlining the significance of its content.
- The theses should have a clearly defined structure including an introduction accessible to scientists not expert in that particular field.

More information about this series at http://www.springer.com/series/8790

Nishu Goyal

In silico Modeling and Experimental Validation for Improving Methanogenesis from CO_2 via *M. maripaludis*

Doctoral Thesis accepted by
National University of Singapore, Singapore

Springer

Author
Dr. Nishu Goyal
Chemical and Biomolecular Engineering
National University of Singapore
Singapore

Supervisor
Prof. I.A. Karimi
Department of Chemical and Biomolecular Engineering
National University of Singapore
Singapore

ISSN 2190-5053 ISSN 2190-5061 (electronic)
Springer Theses
ISBN 978-981-10-2509-9 ISBN 978-981-10-2510-5 (eBook)
DOI 10.1007/978-981-10-2510-5

Library of Congress Control Number: 2016949597

Printed on acid-free paper

This Springer imprint is published by Springer Nature
The registered company is Springer Nature Singapore Pte Ltd.
The registered company address is: 152 Beach Road, #22-06/08 Gateway East, Singapore 189721, Singapore

Supervisor's Foreword

It is my great pleasure to introduce the Ph.D. thesis of Dr. Nishu Goyal, which has been selected as a Springer Thesis for outstanding original work. Dr. Goyal was conferred Ph.D. on 17 December 2015 by the Department of Chemical and Biomolecular Engineering of the National University of Singapore. She began her Ph.D. in July 2011, after securing an M.Tech. (Biomedical Engineering) from the Indian Institute of Technology Bombay, India, and gaining some valuable work experience in Strand Life Sciences Pvt Ltd., a leading bioinformatics company in Bangalore, India. For her graduate studies at NUS, she was awarded the highly prestigious President Graduate Fellowship. With interest and experience in microbiology, genomics, and informatics, she chose the area of systems biology as her Ph.D. topic under my supervision. Given the global issue of increasing CO_2 emissions and a need for sustainable energy, she decided to focus on the possibility of converting carbon dioxide into a cleaner energy fuel such as methane via biochemical pathways. To this end, she conducted an exhaustive search and identified the potential for using hydrogenotrophic methanogens to convert CO_2 to methane. She selected *M. maripaludis*, a mesophilic, gram-negative anaerobe with the ability to utilize CO_2 as the sole carbon substrate for growth and methanogenesis, as the most attractive microbe.

Her first task in the thesis was to develop the first constraint-based genome-scale metabolic model (*i*MM518) for *M. maripaludis* to quantify the various intra- and extracellular fluxes during methanogenesis from CO_2. She used *i*MM518 to explain a variety of experimental phenotypes known in the literature. Then, she identified several genetic manipulations that can enhance methanogenesis. Since virtually no experimental flux data existed in the literature for more accurate validation, Nishu performed anaerobic batch cultivations and measured key extracellular fluxes along with specific growth rates in the presence of CO_2 as the sole carbon substrate. For analysing her data and calibrating her model, she developed a novel process simulation approach to estimate the key maintenance energy parameters of a cell. Her experiments revealed the beneficial impact of free nitrogen on methanogenesis. Therefore, she studied the effect of diazotrophy (growth on free N_2) on

methanogenesis in *M. maripaludis*. Her experiments have suggested 2.5 times higher conversion yield for CO_2 to methane during diazotrophy. During her work, she also constructed a detailed, integrated, and comprehensive picture of the entire metabolism of *M. maripaludis*, which is also missing in the literature.

In brief, her work demonstrates a synergistic mix of modelling and experiments. Its framework for systematically and quantitatively studying the metabolism in *M. maripaludis* at the genome-scale by combining constraint-based metabolic modelling and experimental flux data under different culture conditions is general, and applicable to any other CO_2-fixing methanogen. She has published three papers in international refereed high-impact journals and presented her work at several prestigious international conferences.

Singapore
August 2016

Prof. I.A. Karimi

Parts of this thesis have been published in the following journal articles:

Publications and Conferences

Journal Publications

1. **N. Goyal**, Z. Zhi, and I. A. Karimi. "Genome-scale metabolic model of *M. maripaludis* S2 for CO_2 capture and conversion to methane". *Molecular BioSystems* (2014), 10, 1043–1054.
2. **N. Goyal**, Z. Zhi, and I. A. Karimi. "Flux measurements and maintenance energy for CO_2 Utilization by *M. maripaludis*". *Microbial Cell Factories* (2015), 14, 146.
3. **N. Goyal**, Z. Zhi, and I. A. Karimi. "Metabolic processes in *M. maripaludis* for industrial and environmental applications". *Microbial Cell Factories* (2016), 15, 107.
4. **N. Goyal**, Z. Zhi, and I. A. Karimi. "Diazotrophy enhances CO_2 to methane conversion in *M. maripaludis*" (Under review by *Biomass and Bioenergy*).
5. M. Padhiary, K. Walczak, **N. Goyal**, and Z. Zhou. "Bioelectrocatalyzed reduction of CO_2 to higher alcohols and acids using acetogens and acetate-utilizing *Clostridium* strains" (Under review by *Energy and Environmental Science*).

Conference Proceedings

1. **N. Goyal**, H. Widiastuti, I. A. Karimi and Z. Zhi. "Genome-scale metabolic network reconstruction and *in silico* analysis of *M. maripaludis* S2" *Computer-Aided Chemical Engineering* (2013), Vol 32, 181–186. Lappeenranta, Finland.
2. **N. Goyal**, I. A. Karimi and Z. Zhi. "Genome based metabolic flux analysis (MFA) of *M. maripaludis* for improved methane productivity" (264e), *AIChE Annual Meeting* (2014), Atlanta, Georgia, USA.
3. **N. Goyal**, I. A. Karimi and Z. Zhi. "Experimental validation of *in silico* flux predictions from a genome-scale model (*i*MM518) for CO_2 utilization by *M. maripaludis*" *Computer-Aided Chemical Engineering* (2015), Vol 37, 2153–2159. Copenhagen, Denmark.
4. **N. Goyal**, I. A. Karimi and Z. Zhi. "Influence of nitrogen limitation on methanogenesis and growth in *M. maripaludis*" (250). *International Conference on Carbon Dioxide Utilization* (2015), Singapore.

Acknowledgements

Ph.D. has been a great learning experience for me and I could not have reached its completion without the invaluable support of many. I take this wonderful opportunity to express my sincere gratitude to all those who have helped me in shaping my research career and making my stay in Singapore a truly memorable one.

First of all, I express my greatest gratitude to my research supervisor Prof. I.A. Karimi, ChBE, for providing me the opportunity to pursue Ph.D. under his guidance. He taught me to be patient, tenacious, and attentive to minute details and helped me to develop as an independent researcher. His critical comments and suggestions were invaluable for my research and publications. I am extremely thankful to him for supporting me to present my research in national and international conferences that helped me to evaluate myself among many researchers on the same platform. It was indeed a privilege to work with Prof. Karimi.

I am thankful to Prof. Zhi Zhou, CEE, for believing in me and for providing his experimental laboratory facilities to validate our *in silico* predictions. Without his timely inputs, guidance, and encouragement the work would not have reached its completion.

I extend my sincere thanks to Thesis Advisory Committee (TAC) members Chen Shing Bor, Associate Professor, ChBE, and Dr. Yan Ning, Assistant Professor, ChBE, for their kind acceptance to be in examination panel and for providing me valuable comments and suggestions during the oral qualifying examination. I also wish to admire and thank all the unknown reviewers of our publications, who provided constructive feedbacks on manuscripts and helped us to bring the best out of this research. I also take this excellent opportunity to thank online search engines, researchers who shared their research in the form of website notes and literature and freely available online databases used to strengthen this research.

I sincerely thank Centre for Development of Teaching and Learning (CDTL) staff for organizing technical workshops and seminar and ChBE laboratory/ administrative staff for their constant cooperation and support. I also thank ChBE department for financially supporting all my conference visits.

My affectionate thanks go to my labmates (Kunna, Sadegh, Hanifah, Mrutyunjay, Kefeng, Vasanth, Rajnish, Karthik, Pulkit, and Sushant) and all my

friends who made my journey more comfortable and enjoyable at NUS. They were primal in supporting me during stress and difficult moments.

Most Importantly, I thank my entire family for their boundless love, encouragement, and moral support. They have always been a constant source of motivation in achieving my goals.

Singapore Nishu Goyal
July 2015

Declaration

I hereby declare that this thesis is my original work and it has been written by me in its entirety. I have duly acknowledged all the sources of information which have been used in the thesis.

This thesis has also not been submitted for any degree in any university previously.

July 2015 Nishu Goyal

Contents

Nomenclature

Symbols

I	Number of metabolites
J	Number of reactions
t	Time (h)
v	Vector of reaction fluxes (mmol/gDCW-h)
b	$I \times 1$ vector of net metabolite fluxes (mmol/gDCW-h)
S	Matrix of stoichiometric coefficient of the reactants and products (dimensionless)
Z	Objective function
μ	Specific growth rate (/h)
c_j	Weight associated with the reaction fluxes (dimensionless)
v_j	Reaction flux (mmol/gDCW-h)
X	Biomass (gram dry cell weight)
C_i	Specific concentration of metabolite i (mmol/gDCW)
α_j	Lower bound for reaction flux (mmol/gDCW-h)
β_j	Upper bound for reaction flux (mmol/gDCW-h)

Abbreviations

3-HP	3-Hydroxypropionate
ACS	Acetyl-CoA synthetase
ADP	Adenosine diphosphate
ADTH	2-amino-3,7-dideoxy-D-threo-hept-6-ulosonate
AMP	Adenosine monophosphate
AroAAs	Aromatic amino acids
ATP	Adenosine triphosphate
BCAAs	Branched-chain amino acids
CBB	Calvin benson-bassham
CoA	Coenzyme A
COBRA	COnstraint-Based Reconstruction and Analysis

CODH	Carbon monoxide dehydrogenase
CoM	Coenzyme M
COM-S-S-COB	Coenzyme M 7-mercaptoheptanoylthreonine-phosphate heterodisulfide
CTP	Cytidine triphosphate
CUR	Carbon dioxide uptake rate
CysRS	Cysteinyl-tRNA synthetase
Cys-tRNA	Cysteinyl-tRNA
DCP	Dry Cell Protein
DCW	Dry Cell Weight
DHQ	3-dehydroquinate
DKFP	6-deoxy-5-ketofructose 1-phosphate
E4P	Erythrose-4-phosphate
Ech	Energy-converting hydrogenase
EMP	Embden–Meyerhof–Parnas
EPC	Electronic pneumatic control
F420(ox)	Oxidized coenzyme F420
F420(rd)	Reduced coenzyme F420
F6P	Fructose-6-phosphate
FBA	Flux balance analysis
FBP	Fructose-bisphosphatase
Fd(rd)	Reduced ferredoxin
Fd(ox)	Oxidized ferredoxin
Fdh	Formate dehydrogenase
Fru/Frc	F420 reducing hydrogenase
Ftr	Formyltransferase
FVA	Flux variability analysis
Fwd/Fmd	Tungsten/Molybdenum containing formylMFR dehydrogenase
G3P	Glyceraldehyde-3-phosphate
GAM	Growth-associated maintenance
GAPDH	G3P dehydrogenase
GAPN	$NADP^+$-dependent G3P dehydrogenase
GAPOR	Fd-dependent G3P dehydrogenase
GHG	Greenhouse gas
GK	Glucokinase
GMP	Guanosine monophosphate
GPR	Gene–protein reaction
Hdr	Heterodisulfide reductase
HHV	High Heating Value
Hmd	5,10-methenylTHMPT hydrogenase
HS-COM	Coenzyme M (2-mercaptoethanesulfonate)
HUR	Hydrogen Uptake Rate
IPMS	2-isopropylmalate synthase
LNG	Liquefied natural gas
LP	Linear programming

McC	Complex medium
Mch	Methylene-THMPT cyclohydrolase
McN	Minimal medium
McNA	Minimal medium plus sodium acetate
Mcr	Methyl-COM reductase
MECs	Microbial electrolysis cells
MER	Methane evolution rate
Mer	Methylene-THMPT reductase
Methyl-S-COM	2-(Methylthio)-coenzymeM
MFA	Metabolic flux analysis
MFCs	Microbial fuel cells
MFR	Methanofuran
Mtd	Methylene-THMPT dehydrogenase
Mtr	Methyltransferase
NAD	Nicotinamide adenine dinucleotide
NGAM	Non-growth-associated maintenance
NOPPP	Non-oxidative PPP
OD	Optical density
ORFs	Open-reading frames
PABA	p-aminobenzoic acid
PEG	Polyethylene glycol
PFK	Phosphofructokinase
PFORs	Pyruvate: ferredoxin oxidoreductases
PMF	Proton motive force
PORs	Pyruvate oxidoreductases
PPC	Phosphenolpyruvate carboxylase
PPP	Pentose phosphate pathway
PPS	Phosphoenolpyruvate synthase
ProRS	Prolyl-tRNA synthetase
PRPP	5-Phosphoribosyldiphosphate
PYC	Pyruvate carboxylase
rDNA	Recombinant DNA technology
SBML	Systems Biology Markup Language
SepCysS	Sep-tRNA:Cys-tRNA synthase
Sep-tRNA	O-phosphoseryl-tRNA
SH-CoB	Thio-coenzyme B
SSE	Sum of Squares of Errors
TCA	Tricarboxylic acid
THMPT	Tetrahydromethanopterin
TKL	Transketolase
TSSE	Total sum of squares of errors
UMP	Uridine monophosphate
Vhu/Vhc	F420 non-reducing hydrogenase

List of Figures

List of Tables

Chapter 1
Introduction

Energy consumption is increasing worldwide by approx. 2.3 % every year [1]. The primary energy sources are petroleum (~36.0 %), coal (~27.4 %) and natural gas (~23.0 %). In total, 86.4 % energy consumption is met by the consumption of fossil fuels. The burning of fossil fuels emits around 21.3 billion tons of carbon dioxide (CO_2) in the atmosphere per year and hence leads to serious environmental effects such as global warming.

In order to address the rising energy demands and reduce environmental impact, a readily available carbon neutral clean energy fuel is needed. Considerable research efforts are in progress to convert CO_2 to valuable fuels and chemicals via metal catalysts [2], photocatalysts [3], electrocatalytic reduction [4], and nanotechnology [5] (Fig. 1.1). These energy solutions are suffered by low product yield, high infrastructure and maintenance costs, extreme temperature and pressures, etc. Hence new fields of sustainable and cheap energy solutions are gaining popularity.

Genetic engineering of microorganisms for fuels and value-added chemicals has grown tremendously over the past decade [6]. Biofuels such as biogas, biodiesel and bioethanol are renewable energy sources which are receiving increasing attention due to low carbon emissions compared to fossil fuels. However various social, economic, environmental and technical issues exists such as moderating oil prices, food vs fuel debate, carbon emission levels, sustainable production, deforestation, soil erosion, and impact on water resources. In this thesis, we evaluated an interesting biological approach for CO_2 capture and conversion to methane, a clean energy fuel.

N. Goyal, *In silico Modeling and Experimental Validation for Improving Methanogenesis from CO_2 via M. maripaludis*, Springer Theses,
DOI 10.1007/978-981-10-2510-5_1

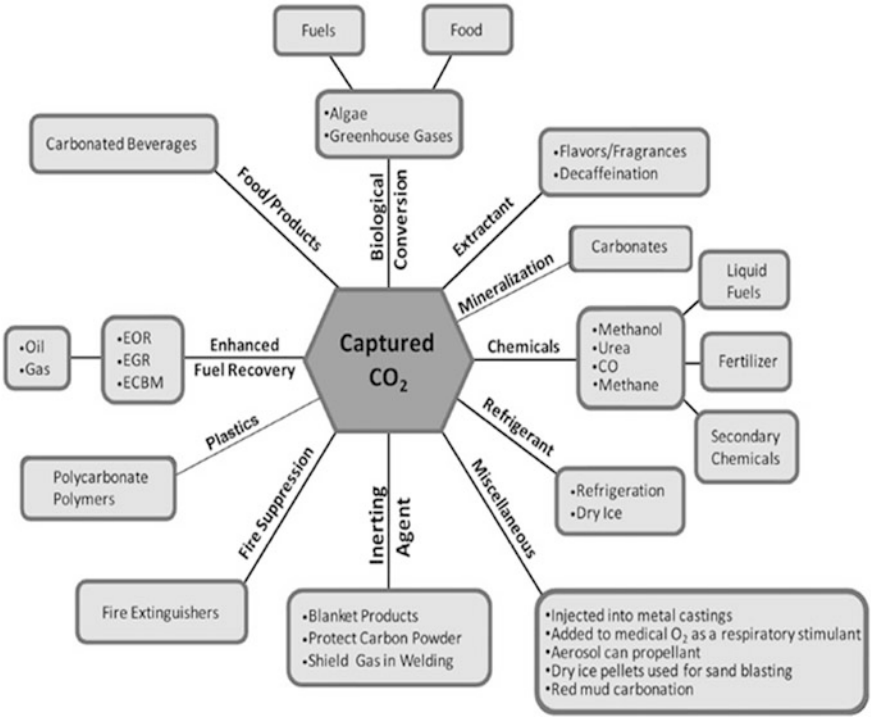

Fig. 1.1 A general picture of fuels and chemicals that can be obtained from CO_2 via various conversion processes [7]

1.1 Methane, a Useful Fuel

Carbon neutral fuel refers to those synthetic fuels, such as methane, gasoline, diesel fuel or jet fuels, which are produced from renewable or nuclear energy. For example, hydrogenation of CO_2 recycled from power plant flue gas, CO_2 derived from carbonic acid in sea water, electrolysis of water to make hydrogen, etc. These fuels do not result in the net increase of atmospheric carbon and displace fossil fuels. Such renewable fuels have the potential to alleviate the cost and dependency of fossil fuels.

Methane is considered as an excellent carbon neutral fuel due to its volumetric energy content or high heating value (HHV = 40 MJ/m^3 or 1075 BTU/ft^3). Due to its physical characteristics (adiabatic coefficient = 1.31 and initial specific volume = 1.39 m^3/kg), methane can be compressed and stored in chemical industries and transported as a refrigerated liquid (liquefied natural gas, or LNG). It has significant benefits:

Renewable energy source: Biomethane is a renewable source of energy produced worldwide from "fresh" organic matter and is a major component ($\sim$75 %

methane, 15 % ethane, and 5 % hydrocarbons such as propane and butane) of natural gas used for heating and electricity.

Rocket fuel and raw material: Methane in liquefied form can also be used as rocket fuel [8]. It is also a raw material for manufacture of methanol, formaldehyde, nitromethane, chloroform, carbon tetrachloride, etc.

Reduce Greenhouse Gas (GHG) emissions: Methane is 20 times more potent gas than CO_2 and hence use of methane as biofuel in place of fossil fuels reduces GHG emissions in the atmosphere.

1.1.1 Production Routes

1.1.1.1 Industrial

Methane is synthesized commercially by the distillation of bituminous coal and by heating a mixture of carbon and hydrogen. Substances released from bituminous coal when it is distilled, in addition to methane, include water, carbon dioxide, ammonia, benzene, toluene, naphthalene, and anthracene. In addition, methane is produced in industries through Sabatier process, discovered by French chemist Paul Sebatier during 1910s, via hydrogenation of carbon dioxide at elevated temperature (300–400 °C) in the presence of nickel as a catalyst. The reaction is represented as follows:

$$CO_2 + 4H_2 \rightarrow CH_4 + 2H_2O \qquad (\Delta G = -130.59\,\text{kj/mol})$$

Methane is an undesirable byproduct in the Fischer-Tropsch process where mixture of carbon monoxide and hydrogen (syngas) are converted into hydrocarbon chains of varying lengths:

$$CO + 3H_2 \rightarrow CH_4 + H_2O \qquad (\Delta G = -150.69\,\text{kj/mol})$$

1.1.1.2 Biological

Biochemical conversion of CO_2 to methane (CH_4) via microbes is an interesting approach for CO_2 capture and utilization. Methanogens are *Archaebacteria*, capable of producing methane as a major catabolic product using three different pathways: CO_2-reducing, methylotrophic, and aceticlastic shown in Fig. 1.2 [9]. All three pathways reduce CO_2 to CH_4 and create an electrochemical gradient across the cell membrane to produce ATP. During hydrogenotrophic pathway, CO_2 is reduced to methane with the help of electron donors such as H_2/formate. During methylotrophic pathway, C1 compound i.e. methanol, methyl-amines, methyl-sulfides disproportionate and one molecule of C-1 compound provide electrons to reduce

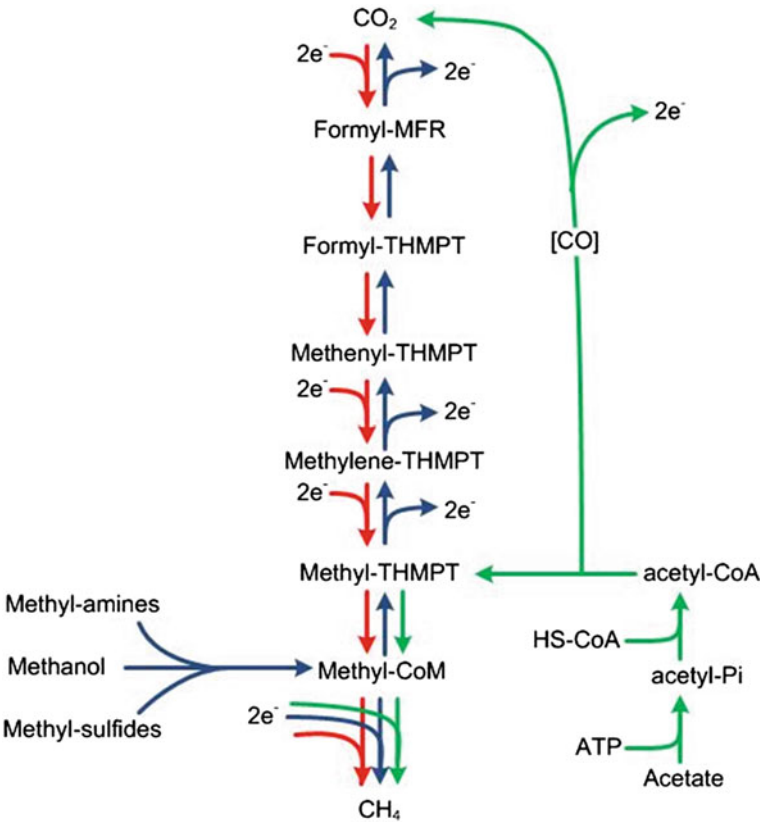

Fig. 1.2 The hydrogenotrophic (*red*), the methylotrophic (*blue*), and the aceticlastic (*green*) pathway of methanogenesis

additional three molecules to methane. During aceticlastic pathway, methanogens splits acetate to generate CO_2 and methane. Ruminants (e.g. cattle, sheep, and goats) produce 86 million metric tons (Tg) of CH_4 per year due to the presence of methanogens in the rumen [10]. Identification and achievement of desirable genetic traits in methanogens to enhance CO_2 to CH_4 conversion is crucial, and can be aided by in silico metabolic modeling [11].

1.2 *M. maripaludis* S2, an Interesting Biocatalyst

Several methanogens such as *Methanosarcina barkeri* [12], *Methanococcus jannaschii* [13], *Methanococcus voltae* [14], and *Methanobacterium thermoautotrophicum* [15] have been studied in the literature. *M. maripaludis* S2 (mmp), also

known as *M. maripaludis* LL, is a model organism among hydrogenotrophic methanogens. It is mesophilic, gram-negative anaerobe that has the ability to utilize CO_2 as the sole carbon substrate for growth and methanogenesis via a modified Wood-Jungdahl pathway, also known as Wolfe cycle [16]. Its unique ability to consume both CO_2 and N_2 demonstrate its potential for treating industrial flue gases comprising primarily of CO_2 (8–14 %) and N_2 (70–80 %) [17, 18].

M. maripaludis is one of the fastest growing methanogens with a doubling time of 2 h at 35–39 °C, and is an excellent laboratory strain for molecular and biochemical studies [19–22]. The presence of selectable resistance markers [23], efficient transformation methods [24], gene deletion or substitution strategies [21, 25], and integrative and shuttle expression vectors [26] make it possible to manipulate the genome of *M. maripaludis*. For instance, acetate auxotrophs were isolated using random insertional mutagenesis by transforming the wild type *M. maripaludis* with pWDK104 vector [27]. Four mutations were made in and around *nifH* gene using transposons insertion mutagenesis for studying N_2-fixation [28]. However, most such studies have been experimental.

1.3 In Silico Metabolic Modeling

Recent advances in synthetic biology have accelerated the ability to engineer existing or novel metabolic pathways in a microbial cell to enhance biofuel production for industrial applications. *In silico* genome-scale metabolic modeling and analysis is a systematic, proven, and attractive approach for exploring metabolic manipulations in an organism to enhance its desirable traits [29, 30]. It helps to develop insights into active pathways, genes, proteins, and metabolites and their interactions in a microbe.

The first genome-scale metabolic model was developed in 1995 for *Haemophilus influenza* [31]. Since then, many reconstructed in silico models for bacteria (*Escherichia coli* [32], *Rhodococcus erythropolis* [33], *Zymomonas mobilis* [34]) archaea (*Methanosarcina barkeri* [12], *Methanosarcina acetivorans* [35]), and eukarya (*Mus musculus*) [36] have been reported in the literature. The predictions from such models add a level of assurance and guidance for experimentation with organisms.

Only three genome-scale metabolic models are available to date for archaea. These are *Methanosarcina barkeri* [12], *Methanosarcina acetivorans* [35], and *Sulfolobus Solfataricus* P2 [37]. While the genome of *M. maripaludis* S2 is fully sequenced with a size of 1.66 Mb and 1722 protein coding genes [19], no genome-scale metabolic model exists till date. A reconstructed model would greatly aid experimental work by helping to predict various cellular phenotypes including growth and quantify the impact of complex intracellular interactions during methanogenesis.

1.4 Scope of the Thesis

1.4.1 Objectives

As mentioned earlier, approx. 87 % of the global primary energy consumption is met by fossil fuels such as coal, petroleum and natural gas. Consumption of dry natural gas ("wet natural gas" when hydrocarbons other than methane are present) doubled from 1980 (53 trillion cubic feet) to 2010 (113 trillion cubic feet) dominated mainly by USA, Russia, Iran, and China. While natural gas lowers CO_2 emissions by displacing coal or oil, the share is not enough to cap carbon emissions in the atmosphere. New technologies such as carbon capture and storage are needed to get rid of carbon emissions.

We identified a methanogenic strain, *M. maripaludis* S2, from the literature, best suited for genetic manipulations. It rapidly grows (without requiring extreme pressure and temperature) on CO_2 as the sole carbon substrate and H_2/formate as the electron donor to reduce it to methane. This creates synergy with renewable energy sources such as solar and wind, where electricity storage becomes critical due to their intermittent nature and the surplus electricity can be converted to H_2 for use in this microbial conversion.

The major objectives of this thesis are:

- To review the metabolic processes in *M. maripaludis* with industrial and environmental applications
- To develop the first systems biology metabolic model of *M. maripaludis* S2 for understanding CO_2 capture and its conversion to methane
- To experimentally quantify three key extracellular fluxes (CO_2, H_2, and CH_4) along with specific growth rates (μ) during growth on NH_4^+ or N_2 in an environment where CO_2 is the sole carbon substrate
- To verify in silico predictions with experimentally measured fluxes and determine the maintenance energy parameters for *M. maripaludis* during growth on NH_4^+ or N_2
- To compare the influence of two different nitrogen sources (NH_4^+ or N_2) on growth and methanogenesis in *M. maripaludis*.

1.4.2 Organization

This thesis is organized into six chapters and the highlights of each chapter are as follows:

This chapter briefly introduces methane as a useful energy source, *M. maripaludis* as a whole cell biocatalyst, role of in silico metabolic modeling in understanding methanogenesis at genome-scale and defines the scope of this thesis.

Chapter 2 begins with an introduction of CO_2 fixing microbes followed by a detailed review on the biochemistry and genetics of *M. maripaludis* S2. Although there are more than 100 papers published on the metabolic pathways and genetics of *M. maripaludis*, a consolidated paper summarizing its metabolic processes and potential applications was lacking in the literature. This chapter further brief in silico mathematical approaches used to generate in silico models and briefly introduces the concept of electromethanogenesis. A part of this chapter is under publication by "*Microbial Cell Factories*".

Chapter 3 describes the detailed procedure of developing a constraint-based genome-scale metabolic model of *M. maripaludis* S2 and reports possible annotations for Open Reading Frames (ORFs) with unknown functions. This chapter also covers the model validation based on the limited experimental data available in the literature and test the model ability to predict cellular behavior. We have published this work in journal "*Molecular BioSystems*" [38].

Chapter 4 studies the dynamic batch culture study on *M. maripaludis* and measure cell growth and three extracellular fluxes, namely CO_2 and H_2 uptake, and CH_4 evolution. This is the first study to report these fluxes under an environment where CO_2 is the sole carbon substrate. We propose a novel process simulation approach for calculating extracellular fluxes and describe a method to estimate the maintenance energy parameters of a cell using a genome-scale model and experimentally measured compositional data. This work received encouraging comments from reviewers and is published by journal "*Microbial Cell Factories*".

Chapter 5 compares the impacts of two different nitrogen sources (N_2 and NH_4^+) on methane production in *M. maripaludis*. The growth rates and methane evolution rates (MERs) for *M. maripaludis* were measured and compared. We showed a significant enhancement of methanogenesis during N_2 fixation compared to NH_4^+. We quantified growth rates and fluxes during N_2-fixation using our novel process simulation approach and estimated maintenance energy parameters. This work is under review by journal "*Biomass and Bioenergy*".

Chapter 6 highlights the key contributions and discusses future recommendations for an improved understanding of methanogenesis from *M. maripaludis*. It reports some preliminary work carried out on single-chamber electromethanogenesis as part of this thesis.

References

1. Global Energy Trends—BP Statistical Review (2014) http://euanmearns.com/global-energy-trends-bp-statistical-review-2014/
2. Park S, Bézier D, Brookhart M (2012) An efficient iridium catalyst for reduction of carbon dioxide to methane with trialkylsilanes. J Am Chem Soc 134:11404–11407
3. In S-I, Vaughn DD, Schaak RE (2012) Hybrid CuO–TiO2–xNx hollow nanocubes for photocatalytic conversion of CO_2 into methane under solar irradiation. Angew Chem 124:3981–3984

4. Li W (2010) Electrocatalytic reduction of CO_2 to small organic molecule fuels on metal catalysts. ChemInform 1056:55–76
5. Earl Boysen NCM (2011) Nanotechnology for dummies. 2nd edn
6. Zhang ZY, Maekawa T (1993) Kinetic study on fermentation from CO_2 and H_2 using the acclimated-methanogen in batch culture. Biomass Bioenergy 4:439–446
7. Dodge E (2014) Carbon dioxide can be a resource rather than a waste product
8. Brilman W, Alba LG, Veneman R (2013) Capturing atmospheric CO_2 using supported amine sorbents for microalgae cultivation. Biomass Bioenergy 53:39–47
9. Ferry JG (1994) Methanogenesis: ecology, physiology, biochemistry & genetics. Springer
10. Liu Y, Whitman WB (2008) Metabolic, phylogenetic, and ecological diversity of the methanogenic archaea. Ann N Y Acad Sci 1125:171–189
11. Stephanopoulos G, Aristidou AA, Nielsen J (1998) Metabolic engineering: principles and methodologies. Academic Press
12. Feist AM, Scholten JC, Palsson BØ, Brockman FJ, Ideker T (2006) Modeling methanogenesis with a genome-scale metabolic reconstruction of *Methanosarcina barkeri*. Mol Syst Biol 2
13. Tsao JH, Kaneshiro SM, Yu SS, Clark DS (1994) Continuous culture of *Methanococcus jannaschii*, an extremely thermophilic methanogen. Biotechnol Bioeng 43:258–261
14. Whitman W, Ankwanda E, Wolfe R (1982) Nutrition and carbon metabolism of *Methanococcus voltae*. J Bacteriol 149:852–863
15. Zeikus J, Fuchs G, Kenealy W, Thauer R (1977) Oxidoreductases involved in cell carbon synthesis of *Methanobacterium thermoautotrophicum*. J Bacteriol 132:604–613
16. Thauer RK (2012) The Wolfe cycle comes full circle. Proc Natl Acad Sci 109:15084–15085
17. Jones WJ, Paynter MJB, Gupta R (1983) Characterization of *Methanococcus maripaludis* sp. nov., a new methanogen isolated from salt marsh sediment. Arch Microbiol 135:91–97
18. Lie TJ, Wood GE, Leigh JA (2005) Regulation of nif expression in *Methanococcus maripaludis*: roles of the euryarchaeal repressor NrpR, 2-oxoglutarate, and two operators. J Biol Chem 280:5236–5241
19. Hendrickson EL, Kaul R, Zhou Y, Bovee D, Chapman P, Chung J, Conway de Macario E, Dodsworth JA, Gillett W, Graham DE, et al. (2004) Complete genome sequence of the genetically tractable hydrogenotrophic methanogen *Methanococcus maripaludis*. *J Bacteriol* 186:6956–6969
20. Moore BC, Leigh JA (2005) Markerless mutagenesis in *Methanococcus maripaludis* demonstrates roles for alanine dehydrogenase, alanine racemase, and alanine permease. J Bacteriol 187:972–979
21. Porat I, Kim W, Hendrickson EL, Xia Q, Zhang Y, Wang T, Taub F, Moore BC, Anderson IJ, Hackett M et al (2006) Disruption of the operon encoding Ehb hydrogenase limits anabolic CO_2 assimilation in the archaeon *Methanococcus maripaludis*. J Bacteriol 188:1373–1380
22. Wood GE, Haydock AK, Leigh JA (2003) Function and regulation of the formate dehydrogenase genes of the methanogenic archaeon *Methanococcus maripaludis*. J Bacteriol 185:2548–2554
23. Argyle JL, Tumbula DL, Leigh JA (1996) Neomycin resistance as a selectable marker in *Methanococcus maripaludis*. Appl Environ Microbiol 62:4233–4237
24. Tumbula DL, Makula RA, Whitman WB (1994) Transformation of *Methanococcus maripaludis* and identification of a Pst I-like restriction system. FEMS Microbiol Lett 121:309–314
25. Jones GM, Wu J, Ding Y, Uchida K, Aizawa S, Robotham A, Logan SM, Kelly J, Jarrell KF (2012) Identification of genes involved in the acetamidino group modification of the flagellin N-linked glycan of *Methanococcus maripaludis*. J Bacteriol 194:2693–2702
26. Walters AD, Smith SE, Chong JP (2011) Shuttle vector system for *Methanococcus maripaludis* with improved transformation efficiency. Appl Environ Microbiol 77:2549–2551
27. Ladapo J, Whitman WB (1990) Method for isolation of auxotrophs in the methanogenic archaebacteria: role of the acetyl-CoA pathway of autotrophic CO_2 fixation in *Methanococcus maripaludis*. Proc Natl Acad Sci 87:5598–5602

28. Blank CE, Kessler PS, Leigh JA (1995) Genetics in methanogens: transposon insertion mutagenesis of a *Methanococcus maripaludis* nifH gene. J Bacteriol 177:5773–5777
29. Reed JL, Palsson BO (2003) Thirteen years of building constraint-based *In Silico* models of *Escherichia coli*. J Bacteriol 185:2692–2699
30. Price ND, Reed JL, Palsson BO (2004) Genome-scale models of microbial cells: evaluating the consequences of constraints. Nat Rev Microbiol 2:886–897
31. Fleischmann R, Adams M, White O, Clayton R, Tatusov R, Mushegian A, Bork P, Brown N, Hayes W, White O (1995) Whole-genome random sequencing and assembly of Haemophilus. Science 269:496–512
32. Pramanik J, Keasling JD (1997) Stoichiometric model of *Escherichia coli* metabolism: incorporation of growth-rate dependent biomass composition and mechanistic energy requirements. Biotechnol Bioeng 56:398–421
33. Aggarwal S, Karimi IA, Lee DY (2011) Reconstruction of a genome-scale metabolic network of *Rhodococcus erythropolis* for desulfurization studies. Mol BioSyst 7:3122–3131
34. Widiastuti H, Kim JY, Selvarasu S, Karimi IA, Kim H, Seo JS, Lee DY (2011) Genome-scale modeling and *in silico* analysis of ethanologenic bacteria *Zymomonas mobilis*. Biotechnol Bioeng 108:655–665
35. Satish Kumar V, Ferry JG, Maranas CD (2011) Metabolic reconstruction of the archaeon methanogen *Methanosarcina acetivorans*. *BMC Syst Biol* 5:28
36. Selvarasu S, Karimi IA, Ghim G-H, Lee D-Y (2010) Genome-scale modeling and *in silico* analysis of mouse cell metabolic network. Mol BioSyst 6:152–161
37. Ulas T, Riemer SA, Zaparty M, Siebers B, Schomburg D (2012) Genome-scale reconstruction and analysis of the metabolic network in the hyperthermophilic archaeon *Sulfolobus solfataricus*. PLoS ONE 7:e43401
38. Goyal N, Widiastuti H, Karimi IA, Zhou Z (2014) Genome-scale metabolic model of *Methanococcus maripaludis* S2 for CO_2 capture and conversion to methane. Mol BioSyst 10:1043–1054

Chapter 2
Literature Review

The literature review has been divided into three major sections and each section reviews and analyzes the prior research that discusses the related work. The information presented here gives a summarized overview and help us in exploring the metabolic processes and potential of hydrogenotrophic methanogens as well as deciphering the underlying mechanisms with the help of genome-scale engineering.

2.1 CO_2 Fixing Microbes

Carbon dioxide is an inorganic form of carbon which serves as the substrate for many autotrophic microorganisms [1]. The microbial CO_2 fixation can be very useful for the production of bioenergy, biodiesel, biohydrogen and biodegradable plastics. In 1940, CO_2 fixation by *Propionibacterium pentosaceum* was first reported by Wood and Werkman [2]. Later, CO_2 assimilation by various heterotrophic bacteria (*Aerobacter indologenes*, *Proteus vulgaris*, *Streptococcus paracitrovorus*, and *Staphylococcus candidus*) was reported by Werkman and Wood [3]. Since then series of efforts were made for studying CO_2 assimilation by microorganisms. CO_2 assimilating microorganisms are widespread among both archaeal and bacterial domain. Within archeal domain, they belong to phyla Euryarchaeota and Crenarchaeota. While among bacterial domain, they belong to the phyla Aquificae, Actinobacteria, Chloroflexi (green non-sulfur bacteria), Proteobacteria, Chlorobi, Firmicutes and Thermodesulfobacteria [1].

There are six major CO_2 fixing pathways: first, Calvin cycle or Calvin-Benson-Bassham (CBB) pathway or Reductive pentose pathway found in green plants and many autotrophic bacteria [4]. Second, Reductive TCA cycle or reverse citric acid

Some content of this chapter has been reproduced with permission from Nishu Goyal, Zhou Zhi, and I A Karimi. "Metabolic processes of *M. maripaludis* and potential applications", Microbial Cell Factories (2016), Vol. 15, 107

N. Goyal, *In silico Modeling and Experimental Validation for Improving Methanogenesis from CO_2 via M. maripaludis*, Springer Theses,
DOI 10.1007/978-981-10-2510-5_2

cycle found in Thermoproteus [5]. Third, Reductive acetyl-coenzyme A (acetyl-CoA) pathway or Wood-Ljungdahl pathway generally present in strict anaerobes because of the oxygen sensitivity of its key enzyme acetyl-CoA decarbonylase/synthase (CODH/ACS) [4, 6]. The microbial species having this pathway mainly belong to methanogens and acetogens. Fourth, 3-Hydroxypropionate pathway/Malyl-CoA pathway (3-HP) which was first reported in phototrophic green non-sulfur bacterium [7]. Fifth, 3-Hydroxypropionate/4-hydroxybutyrate cycle reported in the cell extract of *Metallosphaera sedula*, an aerobic autotrophic member of sulfolobales [8] and Last, Dicarboxylate/4-hydroxybutyrate cycle found to be operating in *Ignicoccus hospitalis* (Desulfurococcales) [9].

Till date, the biological fixation of CO_2 by microalgae has been investigated for global reduction of CO_2 levels [10]. However, harvest has been an expensive and problematic part of industrial production of microalga biomass. In this thesis, we explore the potential of a hydrogenotroph, *M. maripaludis.* This is a very useful model organism among hydrogenotrophic methanogens that offers several advantages. (1) Rapidly growing archaea, with a doubling time of 2 h [11]. (2) Mesophilic, grows best at 35–39 °C. (3) Robust set of genetic tools for molecular and biochemical studies. (4) Cells easy to lyse and makes the isolation of DNA and other components easier. (5) Non-pathogenic. (6) No need of biofuel harvesting.

2.2 *M. maripaludis*—A CO_2 Fixer

Methanococci are non-pathogenic, mesophilic, strictly anaerobic, hydrogenotrophic, and methanogenic archaebacteria. They comprise four species: *M. maripaludis*, *M. vannielii*, *M. voltae*, and *M. aeolicus* [12]. In this study, we focus on *M. maripaludis* (Fig. 2.1), whose type strain *M. maripaludis* JJ was isolated from salt

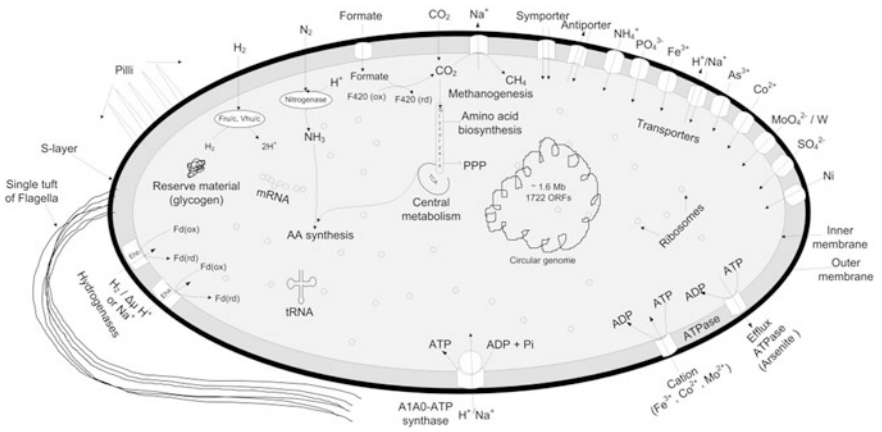

Fig. 2.1 A schematic representation of a typical *M. maripaludis* cell

marsh sediments in South Carolina [11]. Since then, numerous strains have been isolated from estuarine sites in South Carolina, Georgia, and Florida [13]. Table 2.1 lists the characteristics of five fully sequenced strains (S2, C5, C6, C7 and X1).

M. maripaludis is a fast growing microbe with a doubling time of 2 h and optimum growth temperature at 38 °C. It reduces CO_2 to methane via a modified Wood-Ljunghdahl pathway, also known as Wolfe cycle [14]. Unlike other microorganisms that need complex carbon substrates such as pentoses, hexoses, alcohols, and their derivatives for their growth, *M. maripaludis* can use simple substrates such as CO_2 or formate as the sole carbon sources, and N_2 as the sole nitrogen source [15]. However, it needs H_2 or formate (HCO_2^-). as an energy source [16–18]. In other words, given a renewable source of H_2,

M. maripaludis has the potential to convert flue gas emissions (majorly consist of CO_2 and N_2) into a useful fuel (methane). In fact, *M. maripaludis* S2 has been a well-studied model organism in the literature [22].

In spite of more than 100 publications on the biochemistry of *M. maripaludis*, a consolidated review is missing in the literature. This chapter reviews existing literature on *M. maripaludis*, and explores its potential industrial and environmental applications. Figure 2.2 shows an overview of eight major metabolic subsystems in *M. maripaludis*: methanogenesis, reductive tricarboxylic acid (TCA) cycle, non-oxidative pentose phosphate pathway (PPP), glucose/glycogen metabolism, nitrogen metabolism, amino acid metabolism, and nucleotide metabolism.

Reduction of CO_2 to methane via methanogenesis is essential for the energy needs of *M. maripaludis* [23, 24], and therefore methanogenesis forms the foundation for its survival and growth. In other words, methanogenesis is coupled with cell growth, and both compete for the carbon source. The remaining seven subsystems provide the essential precursors for cell growth via two key intermediates: acetyl CoA and pyruvate.

2.2.1 Taxonomy, Cell Structure, and Cultivation

Identification and classification

In late 1970s, 16S rRNA gene sequences were adopted for phylogenetic analyses, and *Archaea* was classified as the third domain of life by Carl Woese and his colleagues [23]. *Archaea* is a diverse group of microorganisms widely distributed in extreme habitats, such as hot springs for the phylum Crenarchaeota and salt lakes for the phylum Euryarchaeota. The phylum Euryarchaeota includes eight classes: Methanobacteria, Methanococci, Methanomicrobia, Halobacteria, Thermoplasmata, Thermococci, Archaeoglobi, and Methanopyri. The distinctive features of the Methanococci include rapid growth in both mesophilic and thermophilic temperatures, proteinaceous S-layer as the cell envelope, and a nutritional requirement for selenium. The Methanococci include a single order Methanococcales, which includes methanogens characterized by a coccoid shape and the presence of

Table 2.1 Characteristic features of *M. maripaludis* strains

Strains	Source/habitat	Substrate	Optimum temperature	Optimum pH	mol% GC	Growth rate (/h)	Sequenced by	Total genome size (bp)	Number of ORFs
M. maripaludis S2	Salt marsh sediment [13]	HCOOH, or H_2 and CO_2	38 °C	6.8–7.2	34.4 ± 0.1	0.30	[22]	1,661,137	1772
M. maripaludis C5	Airport Marsh [13]	HCOOH, or H_2 and CO_2	35–40 °C	6–8	33.1 ± 0.1	0.21	[19]	1,789,046	1889
M. maripaludis C6	Roger's Marsh [13]	HCOOH, or H_2 and CO_2	35–40 °C	6-8	34.2 ± 0.1	0.06	[19]	1,744,193	1888
M. maripaludis C7	Roger's Marsh [13]	HCOOH, or H_2 and CO_2	35–40 °C	6–8	33.7 ± 0.1	0.20	[19]	1,772,694	1855
M. maripaludis X1	Thermophilic saline oil reservoir [20]	HCOOH, or H_2 and CO_2	NA	NA	32.9 ± 0.1	NA	[21]	1,746,697	1892

NA *Not available*

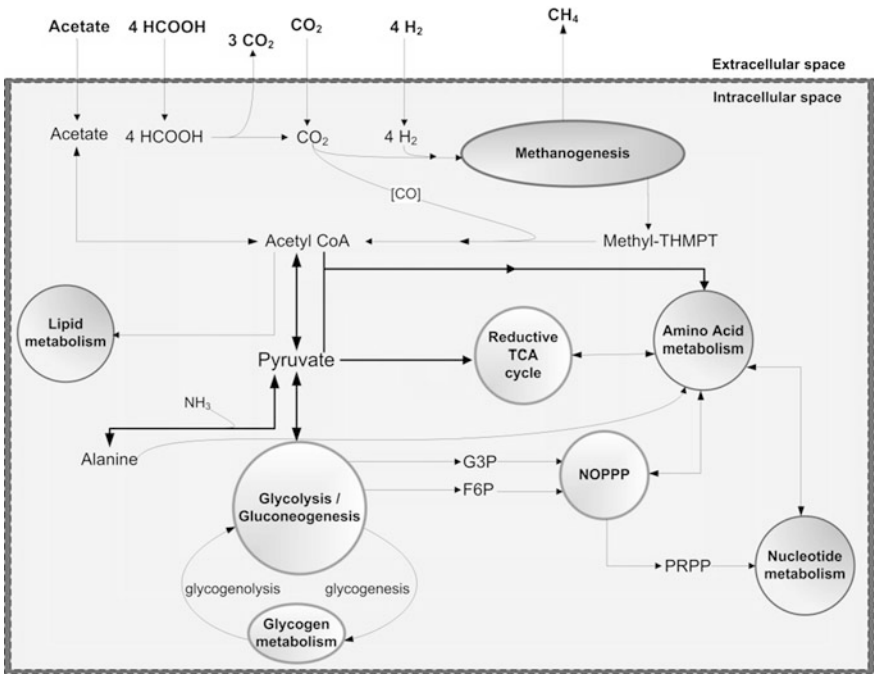

Fig. 2.2 Simplistic overview of eight major metabolic subsystems in *M. maripaludis*

glycolipids and polar lipids in varying compositions [18]. The order Methanococcales is composed of two families: *Methanococcaceae* and *Methanocaldococcaceae*. They differ in 12 % 16S rRNA sequences and growth temperatures [25]. *Methanococcaceae* are extremely thermophilic or mesophilic, while *Methanocaldococcaceae* are all hyperthermophilic. The family *Methanococcaceae* is further subdivided into two genera, namely *Methanococcus* and *Methanothermococcus* based on their different optimum growth temperatures. The core lipid of *Methanococcus* is mainly archaeol and hydroxyarchaeol, while caldarchaeol is additionally present in *Methanothermococcus* [26]. The most abundant polyamine is spermidine in *Methanococcus* and *Methanothermococcus*. The genus *Methanococcus* is subdivided into four species, *M. aeolicus, M. maripaludis, M. vannielii, and M. voltae,* based on 16S rRNA sequences, DNA relatedness, cellular protein patterns, and phenotypic methods [12]. The detailed characteristics of each species have been described previously [25]. *M. maripaludis* species have five sequenced strains: *M. maripaludis* S2, *M. maripaludis* C5, *M. maripaludis* C6, *M. maripaludis* C7, and *M. maripaludis* X1, which were classified based on their 54–69 % DNA relatedness and 99.2 % sequence similarity with 16S rRNA sequences [12].

Cell structure

Methanococcus has a spherical shape. Its cell wall is fragile and its morphology is affected by its physiological state and the ionic strength of growth medium. *M. maripaludis* cells are weakly-motile cocci with a diameter ranging from 0.9 to 1.3 μm [11]. They are non-spore forming mesophile, and grow best at a temperature between 20 and 45 °C and a pH between 6.5 and 8.0 [27]. The cell envelope of *M. maripaludis* is a single electron dense layer. The cell wall is a proteinaceous S-layer, but lacks peptidoglycan molecules. The molecular mass of S-layer proteins was found to be in the range of 59,064 and 60,547 Da [28]. The proteinaceous cell wall of *M. maripaludis* lyses rapidly in low concentrations of detergents [11] and buffers of low osmolarity [29], which makes the isolation of DNA easier. Despite the differences in the predominance of some amino acids, the primary structure of S-layer proteins shows a high degree of identity (38–45 %) [28]. Ether lipids recovered from *M. maripaludis* mainly include glycolipid (14.2 mg ether lipid/g dry cell weight) and polar lipids (0.4 mg ether lipid/g dry cell weight) [30]. The S-layer proteins and flagellins of *M. maripaludis* have been discussed in the literature [31, 32].

The motility in methanococci is due to the presence of flagella. However, efficient attachments to the surfaces in *M. maripaludis* require both flagella and pili [33]. Bardy et al. [34] demonstrated the presence of *flaK* and preflagellin peptidase activity in *M. maripaludis*, but the exact role of this peptidase in the secretion of archaeal flagellins and assembly of flagella is unknown. To understand the proper assembly and function of flagella in *M. maripaludis*, Chaban et al. [35] performed systematic deletions of *fla* genes in the flagella operon that consists of three flagellin genes (*flaB1, flaB2*, and *flaB3*) and eight others (*flaC to flaJ*). Their results showed that individual deletions of *flaB1, flaB2, flaC, flaF, flaG*, *flaH* and *flaI* resulted in non-motile and non-flagellated cells. *flaJ* was homologus to the integral membrane proteins in the type IV pili system, and is necessary for flagellation in a closely related methanogen *M. voltae*. Thus, its deletion was exempted. The experiments on deletions of *fla*D and *fla*E failed several times for unknown reasons, which requires further research [36]. Interestingly, an acetyltransferase gene involved in sugar biosynthesis in *M. maripaludis* was found to affect flagellin N-linked glycosylation and proper assembly of both flagella and pili [37]. The deletion of this gene resulted in completely nonglycosylated flagellins and defective pilus anchoring [37]. The composition of a novel N-linked flagellar glycan in *M. maripaludis* was identified in 2009 [38]. A genetic analysis for the type IV pili formation in *M. maripaludis* was conducted, but specific roles of these pili are still unknown [39]. However, if archaeal pili are similar to bacterial pili, then archaeal pili could be involved in functions related to cell-to-cell twitching motility, attachment, biofilm formation, etc.

Growth media, Culture conditions, and Storage

M. maripaludis is a routinely cultured hydrogenotrophic methanogen. It can grow anaerobically on minimal medium (McN), complex medium (McC), and minimal

medium plus sodium acetate (McNA) [13]. Plate colonization of *M. maripaludis* on solidified agar medium with 50–100 % plating efficiency and maximum colony size was achieved by optimizing the inoculation method, H_2S concentration, and agar moisture content [40]. The preferred carbon and energy source is CO_2–H_2 (20:80 v/v) at a pressure of about 275 kPa. In the absence of H_2, formate can serve as the sole carbon and energy source in the presence of N_2–CO_2 (80:20 v/v) [41, 42]. However, excess of either H_2 or formate decreases the ratio of growth yield to methane significantly [17].

Amino acids and vitamins may affect [43] the growth rate and cell yield (mg dry cell weight/ml) of methanococci. Some of the facultative autotrophic strains, such as Strain D1, Strain C5, Strain C9, and Strain C14, assimilated large amounts of amino acids, but the growths of *M. vannielli* and *M. aeolicus* were unaffected. The growth of *M. maripaludis* was moderately stimulated, possibly because *M. maripaludis* was capable of utilizing alanine as the sole nitrogen source in the absence of other nitrogen sources, while *M. vannielli* and *M. aeolicus* could not use alanine as the sole nitrogen source. Although exogenous amino acids can substitute for 40–60 % of the total cell carbon by some autotrophic methanococci, they were not the major nitrogen sources and were not extensively metabolized. The growth of 16 autotrophic isolates, such as *M. maripaludis*, *M. vannielii*, *M. deltae*, and *M. aeolicus*, remained unaffected by the mixture of water soluble vitamins [43]. Pantothenate was the only vitamin that stimulated the growth of *M. voltae* [44].

Long-term storage of *M. maripaludis* cultures in glycerol stock solutions has been reported [13]. Cultures were grown to the early stationary phase, concentrated by centrifugation, and cell pellets were resuspended in media containing 25 % glycerol and then stored at −70 °C. The addition of glycerol stabilizes frozen microorganisms, prevents damage to cell membranes, and keeps the cell alive for many years.

2.2.2 *Metabolic Processes in* M. maripaludis

In this section, we focus on metabolic processes, energy production, and genome-scale modeling. Specifically, we discuss methanogenesis, acetyl-CoA synthesis, pyruvate synthesis, glycolysis/gluconeogenesis, reductive tricarboxylic acid (TCA) cycle, non-oxidative pentose phosphate pathway (PPP), nitrogen metabolism, amino acid metabolism, nucleotide metabolism, molecular biology tools, genome-scale model, and applications.

2.2.2.1 Methanogenesis

Methanogenesis (Fig. 2.3) is the biological production of methane from the reduction or disproportionation of simple carbon substrates (e.g. CO_2, formate, acetate and methanol) as per the following reactions:

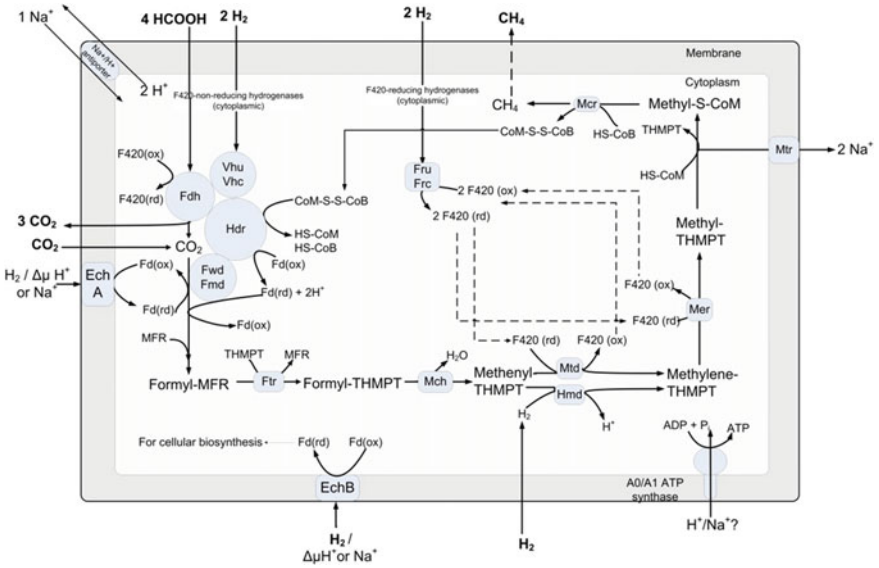

Fig. 2.3 Energy producing pathway in *M. maripaludis*

$$\begin{aligned}
CO_2 + 4H_2 &\rightarrow CH_4 + 2H_2O & \Delta G^0 &= -131\,\mathrm{kJ/mol}\\
4HCOOH &\rightarrow 3CO_2 + CH_4 + 2H_2O & \Delta G^0 &= -119\,\mathrm{kJ/mol}\\
CH_3COOH &\rightarrow CH_4 + CO_2 & \Delta G^0 &= -36\,\mathrm{kJ/mol}\\
4CH_3OH &\rightarrow 3CH_4 + CO_2 + 2H_2O & \Delta G^0 &= -106\,\mathrm{kJ/mol}
\end{aligned}$$

While formate, acetate, and methanol oxidize/reduce by themselves, CO_2 needs an electron donor such as H_2 [11], formate [41], or electricity [45]. In *M. maripaludis*, methanogenesis can occur via the reduction of CO_2 with H_2/formate/electricity, or the disproportionation of formate. Lohner et al. [45] demonstrated H_2-independent electromethanogenesis from CO_2 in both wild-type *M. maripaludis* strain S2 and hydrogenase mutant strain MM1284. Mutant strain under the same conditions reduced methane production rates by a factor of 10 compared to those observed with the wild-type strain S2 [45]. However, the attempts to quantify biomass growth were inconclusive.

The formate-dependent methanogenesis involves an additional endergonic step where formate is oxidized to CO_2 via formate dehydrogenase with a simultaneous reduction of coenzyme F420 [42]. The reduced coenzyme F420 serves as the electron carrier for two intermediary steps in methanogenesis. However, H_2 is probably not an intermediate during formate-dependent methanogenesis [41, 46]. As shown in Fig. 2.3, the resulting CO_2 participates in the first step of methanogenesis.

A recent study [17] showed the effects of H_2 and formate limitation/excess on growth yield and regulation of methanogenesis using a continuous culture of *M. maripaludis*. They concluded that the growth yield (g dry cell weight

(DCW)/mol CH_4) decreased remarkably with excess H_2 or formate. While they speculated energy spilling or dissipation to be a possible cause, the exact cause is still unclear. While *M. maripaludis* can also assimilate other carbon substrates, such as acetate and pyruvate, they are not the physiologically relevant substrates for methane production [47, 48]. No methane production from acetate (17), and extremely low methane (only 1–4 % compared to that for H_2) has been reported from pyruvate [48].

Mechanism

The structures and functions of the cofactors and coenzymes involved in methanogenesis are listed in Table 2.2. The first step in methanogenesis is the reduction of CO_2. It involves the simultaneous oxidation of low-potential reduced ferredoxins and the capture of CO_2 by methanofuran (MFR) to form formyl-MFR (ΔG^0 = 0 kJ/mol) [55]. These extremely low-potential ferredoxins could come from two pools [56]. One is EchA that not only uses one H_2, but also consumes proton-motive force (PMF) to generate ferredoxins. This accounts for only 4 % of the reduce ferredoxins as shown in a $\Delta 5H_2$ase mutant [46]. The second and the major pool is Vhu/Hdr bifurcation complex that consumes two H_2 and generates one pair of relatively high potential electrons to reduce CoB-S-S-CoM and another pair of extremely low potential electrons to reduce the ferredoxins. The formyl group from formyl-MFR is then transferred to THMPT (ΔG^0 = −5 kJ/mol) to form formyl-THMPT, and the latter is then dehydrated to methenyl-THMPT (ΔG^0 = −5 kJ/mol) [57]. In the next two steps, the reduced F420 supplies electrons to reduce methenyl-THMPT to methylene-THMPT (ΔG^0 = +6 kJ/mol) and methylene-THMPT to methyl-THMPT (ΔG^0 = −6 kJ/mol) [58]. These reactions are fully reversible, as evidenced by their near zero free energy changes. The oxidized F420 is then reduced (ΔG^0 = −11 kJ/mol) in the presence of H_2 [55]. Next, the methyl group from methyl-THMPT is transferred to coenzyme M (HS-CoM) in an exergonic step (ΔG^0 = −30 kJ/mol) coupled with $2Na^+$ translocation by a membrane-bound enzyme complex [59]. This reaction builds up an electrochemical Na^+ gradient, which drives energy production via ATP synthase [55]. The final step of methanogenesis is the reductive demethylation of methyl-S-CoM to methane and CoM-S-S-CoB (ΔG^0 = −30 kJ/mol). Subsequently, this CoM-S-S-CoB gets reduced with the help of H_2 to form HS-CoM and HS-CoB (ΔG^0 = −39 kJ/mol) [60]. This reduction of CoM-S-S-CoB mediates via an electron bifurcation mechanism [55]. This step along with the earlier step involving the Na^+ translocation supplies the major energy demand of *M. maripaludis*.

Hydrogenases

The key to the survival of *M. maripaludis* on CO_2 is its ability to take up external H_2 and perform $H_2 \rightarrow 2H^+ + 2e^-$ with the help of seven hydrogenases (Fig. 2.3). These are Fru, Frc, Vhu, Vhc, Hmd, EchA, and EchB, which can be categorized in different manners. The first five are cytoplasmic and the last two are membrane-bound [61]. Fru and Frc use cofactor F420 [53], Vhu and Vhc use

Table 2.2 Structure and functions of unusual coenzymes involved in methanogenesis

Cofactor/coenzyme	Structure	Function	Reference
Methanofuran	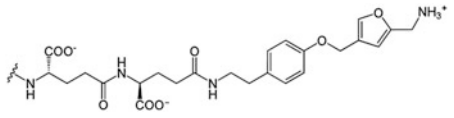	Carbon-carrier cofactors involved in the first step of the methanogenic reduction of CO_2 to formyl-methanofuran	[49, 50]
Tetrahydro-methanopterin	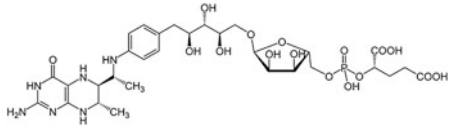	Carries single carbon fragments between formyl and methyl oxidation levels in methanogens, typically formyl, methenyl, methylene or methyl group	[14, 50]
Coenzyme B	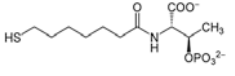	Function as electron carrier in metabolism of methanogens	[50, 51]
Coenzyme M	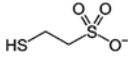	Required for methyl-transfer reactions in the metabolism of methanogens. HS-CoB reacts with Methyl-S-CoM to release methane and CoM-S-S-CoB in the final step of methanogenesis	[50, 52]

(continued)

Table 2.2 (continued)

Cofactor/coenzyme	Structure	Function	Reference
Coenzyme F420	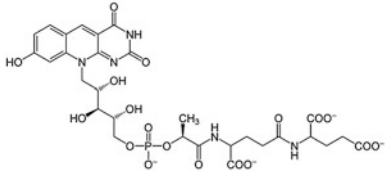	Major electron transfer currency. Transfer electrons from H_2 to the consecutive intermediates of methane biosynthesis e.g. coenzyme F420 hydrogenase, 5,10-methylene-THMPT reductase and methylene-THMPT dehydrogenase	[50, 53]
Cofactor F430	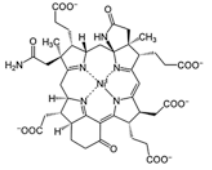	This cofactor is the prosthetic group of the methyl-CoM reductase which catalyzes the release of methane and CoB-S-S-CoM in the final step of methanogenesis	[50, 54]

ferredoxin and CoM/CoB [62], Hmd uses direct H_2 [53], and EchA and EchB use ferredoxins as electron carriers [46]. *M. maripaludis* needs four pairs of electrons to reduce one mole of CO_2 to methane. Fru/Frc can supply two pairs, Vhu/Vhc can supply two pairs, Hmd can supply one pair, and EchA/EchB can supply one pair each. Of these, Fru/Frc and Vhu/Vhc play a major role in H_2 uptake.

Fru and Frc reduce two molecules of coenzyme F420 with the help of two H_2 [53]. One F420(rd) gets oxidized by reducing methenyl-THMPT and the other by reducing methylene-THMPT.

Vhu and Vhc facilitate the flow of electrons from H_2 to heterodisulfide reductase (Hdr) complex [62], which in turn catalyzes the reductions of CoM/CoB and ferredoxins via an electron bifurcation mechanism [60]. These reduced ferredoxins are the major electron suppliers during the first step of methanogenesis.

Hmd uses H_2 to reduce methenyl-THMPT to methylene-THMPT [53] without any carrier. As shown in Fig. 2.3, Mtd also catalyzes the same reaction, but with the help of reduced F420 as an electron carrier. Hendrickson et al. [53] demonstrated that during the growth on H_2 and CO_2, Hmd is not essential in the presence of active Fru/Frc, but it is essential otherwise. In contrast, the ΔFru, ΔFrc, and ΔHmd mutants grew normally during formate-dependent growth.

EchA generates a small portion of low-potential reduced ferredoxins required for the first step of methanogenesis. Its role in *M. maripaludis* is anaplerotic, because it is required only under certain conditions such as (1) to replenish the intermediates of methanogenesis cycle, and (2) imperfect coupling during electron bifurcation [46]. Lie et al. [46] showed this by eliminating all nonessential pathways of H_2 metabolism and using formate as the sole electron donor. In this case, both Hdr complex and EchA independently provided electrons for growth.

In contrast, EchB supplies electrons to anabolic oxidoreductases for the synthesis of precursors such as pyruvate and acetyl CoA [61, 215]. EchB mutants affect the autotrophic growth severely, but it is unclear how they still survive. When conditions limit growth, anabolic CO_2 fixation is unimportant, but methanogenesis continues. Under such a scenario, EchA is essential, but EchB could be detrimental [46].

During formate-dependent growth, the H_2 required for the essential anaplerotic (EchA) and anabolic (EchB) functions has to be produced from formate. This H_2 production can occur via two pathways as demonstrated by Lupa et al. [42] in *M. maripaludis*. One involves Fdh1-Fru/Frc, and the other involves Fdh1-Mtd-Hmd. Of these, the former seems to be predominant ($\sim$90 %), as the deletion of either Fdh1 or Fru/Frc reduced H_2 production rates severely.

Energy Generation/Conservation

In most organisms, electron movement along the cell membrane is the key to energy transduction. Substrate oxidation releases electrons that move along the membrane-bound cytochrome carriers and extrudes protons out of the cell to generate a potential gradient. The potential difference drives the protons back into the cell, while synthesizing ATP from ADP and Pi via ATP synthase [63].

Hydrogenotrophic methanogens such as *M. maripaludis* lack such an electron transport chain [64]. In place of cytochrome carriers, *M. maripaludis* uses methyl-THMPT: HS-COM methyltransferase (Mtr), the only membrane-bound enzyme complex in the core methanogenic pathway, to extrude Na^+/H^+ out of the cell [55, 59]. This creates a Na^+/H^+ ion motive force (positive outside), which on their translocations into the cell generate ATP via an A1A0-type ATP synthase [65]. However, a direct experimental evidence specifically for Na^+ or H^+ gradient does not exist in the literature for *M. maripaludis*. To conserve ATP, *M. maripaludis* uses reduced ferredoxins as low-potential electron carriers for the highly endergonic reduction of CO_2 to formyl-MFR. As discussed earlier, these ferredoxins are supplied predominantly by the Hdr complex [60] and supplemented by EchA.

The genome sequence of *M. maripaludis* indicates the presence of membrane-bound A1A0-type ATPases (chimeric ATP synthases) instead of the F1F0-type ATPases found in Bacteria and Eukarya [22, 66]. The catalytic unit of the A1A0-type ATPase is structurally homologous to the V-type ATPase and functionally homologous to the F1F0-type ATPase [67]. But, the membrane-embedded motors in the A1A0-type ATP synthases are exceptional due to their novel functions and structural features [68].

2.2.2.2 Acetyl-CoA Synthesis

M. maripaludis can synthesize acetyl-CoA from either CO_2 or acetate [16, 47]. The CO_2-based synthesis occurs with the help of CODH/ACS [16]. Sequencing studies have confirmed the existence of CODH/ACS in a single cluster (MMP0980-MMP0985) [22]. During the CO_2-based synthesis, methyl-THMPT, an intermediate of methanogenesis, contributes the methyl carbon of acetyl-CoA while CO, which is generated during reduction of CO_2 in the presence of reduced ferredoxins by CO dehydrogenase (CODH), contribute the carboxyl carbon [16]. The acetate-based synthesis is accomplished by AMP-forming acetate CoA ligase (MMP0148, *acs*A) in *M. maripaludis* [47]. Shieh et al. [47] showed that *M. maripaludis* can assimilate up to 60 % of its cellular carbon from exogenous acetate. Sequencing study also showed the presence of ADP-forming acetyl-CoA synthetase gene (MMP0253, *acd*) in *M. maripaludis* [22], catalyzes acetate formation and ATP synthesis from acetyl CoA, ADP and Pi. However, no experimental study exists in the literature to demonstrate the biosynthesis of free acetate by *M. maripaludis*.

2.2.2.3 Pyruvate Synthesis

Pyruvate is the entry point into glycolysis, citric acid cycle, and amino acid metabolism. Acetyl-CoA is converted to pyruvate through pyruvate: ferredoxin oxidoreductases (PORs) [53, 69, 70] as follows:

$$\text{Acetyl} - \text{CoA} + \text{CO}_2 + 2\,\text{Fd(rd)} + 2\text{H}^+ \leftrightarrow \text{Pyruvate} + \text{CoA} + 2\,\text{Fd(ox)}$$

This is reversible in that PORs also catalyze pyruvate oxidation to acetyl-CoA in the absence of H_2 [48]. However, pyruvate oxidizes very slowly in *M. maripaludis* and PORs appear to function mainly in the anabolic directions during growth [69].

The PORs containing five polypeptides in *M. maripaludis* are encoded by a gene cluster (*por*ABCDEF). Of these, *por*EF is unique to *M. maripaludis*, because the N-terminal sequences of the first four polypeptides (*por*ABCD) are similar to those in other *Archaea* [70]. The importance of *por*EF in *M. maripaludis* was highlighted by Lin et al. [71]. They showed that *por*EF mutants of *M. maripaludis* JJ grew extremely slowly. In addition, pyruvate-dependent methanogenesis was completely inhibited. Interestingly, *por*F mutant failed to restore growth, but restored methanogenesis to wild-type levels. In contrast, *por*E mutant restored growth partially, but did not restore methanogenesis. This indicates that *por*F function as an electron donor to PORs.

Pyruvate is also a precursor for alanine biosynthesis via alanine dehydrogenase (MMP1513, *ald*) [72]. The same enzyme catalyzes the reverse reaction also, i.e. alanine to ammonia and pyruvate, in *M. maripaludis*. In addition, alanine transaminase that catalyzes the conversion of alanine to pyruvate in several organisms including *Pyrococcus furiosus*, *Escherichia coli*, *Mus musculus,* and *Homo sapiens*, may also exist in *M. maripaludis*. Our inference is based on our BLASTp search with the protein sequences of *M. maripaludis*. Our search located proteins with high similarity (E-value = 7e-63) to the alanine transaminase from *P. furiosus*. *M. maripaludis* takes alanine with the help of alanine permease and alanine racemase. While the former transports both L-alanine and D-alanine into the cell, the latter is essential to convert D-alanine to L-alanine [72, 73], because alanine dehydrogenase is specific for L-alanine.

2.2.2.4 Glycolysis/Gluconeogenesis and Glycogenolysis/Glyconeogenesis

M. maripaludis does not assimilate carbohydrates such as pentoses and hexoses, as it lacks the required transporters [22]. However, it has all the enzymes and cofactors required for glycolysis/gluconeogenesis and glycogenolysis/glyconeogenesis with some unique features. In fact, studies have shown that methanococci such as *M. maripaludis* synthesize and store glycogen as a reserve metabolite, and use it for methane generation in the absence of exogenous substrates [74]. The bifunctional activity of ADP-dependent phosphofructokinase (PFK)/glucokinase (GK) has been demonstrated experimentally in both *M. jannaschii* [75] and *M. maripaludis* [76]. Castro-Fernandez et al. [76] measured the activities of glucose phosphorylation versus dephosphorylation. They unexpectedly observed that the latter was 2-folds more efficient than the former. Based on these observations, they indicated that

M. maripaludis can catalyze D-glucose formation, and suggested the possibility of methane production from glycogen or D-glucose during starvation in *M. maripaludis*.

Unlike non-methanogenic *Archaea* that use ED pathway, *M. maripaludis* [74] uses a modified Embden-Meyerhof-Parnas (EMP) pathway with some unique features. These include the reduction of ferredoxins instead of NAD (e.g. PORs and GAPOR) [77], ADP-dependent kinases [75], zero or very low ATP yields [78], highly divergent phosphoglucose isomerase [79], and phosphoglycerate mutase [80]. Of the eight enzymatic steps (5–13) from pyruvate to glucose-6-phosphate (Fig. 2.4), five are reversible and catalyzed by the same enzyme, and the rest are irreversible (5, 9, and 12). However, even for these three irreversible steps, reverse steps are catalyzed by alternative enzymes [phosphenolpyruvate synthase (PPS), glyceraldehyde-3-phosphate dehydrogenase (GAPDH), and fructose-bisphosphatase (FBP)]. In other words, all the steps leading to glucose-6-phosphate from pyruvate are reversible in principle. Glycogen in *M. maripaludis* is then synthesized by converting (1) glucose-6-phosphate to glucose-1-phosphate via phosphoglucomutase

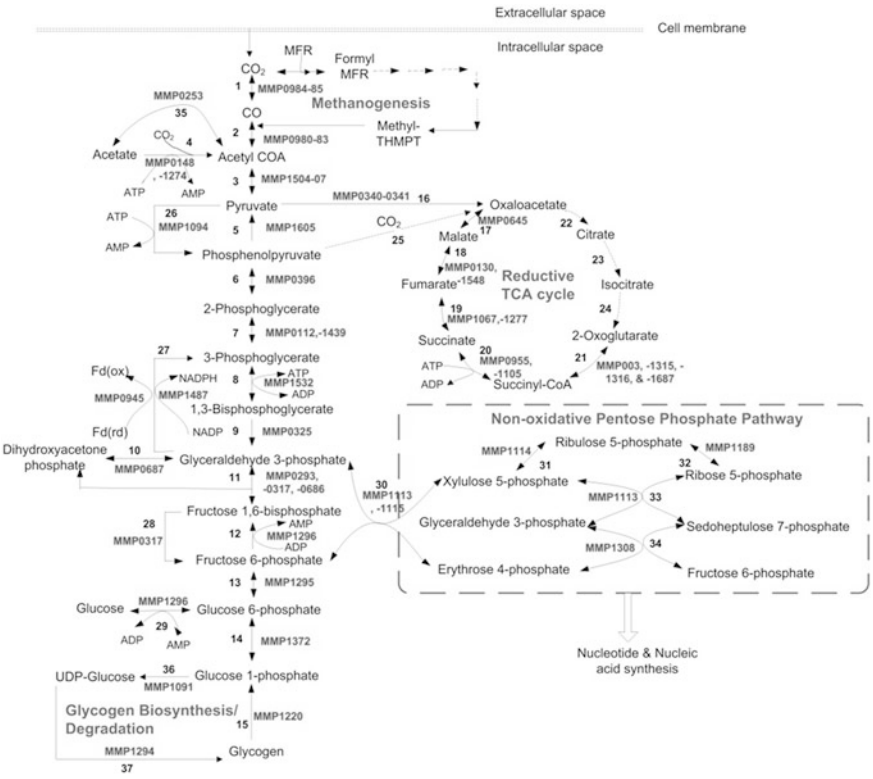

Fig. 2.4 Diagram outlining the reactions and associated ORF and enzymes involved in glycolysis/gluconeogenesis, TCA, and PPP of *M. maripaludis*

(MMP1372), (2) glucose-1-phosphate to UDP-glucose via UTP-glucose-1-phosphate uridylyltransferase (MMP1091), and (3) the growing polymeric chain of UDP-glucose to glycogen via glycogen synthase (MMP1294) with the release of UDP molecule [22]. On the other hand, glycogen in *M. maripaludis* degrades to glucose-6-phosphate by converting (1) glycogen to glucose-1-phosphate via glycogen phosphorylase (MMP1220), and (2) glucose-1-phosphate to glucose-6-phosphate via glucose phosphomutase (MMP1372) [22, 74]. The low activity of PFK in comparison to FBP in *M. maripaludis* suggests that glyconeogenesis is the predominant function of EMP pathway in *M. maripaludis* pointing to the storage of glycogen as a reserve material [74]. This predominance of the anabolic direction is further confirmed by the high activities of the reversible hexose phosphate conversions (via glucose phosphomutase, glucose-6-phosphate isomerase, and fructose-bisphosphate aldolase) and triose phosphate conversions for pentose biosynthesis (via enolase, 2,3-bisphosphoglycerate mutase, and glyceraldehyde-3-phosphate dehydrogenase). Yu et al. [74] further showed that glycogen content increased from 0.11 % ± Solid lines show the presence of enzymes and dotted lines show the absence of enzyme in *M. maripaludis*. Numbers mentioned in diagram indicate enzymes as follows: 1. carbon-monoxide dehydrogenase (1.2.7.4, *codh* and *por*EF); 2. acetyl CoA decarbonylase (2.1.1.245, *acds*); 3. pyruvate:ferredoxin oxidoreductase/synthase (1.2.7.1, *por*ABCD); 4. acetyl CoA synthetase (AMP forming) (6.2.1.1, *acs*A); 5. phosphenolpyruvate kinase (2.7.1.40, *pyk*); 6. enolase (4.2.1.11, *eno*); 7. 2,3-bisphosphoglycerate mutase (5.4.2.12, *pgm*); 8. phosphoglycerate kinase (2.7.2.3, *pgk*); 9. glyceraldehyde-3-phosphate dehydrogenase (1.2.1.59, *gapdh*); 10. triosephosphate isomerase (5.3.1.1, *tpi*); 11. fructose-bisphosphate aldolase (4.1.2.13. *fbp*); 12. phosphofructokinase (2.7.1.147, *pfk*); 13. glucose-6-phosphate isomerase (5.3.1.9, *pgi*); 14. Phosphoglucomutase (5.4.2.8, *pgm*); 15. glycogen phosphorylase (2.4.1.1, *glg*P); 16. pyruvate carboxylase (6.4.1.1, *pyc*B); 17. malate dehydrogenase (1.1.1.37, *mdh*) 18. fumarate hydratase (4.2.1.2, *fum*A); 19. succinate dehydrogenase/fumarate reductase (1.3.5.4/1.3.4.1, *sdh*A); 20. succinyl-CoA synthetase (6.2.1.5, *suc*C and *suc*D); 21. 2-oxoglutarate oxidoreductase (1.2.7.3, *kor*ABDG); 22. citrate synthase; 23. aconitate; 24. isocitrate dehydrogenase; 25. phosphoenolpyruvate carboxylase; 26. phosphoenolpyruvate synthase (2.7.9.2, *pps*A); 27. NADP-dependent glyceraldehyde-3-phosphate dehydrogenase (1.2.1.9, *gapn*) OR ferredoxin-dependent glyceraldehyde-3-phosphate dehydrogenase (1.2.7.6, *gapor*); 28. fructose-bisphosphatase (3.1.3.11, *fbp*); 29. ADP-specific phosphofructokinase (2.7.1.147, *pfk*); 30. transketoloase (2.2.1.1, *tkl*); 31. ribulose-phosphate 3-epimerase (5.1.3.1, *rpe*); 32. ribose-5-phosphate isomerase (5.3.1.6); 33. transketoloase (2.2.1.1, *tkt*); 34. translaldolase (2.2.1.2, *tal*); 35. Acetate CoA synthetase (ADP-forming) (6.2.1.13, *acd*); 36. UTP-glucose-1-phosphate uridylyltransferase (2.7.7.9); 37. starch synthase (2.4.1.21, *glg*A)

0.05 % DCW($A_{660} \leq 0.5$) to 0.34 % ± 0.19 % DCW (A_{660}1.0–1.6) during growth, while glycogen consumption depended on the substrate for methanogenesis.

Given the key role of glycolysis/gluconeogenesis in *M. maripaludis*, it is critical to understand their regulation. In general, a pathway can be regulated by (1) substrate availability, (2) up- or down-regulating enzyme activities for rate-limiting

steps, (3) allosteric regulation of enzymes, and (4) covalent modifications of substrates such as phosphorylations. Essentially, the enzymes catalyzing irreversible steps are most suited for regulation [81]. In most *Archaea*, nonphosphorylating $NADP^+$-dependent glyceraldehyde-3-phosphate (G3P) dehydrogenase (GAPN), phosphorylating glyceraldehyde-3-phosphate dehydrogenase (GAPDH), and glyceraldehyde-3-phosphate ferredoxin oxidoreductase (GAPOR) act as the regulatory points in glycolysis [82–84]. The genome sequence of *M. maripaludis* codes for all three genes, namely GAPN (MMP1487), GAPDH (MMP0325), and GAPOR (MMP0945) [22]. GAPOR catalyzes ferredoxin-dependent G3P oxidation, GAPN catalyzes NADP-dependent G3P oxidation, and GAPDH catalyzes G3P synthesis. Based on activity, transcript, and flux balance analyses in *M. maripaludis*, Park et al. [85] showed that GAPOR is a post-transcriptionally regulated enzyme that is completely inhibited by the presence of 1 μM ATP, and (unlike GAPN) is most likely involved only under non-optimal growth conditions.

Yu et al. [74] mentioned pH-dependent PFK (optimum pH = 6.0) as an important regulatory enzyme in *M. maripaludis*. The activation and inhibition of PFK was found to be dependent on the presence/absence of various substrates such as ADP, AMP, Pi, cAMP, and citrate. Yu et al. [74] also reported that full activity of pyruvate kinase, another key enzyme in glycolysis, depended on Mn^{2+}. In contrast to Mn^{2+}, Fe^{2+} showed 70 % activity, and Mg^{2+} showed 20 % activity of pyruvate kinase, while Zn^{2+}, Cu^{2+}, Co^{2+}, and Ni^{2+} showed zero activity. The activity of phosphoglycerate mutase was unaffected by Mg^{2+} and AMP, and depended on the presence of reduced dithiothreitol, cysteine hydrochloride, and glutathione.

2.2.2.5 Tri-Carboxylic Acid (TCA) Cycle

TCA cycle plays an important role in generating electron carriers such as NADH and FAD for energy production [86]. Most aerobes have an oxidative TCA cycle to oxidize complex carbon molecules, such as sugars, to CO_2 and H_2O to generate energy [86]. However, most anaerobes have reductive TCA cycles to reduce CO_2 and H_2O to synthesize carbon compounds. Methanogens being anaerobes also have reductive TCA cycles. Furthermore, their TCA cycles are incomplete, as they lack several steps and enzymes [87]. *M. maripaludis* in particular lacks phosphoenolpyruvate carboxykinase, citrate synthase, aconitate, and isocitrate dehydrogenase [47, 88]. The missing steps in *M. maripaludis* are shown as dashed lines in Fig. 2.4. As shown, pyruvate is the entry metabolite in *M. maripaludis* for TCA cycle. In the absence of phosphenolpyruvate carboxylase (PPC), *M. maripaludis* converts pyruvate to oxaloacetate via pyruvate carboxylase (PYC). Oxaloacetate is then reduced to 2-oxoglutarate via a series of intermediates (Malate, Fumarate, Succinate, Succinyl CoA) in the TCA cycle. Hendrickson et al. [22] sequenced the genome of *M. maripaludis* and noted that 2-oxoglutarate oxidoreductase, the last enzyme in the TCA cycle has four subunits (MMP0003, MMP1315, MMP1316, and MMP1687) that are not contiguous. This is in contrast to PORs that are also oxidoreductases, but have contiguous subunits (MMP1502-MMP1507).

Regulation of TCA cycle in *M. maripaludis* in particular, and *Archaea* in general, is poorly understood. However, 2-oxoglutarate plays an important role in nitrogen regulation [89]. In *M. maripaludis*, NrpR protein represses N_2-fixation in ammonia-rich conditions by binding to the *nif* promoters [90]. In the absence of ammonia, 2-oxoglutarate is unable to synthesize glutamate, hence its level increases. High levels of 2-oxoglutarate acts as the inducer and prevents binding of NrpR to *nif* promoters, resulting in activation of N_2-fixation and glutamine synthetase to bring down 2-oxoglutarate levels.

The TCA regulation in *Methanobacterium thermoautotrophicum,* another methanogen with an incomplete reductive cycle similar to that in *M. maripaludis*, can shed some light on the regulation. As reported by Eyzaguirre et al. [58] for *M. thermoautotrophicum, M. maripaludis* may also exhibit unidirectional synthesis of phosphenolpyruvate via phosphenolpyruvate synthetase (*pps*A). The activity of this enzyme may be inhibited by AMP, ADP, and 2-oxoglutarate. Similarly, PYC, the ATP-dependent enzyme responsible for pyruvate carboxylation in *M. maripaludis*, may exhibit anabolic function as reported by Mukhopadhyay et al. [58] in *M. thermoautotrophicum.* Furthermore, its activity may depend on biotin, ATP, Mg^{2+} (or Mn^{2+}, Co^{2+}), pyruvate, and bicarbonates, and it may be inhibited by ADP and 2-oxoglutarate.

2.2.2.6 Pentose Phosphate Pathway (PPP)

PPP is essential for the syntheses of nucleotides and nucleic acids in *M. maripaludis*. Glyceraldehyde-3-phosphate and fructose-6-phosphate synthesized during glycolysis/gluconeogenesis form the feeds to PPP and produce xylulose-5-phosphate and erythrose-4-phosphate (E4P) via transketolase (TKL) in the first step. Yu et al. [68] proposed a non-oxidative PPP (NOPPP) in *M. maripaludis* (Fig. 2.4). They suggested the presence of this pathway based on zero activities of oxidative enzymes [glucose-6-phosphate dehydrogenase and 6-phosphogluconate dehydrogenase] and high activities of non-oxidative enzymes [transketolase (MMP1113, MMP1115), transaldolase (MMP1308), ribose-5-phosphate 3-epimerase (MMP1114), and ribulose-5-phosphate isomerase (MMP1189)] [22, 74]. Tumbula et al. [91] supported this observation by ruling out oxidative PPP based on the labelling patterns of riboses after supplementing the medium with 2-^{13}C acetate. They argued that E4P cannot be the precursor for aromatic amino acids (AroAAs), if NOPPP is its only route. Therefore, they conjectured an alternative route (carboxylation of a triose such as dihydroxyacetone phosphate) for E4P. Porat et al. [92] on the other hand showed that E4P is not a precursor for AroAAs in *M. maripaludis*. They proposed two alternative routes for the syntheses of AroAAs based on the presence of dehydroquinate dehydratase. The details of these routes are provided in the amino acid metabolism. NOPPP is mainly regulated by substrate availability [93, 94]. However, no such regulation has yet been demonstrated in *M. maripaludis*.

2.2.2.7 Nitrogen Metabolism

M. maripaludis is capable of utilizing three nitrogen sources: ammonia, alanine, and free nitrogen with ammonia being the most preferred source for growth [72, 95].

Ammonia assimilation occurs in *M. maripaludis* via glutamine synthetase (encoded by *gln*A) which synthesizes glutamine from glutamate and ammonia [96]. Glutamine then serves as the precursor for protein synthesis. Cohen-Kupiec et al. [96] observed that *gln*A mutants are unable to grow even in the presence of exogenous glutamine and alanine indicating the essentiality of *gln*A and absence of glutamine transporters. As discussed before, alanine uptake occurs in *M. maripaludis* via alanine racemase and alanine permease [72]. Moore et al. [72] confirmed that alanine converts to pyruvate and ammonia by alanine dehydrogenase.

Free N_2 fixation in methanogens including *M. maripaludis* has been well established and extensively reviewed in the literature [97, 98]. A comparison of four N_2-fixing hydrogenotrophic methanococci (*M. formicicus, M. maripaludis, M. aeolicus,* and *M. thermolithotrophicus*) is given in Table 2.3 [95, 99–101]. Blank et al. [102] studied N_2 fixation in wild-type *M. maripaludis* and its four mutants using transposon insertion mutagenesis. Kessler et al. [103] characterized the *nif* gene cluster in *M. maripaludis* based on sequence analysis. Six *nif* genes (*nif*H, D, K, E, N, and X) and two homologues of bacterial nitrogen sensor-regulator *gln*B (*i* and *ii*) lie between *nifH* and *nifD* in a single operon in *M. maripaludis* (Fig. 2.5a). Although the conserved order of *nif* genes resembles that in *Bacteria*, the presence of single operons and two homologues between *nif* genes is unique to *Archaea.*

As shown in Fig. 2.5b, N_2 fixation is effected by multiprotein nitrogenase complex comprising an Fe protein and a MoFe protein [105]. In the presence of N_2, oxidized Fe protein reduces by taking electrons from reduced ferredoxin. Reduced Fe oxidizes in the presence of ATP and reduces MoFe protein. MoFe protein donates the electrons to N_2 and reduces it to ammonia in three successive steps: nitrogen to diamine to hydrazine to two ammonia molecules and one H_2. These reductive steps require electrons from reduced ferredoxins, and their relatively high energy demand makes N_2 fixation unfavorable in *M. maripaludis*. Therefore, cells are less likely to activate this fixation, when ammonia or alanine is available [73, 106].

Regulation

Cohen-Kupiec et al. [96] hypothesized that both *nif* and *gln*A are regulated by the same nucleotide binding sequences (Fig. 2.5c) residing in the *nif* promoter region of *M. maripaludis*. Lie et al. [107] confirmed this by isolating NrpR protein that represses both N_2 fixation and *gln*A expression by binding to the aforementioned nitrogen operator sequences (nifOR). While NrpR represses *nif* transcription fully in the presence of ammonia, it represses partially in the presence of alanine, and depresses fully in the presence of free N_2. As discussed before, NrpR in turn is regulated by 2-oxoglutarate levels in the TCA cycle [89]. As shown in Fig. 2.5c, the binding of NrpR to nifOR weakens during nitrogen deficiency, allowing 2-oxoglutarate to induce *nif* transcription. Experiments have demonstrated that cell

Table 2.3 A comparison on characteristics of the N_2-fixing hydrogenotrophs of the order Methanococcales. Modified from [25]

Property	*Methanotorris formicicus*	*Methanococcus maripaludis*	*Methanococcus aeolicus*	*Methanothermococcus thermolithotrophicus*
Type strain	Mc-S-70	JJ	Nankai-3	SN1
Cell diameter (mm)	0.8–1.5	0.9–1.3	1.5–2.0	1.5
Substrates for methanogenesis	H_2 + CO_2, formate	H_2 + CO_2, formate	H_2 + CO_2, formate	H_2 + CO_2, formate
Autotrophy	+	+	+	+
Yeast extract stimulates growth	–	+	–	–
Selenium simulates growth	–	+	+	nd
Nitrogen source	NH_3, N_2, NO_3	NH_3, N_2, alanine	NH_3, N_2	NH_3, N_2, NO_3^-
Sulfur source	S^{2-}	S^{2-}, S^0	S^{2-}, S^0	S^{2-}, S^0, $S_2O_3^{2-}$, SO_3^{2-}, SO_4^{2-}
Temperature range (°C)	55–83	<20–45	<20–55	17–70
Temperature optimum (°C)	75	35–40	46	60–65
pH range	6.0–8.5	6.5–8.0	5.5–7.5	4.9–9.8
pH optimum	6.7	6.8–7.2	7	5.1–7.5
NaCl range (%, w/v)	0.4–6.0	0.3–5	0.3–6	0.6–9.4
NaCl optimum (%, w/v)	2.4	0.6–2	1–2	2–4
Genome size (Mb)	1.82	1.66	1.57	1.69
GC content (mol%)	33	33	32	34
Doubling time (hr)	0.5	2	1.3	~1
Source	Deep-sea black smoker chimney	Salt marsh sediments	Marine sediments	Coastal geothermally heated sea sediments
Reference	[101]	[11]	[100]	[104]

growth with alanine was only marginally lower than that with ammonia, while significantly reduced with free nitrogen [73].

glnB proteins play an important role in nitrogen sensing and regulation in *M. maripaludis*. *gln*B+ strain lost nitrogenase activity within an hour of ammonia addition [108], while *gln*B mutant did not, indicating that these proteins function post-transcriptionally [106]. Kessler et al. [95] also reported the molybdenum dependency of N_2 fixation.

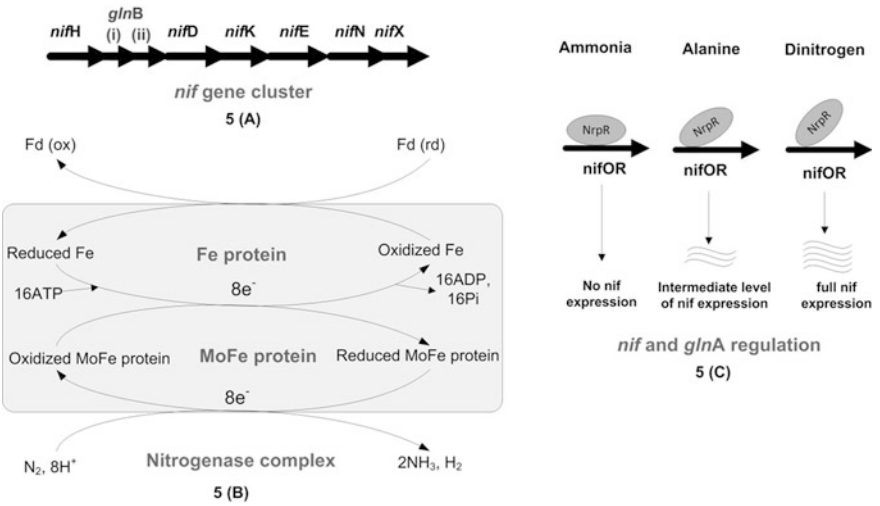

Fig. 2.5 Nitrogen fixation pathway. **a** The *nif* operon in *M. maripaludis*. **b** Nitrogenase complex. **c** Differential binding of *nif* and *gln*A regulation under different nitrogen substrates/nitrogen limiting conditions. Where, nifOR represents *nif* operators

2.2.2.8 Amino Acid Metabolism

M. maripaludis is an autotrophic organism that synthesizes all amino acids required for its growth. Sequence comparisons of archaebacterial genes suggest that amino acid biosynthetic enzymes in *Archaea* share a common ancestry with those in *Eubacteria* and *Eukarya* [109]. For instance, the enzymes of branched-chain amino acids (BCAAs) characterized in three methanococci (*M. aeolicus, M. maripaludis, M. voltae*) were found to be functionally homologous to eubacterial and eukaryotic enzymes with respect to molecular weight, optimum pH, and kinetic properties [109]. Usually, 22 amino acids are required for protein synthesis. 20 amino acids are encoded by the universal genetic codes and the remaining two (selenocysteine and pyrrolysine) are incorporated by unique mechanisms. The 20 amino acids are classified into six groups based on their structures and chemical characteristics of the R group.

In *Methanococcus* spp., the biosynthesis of BCAAs (valine, isoleucine, and leucine) was demonstrated via enzymatic assays [109]. Except *M. voltae* that requires leucine, isoleucine, and acetate for its growth, most species grow autotrophically and possess all the genes and enzymes required for growth. Four enzymes (acetohydroxy acid synthase, acetohydroxy acid isomeroreductase, dihydroxy acid dehydratase, and transaminase B) are required for the syntheses of valine and isoleucine, where 2-ketoisovalerate, an intermediate in valine biosynthesis, acts as a precursor for leucine biosynthesis [109].

The synthesis of alanine occurs from pyruvate via alanine dehydrogenase [72]. Alanine can also serves as the sole nitrogen source during growth [73].

Usually, glycine is synthesized from L-serine via serine hydroxymethyltransferases. *M. thermoautotrophicus* showed the presence of serine hydroxymethyltransferases in the genome [110], but no homologue for this enzyme is present in *M. maripaludis*. Further studies are required to discover the glycine biosynthesis route in methanococci.

The established route of proline biosynthesis involves glutamic acid to proline conversion, but three enzymes of this pathway are absent in most *Archaea* [111]. Graupner et al. [22] demonstrated the synthesis of proline in *M. jannaschii* from cyclization of ornithine via ornithine cyclodeaminase, while no such enzyme has been characterized in *M. maripaludis*, which suggests a possibility of alternate routes.

The biosynthesis of AroAAs (phenylalanine, tyrosine, and tryptophan) is well understood in methanococci. Chorismate acts as the branch point for phenylalanine, tyrosine, and tryptophan synthesis. Unlike *Bacteria*, E4P is not a precursor for chorismate in *M. maripaludis* and an alternate route has been proposed based on the presence of dehydroquinate dehydratase [92]. In this pathway, chorismate is synthesized from 3-dehydroquinate (DHQ) via shikimate pathway. For DHQ synthesis, *M. maripaludis* uses 6-deoxy-5-ketofructose 1-phosphate (DKFP), synthesized after the condensation of methylglyoxal and fructose-1,6-bisphosphate, and L-aspartate-semialdehyde to form 2-amino-3,7-dideoxy-D-threo-hept-6-ulosonate (ADTH), which cyclizes to DHQ [112]. DHQ is not only the precursor for chorismate synthesis, but also acts as a precursor for p-aminobenzoic acid (PABA) synthesis. PABA is an intermediate in *M. maripaludis* during the synthesis of tetrahydromethanopterin, one of the cofactors. [112]. Two biosynthetic routes for the production of AroAAs from chorismate in *M. maripaludis* were proposed previously [92]. To confirm the presence of de novo pathway, deletion strains of MMP1394 encoding 3-dehydroquinate dehydratase were constructed and the mutants were auxotrophic for all three AroAAs and no DHQ activity was detected. To evaluate aryl acid dependent pathway, acids were supplemented to the medium to fulfill the requirements of AroAAs in *M. maripaludis*.

Whole genome sequencing studies on *M. maripaludis* provide information on enzymes/ORFs participating in amino acid biosynthesis. The results indicate that all genes required for the biosynthesis of histidine (*his*A, B, C, D, E, F, G, H, I) were present in *M. maripaludis* except *his*J that encodes for histidinol phosphate phosphatase [22]. Fondi et al. [113] further evaluated the biosynthesis of histidine in *Archaea* and suggested that *his* operon might have been assembled multiple times during evolution because *his* genes scattered throughout the genome. In addition, they showed the existence of *his*N gene for histidinol phosphate phosphatase and *his*B gene for imidazoleglycerol-phosphate dehydratase catalyzing sixth and eight steps of the histidine biosynthesis, which suggests that different molecular mechanisms in *M. maripaludis* may drive piece-wise operon formation for histidine biosynthesis.

Lysine biosynthesis in *M. maripaludis* occurs via diaminopimelate aminotransferase (DapL) pathway [114]. A mutant of *dap*L homolog in *M. maripaludis* resulted in lysine auxotrophy and suggested that *dap*L is essential for lysine biosynthesis.

The specific activities of arginine biosynthetic enzymes in methanogenic *Archaea* was reported by Meile et al. [115]. They also mentioned that although biosynthesis sequences were similar in all microbes, differences existed in reaction steps and regulations of this pathway. Arginine biosynthesis and associated genes/enzymes are well characterized in *M. maripaludis* [22]. The functional conservation of argininosuccinate lyase encoded by *arg*H (catalyze final step in arginine biosynthesis pathway) between *M. maripaludis* and the corresponding *Bacteria* and *Eukarya* was demonstrated [116].

Glutamate is synthesized in *M. maripaludis* via glutamate synthase [96]. Aspartate is synthesized by aspartate aminotransferase and asparagine glutamine-hydrolyzing asparagine synthase (*asnB*). ^{14}C labeling studies on *M. barkeri* and other *Archaea* showed that synthesis of alanine, aspartate, and glutamate occurred from pyruvate, oxaloacetate, and α-ketoglutarate respectively [117].

^{13}C labeling of serine was consistent with its synthesis from pyruvate via 3-phosphoglycerate. *M. maripaludis* contained *serA* and *serB*, but not a homolog for *serC* [22]. Similarly, a homolog for glycine hydroxymethyltransferase encoded by *glyA* is absent for synthesis of glycine from serine.

Stathopoulos et al. [118] challenged the notion that all 20 aminoacyl-tRNA synthetases are essential for the viability of a cell. They knocked out *cysS* gene encoding cysteinyl-tRNA synthetase (CysRS) from *M. maripaludis* and showed that pure *M. maripaludis* prolyl-tRNA synthetase (ProRS) can form cysteinyl-tRNA (Cys-tRNA), implying dual-specificity of enzyme for the loss of CysRS. The report by Stathopoulos et al. [118] was incorrect. While ProRS has low levels of CysRS activity, it is not physiologically significant. Sauerwald et al. [119] demonstrated this by observing that CysRS mutants could not incorporate exogenous cysteine into cellular protein. The tRNA-dependent cysteine biosynthesis pathway in *M. maripaludis* is well established and occurs in two steps: First, O-phosphoseryl-tRNA ligase (SepRS) aminoacylates uncharged Cys-tRNA with 3-phospho-L-serine (Sep) to form O-phosphoseryl-tRNA (Sep-tRNA). Second, Sep-tRNA:Cys-tRNA synthase (SepCysS) transforms Sep to cysteine [119]. Zhang et al. [120] showed that these two enzymes (SepRS and SepCysS) form a stable binary complex and promote the conversion of intermediate Sep-tRNA to cysteinyl-tRNA by sequestering the binding of the intermediate to elongation factor EF-1α or infiltrating into the ribosome.

Methionine biosynthesis in *M. maripaludis* is unclear. Only one ORF, MMP0401, has been identified in *M. maripaludis* via sequencing studies [22] which indicates the synthesis of methionine from homocysteine. The presence of cystathionine β-lyase (*metC*) in *M. maripaludis* indicates the possibility that *M. maripaludis* synthesizes homocysteine (the intermediate precursor of methionine) either by transsulfuration route with cystathione or via direct sulfhydrylation of O-acetylhomoserine [114]. Such gaps in the literature need further investigation of existing routes or novel biosynthetic routes.

Selenocysteine is the selenium containing 21st amino acid that is co-translationally incorporated into proteins, which are known as selenoproteins. The amino acid is coded by UGA, which is normally a termination codon during protein synthesis. Only 20 % of *Bacteria* and 10 % of *Archaea* (*Methanococcus, Methanocaldococcus,* and *Methanopyrus* spp.) were found to have machinery for Sec insertion. In *Eukarya*, sec insertion machinery is common in lower organisms, such as green algae and moulds [121]. Yuan et al. [122] proposed $tRNA^{Sec}$-dependent conversion of *O*-phosphoserine (Sep) to selenocysteine in *Eukarya* and *Archaea*. Genetic analysis of selenocysteine biosynthesis in *M. maripaludis* is reported in the literature [123–125].

Pyrrolysine is the 22nd natural amino acid and is a lysine derivative encoded by UAG. It is used by methanogenic *Archaea* and was discovered in 2002 at the active site of methylamine methyltransferase in *M. barkeri* [126]. *pyl*T gene, whose tRNA product has CUA anticodon, translates to UAG codon as pyrrolysine in some methanogens. The presence of pyrrolysine in *M. maripaludis* is not established, although it has been mentioned in non-pyl-utilizing *Archaea* in the literature [127].

2.2.2.9 Nucleotide Biosynthesis

Nucleotides include purines (adenine and guanine) and pyrimidines (thymine and cytosine). In RNA, adenine base pairs with uracil instead of thymine. The purine and pyrimidine biosynthesis in *M. maripaludis* is very well understood and sequencing study showed the presence of related genes involved in biosynthesis of purines and pyrimidines [22]. 5-phospho-α-D-ribose 1-diphosphate (PRPP) is synthesized from ribose-5-phosphate with the help of PRPP synthetase and combines with glutamine to form 5-phosphoribosylamine, which goes through a series of reactions and forms inosinic acid (IMP). IMP acts as the branch point for adenosine monophosphate (AMP) and guanosine monophosphate (GMP) biosynthesis in the pathway. AMP is synthesized from IMP and adenylosuccinate and converted to other purine nucleotides, such as adenosine diphosphate (ADP) and adenosine triphosphate (ATP). Similarly, xanthosine 5′-monophosphate (XMP) is synthesized from IMP with NAD^+ or $NADP^+$ as acceptors, which is subsequently converted to other purine nucleotides, such as GMP, guanosine diphosphate (GDP), and guanosine triphosphate (GTP). Pyrimidine biosynthesis converts bicarbonate, L-glutamine, ororate, and PRPP, to uridine monophosphate (UMP) for further conversion to uridine triphosphate (UTP) and cytidine triphosphate (CTP) for participation in nucleic acid biosynthesis.

2.2.3 Molecular Biology Tools

M. maripaludis is a well-studied model organism. The 1.6 Mb long *M. maripaludis* genome covers 1722 protein-coding genes and is exceptional in the presence of

unique hydrogenases [53]. Genetic maps are available to help identify the functions of ORFs across methanogens [22, 128, 129]. A set of genetic tools is available for the manipulation of its fully sequenced genome via selectable markers [130], shuttle vectors [131], integrative plasmids and gene replacements [132], and markerless mutagenesis [72].

2.2.3.1 Selectable Markers

It is very difficult to identify antibiotic resistant markers in methanogens due to the absence of peptidoglycans in their cell walls and different ribosome structures. Puromycin resistance in *M. maripaludis* was reported by transforming it with pKAS100 and pKAS102 plasmids [131]. To complement the method of vector transformation, an optimized polyethylene glycol (PEG) method of transformation was used [133]. With the PEG method, transformation frequency increased four to five orders of magnitude (2×10^5 transformants/μg of insertion vector) than with the natural transformation method. Methylation of plasmid with PstI methylase increased the transformation efficiency by at-least four-folds, approaching those obtained for *Escherichia coli* (*E. coli*) and addition of divalent cations inhibit the transformation [133]. Neomycin is the second selectable marker reported previously [130]. Aminoglycoside phosphotransferase genes APH3'I and APH3'II cloned under the control of *Methanococcus voltae* methyl reductase promoter can act as a neomycin resistance marker in *M. maripaludis* [130]. The MIC of neomycin to completely inhibit 5 ml culture of *M. maripaludis* growth was determined to be 1000 μg/ml. Concentration between 500 and 1000 μg/ml delayed its growth. Kanamycin and geneticin are non-inhibitory for *M. maripaludis* cells [134, 135].

2.2.3.2 Shuttle Vectors

Shuttle vector pDLT44 was constructed for *M. maripaludis* JJ using plasmid pURB500 (from *M. maripaludis* C5) and pMEB.2, (*E. coli* vector containing a methanococcal puromycin resistance marker) [136]. The shuttle vector was found to be stable in *E. coli* under ampicillin selection. This was the first report of a plasmid replicated independently in a methanogen and can be manipulated in *E. coli*. Although pURB500 was originated from a methanococcus, it did not replicate in *M. voltae*. In another study, development of expression shuttle and integrative vector for *M. maripaludis* has been reported to use histone promoter (P_{hmvA}) and multiple cloning sites from *M. voltae* for overexpression of *ilvBN* and *ppsA* [137]. These expression vectors may be useful for studying the physiology and biochemistry of *M. maripaludis.* The transformation efficiency may vary from one strain to another [138]. *M. maripaludis* S2 did not show the same high level of transformation as reported for *M. maripaludis* JJ. Therefore, transformation rates were improved by manipulating the shuttle vector. Walters et al. [138] showed that a significantly smaller shuttle vector pAW42 was sufficient to maintain in

M. maripaludis S2 and provides 7000-fold increase in transformation efficiency for pURB500-based vectors.

2.2.3.3 Integrative Plasmid and Gene Replacement

Integration vector pIJA03-cysS for *M. maripaludis* was constructed to determine the essentiality of cysS gene coding for cysteinyl-tRNA synthetase [118]. In the same study, *cysS* gene replacement was carried out by constructing a pBD1 vector by using the plasmid pPH21310. Several other mutants of *M. maripaludis* have been constructed using the technique of integrative plasmids and gene replacement. For example, acetate auxotrophs were isolated by random insertional mutagenesis by transforming the wild type *M. maripaludis* with pWDK104 [139]. Using transposon insertion mutagenesis, mutations were made in and around *nif*H gene and nitrogen fixing abilities of four transformants were studied. In another study of transposon insertion mutagenesis, an 8-kb region corresponding to the *nif* gene cluster was confirmed for N_2-fixation [103].

2.2.3.4 Markerless Mutagenesis

To demonstrate the role of genes that show unusual ability to use D-alanine or L-alanine, markerless mutagenesis in *M. maripaludis* was demonstrated [72]. They used a negative selection based system that used *hpt* and *upt* gene encoding hypoxanthine phosphoribosyltranferase and uracil phosphoribosyltransferase present in *M. maripaludis*. Hpt system was used to produce markerless in-frame deletion mutation in three genes (*ald*, *alr,* and *agcS*) coding for alanine dehydrogenase, alanine racemase, and alanine permease. *Hpt* was used together with *upt* to restore the function of wild type *ald* [72].

2.2.4 Potential Applications

Methanogens play a key role in the global carbon cycle by reducing atmospheric CO_2 [55]. The unique characteristics of *M. maripaludis* in particular, and methanogens in general, offer the potential for several industrial and environmental applications such as wastewater treatment, carbon capture and utilization, and methane from renewable energy via electro-methanogenesis.

2.2.4.1 Wastewater Treatment

Tabatabaei et al. [140] has summarized the characteristics of methanogenic populations used in wastewater treatment. The production of biogas from waste relies on

a symbiotic relationship between syntrophic bacteria (*Syntrophomas*, *Synthrophospora*, and *Syntrophobacter*) and methanogens [141]. Syntrophic acetogenic bacteria convert acid-phase products into acetates and H_2, which are then utilized by methanogenic archaea. If accumulated H_2 is not used by the methanogens, then acetogenesis during anaerobic degradation cannot occur [142]. That is where *M. maripaludis* has a potential to play a key role in maintaining a low partial pressure of H_2 by consuming it rapidly.

In a biogas plant, the actual proportions of acetoclastic and hydrogenotrophic methanogens may depend on the conditions [143]. It has been frequently seen that hydrogenotrophic methanogens dominate at high temperatures (>50 °C). This is primarily because hydrogenotrophic methanogens can degrade acetate with syntrophic bacteria more efficiently at high temperatures than acetoclastic methanogens.

New evidence also suggests that direct electron transfer through nanowires/electrically conductive pili may also be present between bacteria and these methanogens during anaerobic digestion [144–146].

2.2.4.2 Carbon Capture and Conversion

Flue gas exhausts from power plants typically have 3–15 % CO_2 in majority N_2. These CO_2 emissions are the major contributors to global warming and climate change [147]. Reducing CO_2 emissions by capturing and sequestering or converting the CO_2 to fuels and value-added chemicals is an area of active research around the globe. *M. maripaludis* with its ability to uptake CO_2 in the presence of N_2 offers an attractive route to capture and convert CO_2 simultaneously from flue gas emissions to useful fuels such as methane and methanol [108]. In combination with other methanogens such as *M. aeolicus* [100], *M. thermolithotrophicus* [99], *M. formicicus* [101], it is possible to utilize microbe consortia to reduce carbon emissions from power and chemical plants on a large scale, and alleviate environmental and global warming concerns.

2.2.4.3 Methane from Renewable Energy

The main challenge in using methanogens for large-scale biomethane production is the need for H_2. The only viable source for this H_2 is renewable energy sources such as solar, tidal, and wind. The transient nature of these resources raises the need for temporary storage of energy in a stable chemical form. One possibility is to convert surplus renewable electricity directly into methane via electrochemical methanogenesis. This is already established for a mixed-culture of methanogenic microbes comprising *Methanobacterium* sp. (>93 %) and *Methanobrevibacter* ($\sim$5 %) [148]. Recently, Lohner et al. [45] has also demonstrated the uptake of electrons by a hydrogenase-mutant of *M. maripaludis*. However, methane

production relative to the wild type was only 1/10 as discussed before. These studies show that methanogens can be used as biocatalysts for electrochemical conversion of CO_2.

Another alternative is to use surplus renewable electricity for non-microbial electrochemical conversion of CO_2 to formate [149] and then convert formate into methane using *M. maripaludis*.

2.2.4.4 Hydrogen Production

H_2 production by various aerobic and anaerobic microbes has been reported in the literature [150, 151]. The highest rates reported for genetically engineered *E. coli* strains ranges from 1.7 μmol/mg DCW.min to 4.2 μmol/mg DCW.min [152] from formate. The methylotrophs *Methylomonas albus* and *Methylosinus trichosporium* showed H_2 production rates of 1.6 and 0.4 nmol/mgDCW.min respectively from formate [153]. However, the rates reported by wild-type formate-grown *M. maripaludis* S2 are much higher i.e. 1.4 μmol/mg DCW.min [42].

2.2.4.5 Other Applications

Several applications remain unexplored for *M. maripaludis* in spite of its unique advantages such as rapid growth, ease of genetic manipulation, fully sequenced genome, and available genome-scale model. For instance, *M. maripaludis* can potentially be used to produce high value-added pharmaceuticals, vitamins, amino acids, corrinoids, and terpenoids, and these possibilities require further research. An excellent example is geraniol, a useful flavoring agent [154], which can be produced by genetically engineered *M. maripaludis.* Biotransformation of 2,4,5-trinitrotoluene, a priority pollutant, and metabolic conversion of 5-methylfurfurals and 2-methylfufurals (formed during the concentration of aqueous wastes in paper and pulp industries) to furfurals have been studied with *Methanococcus spp.* (strain B) [155, 156]. Such biotransformations can also be explored with *M. maripaludis*. Other possible applications could be the production of liquid biofuels such as methanol, butanol, etc.

2.3 Genome-Scale Engineering

The concept of metabolic pathway manipulation for purpose of using microorganisms with desirable properties is quite old. The methods for identifying superior strains rely heavily on the use of chemical mutagens and creative selection techniques [157]. Despite its success, the genetic and metabolic profiles of these mutant strains are poorly characterized. Recombinant DNA technology (rDNA) introduced a new dimension to the work and genetic modification of enzymatic reactions

allowed precise modifications in metabolic pathways [158]. After the feasibility of rDNA technology, various terms were coined to represent the potential applications of this technology, namely molecular breeding [159], in vitro evolution [158], pathway engineering [160], cellular engineering [160], and metabolic engineering [161]. All convey similar meaning and defined as "directed improvement of product formation or cellular properties through the modification of specific biochemical reaction(s)". Instead of ad hoc target selection process, a rational process to identify the most promising target for metabolic manipulation would save experimental efforts. Therefore, we are witnessing a paradigm shift away from individual enzymatic reactions.

Metabolic engineering focuses on integrated metabolic pathways instead of individual reactions and shifted our attention to the complete biochemical reaction networks instead of its constituent parts. It examines issues of pathway synthesis, thermodynamic feasibility, and pathway flux and its control [161]. Observations about the behavior of overall system provide the best guide for rational analysis. Metabolic engineering needs to be complemented with the appropriate measurements to achieve maximum results. Specific areas of industrial production where metabolic engineering can make significant impact are the production of petroleum-derived thermoplastics by fermentation, biologically active agents such as polyketides, amino acid production, vitamins, organic acids, lipid, oil and a list of other product classes [162–165]. In addition to manufacturing, it can have significant impact on medical field such as identifying targets for drug development [166].

2.3.1 *Systems Biology Models: Kinetic Versus Stoichiometric*

In silico mathematical models can be classified as either kinetic or stoichiometric. Kinetic models describe the dynamic behavior of a cell. They involve temporal ordinary differential equations describing the concentration profiles of metabolites based on rate laws postulated for key metabolic reactions. While kinetic models are simple to construct, they face serious limitations. Firstly, they involve numerous model parameters such as rate constants, which are difficult to measure or even estimate reliably. In most cases, the dynamic data on metabolite concentration profiles is insufficient to fit reliable values for these parameters. Secondly, kinetic models become highly unwieldy and complex, when applied at the genome level. Therefore, most kinetic models are for either subsystems or simplified through appropriate assumptions. Several kinetic models have been developed to understand the effects of metabolic perturbations in subsystems. Some examples are glycolysis in plant tubers [167], mitochondrial respirations [168], calvin cycle [169], microbial growth kinetics during fermentation [170, 171], anaerobic glycolysis of yeast *Saccharomyces cerevisiae* [172], glycogenolysis in mammalian FT skeletal muscle [173], and salicylamide (SAM) metabolism in the perfused rat liver [174] etc.

Stoichiometric models, on the other hand, are inherently non-dynamic and rely on reaction stoichiometry alone. Their main assumption is that the internal metabolites are at pseudo-equilibrium. When such metabolic models are developed based on genome sequence and Gene-Protein-Reaction (GPR) associations, they are called genome-scale metabolic models or constraint-based flux models. Since the first genome-scale metabolic model was constructed for *Haemophilus influenzae* [175], many such models have been constructed for a variety of organisms and experimentally validated. The success rate of in silico predictions is typically about 70–90 % depending on the types of organism and prediction [176]. The constraints in the model is the underlying main concept that separate feasible and infeasible metabolic behavior and are much easier to identify than kinetic parameters, making large scale model building possible [177]. Three main constraints that need to be satisfied by a model are: Firstly, *Physicochemical constraints* defined by conservation laws of mass and energy, dependency of reaction rates on metabolite concentrations, and negative free energy change for spontaneous reactions. Secondly, *Environmental constraints* such as availability of nutrients or electron acceptors etc. imposed as result of specific conditions. Lastly, *Regulatory constraints* i.e. up-regulated/down-regulated gene expressions as the cell undergo environmental perturbations.

In this thesis, we develop a genome-scale metabolic model based on stoichiometric constraint-based approach to predict the behavior of complex biological interactions via FBA. When FBA is applied for the determination of metabolic pathway fluxes, the approach is renamed as Metabolic Flux Analysis (MFA).

2.3.1.1 Constraints-Based Modeling

Drafting a metabolic network

It is a process during which various components of the cellular metabolic pathways e.g. associated genes, proteins, reactions and metabolites are identified through various online databases (KEGG, BioCyc, etc.), genome-wide annotations, published literature, etc. and categorized to form a network [178]. Online resources that are helpful for drafting a metabolic network are extensively reviewed in literature [179]. A number of automated systems to help us in genomics data analysis are also available such as GeneQuiz, Pedant, Magpie, etc. [180]. The reconstructed network or a draft model generated from the well-annotated reactions acts as the starting point of genome-scale modeling. The draft models are manually refined by incorporating genetic, biochemical and functional information before converting into a mathematical model.

Metabolic Flux Analysis (MFA)

MFA is a powerful approach for the determination of metabolic pathway fluxes, whereby intracellular fluxes are calculated using stoichiometric matrix of the reactions and applying mass balance on intracellular metabolites [179]. The metabolic

network is represented in the form of a stoichiometric matrix S, where row represent is the number of metabolites and n is the number of reactions/fluxes occurring in a organism. S_{ij}, the element of a stoichiometric matrix S, corresponds to metabolite i and reaction j. The static models assume a pseudo steady state and transient mass balance represented as follows:

$$\frac{dX}{dt} = S.v - b = 0 \tag{2.1}$$

Here S is the $i \times j$ stoichiometric matrix, v is the vector of n metabolic reactions and b is the vector of net known metabolite uptake by the cell.

Typically Eq. 2.1 represents an underdetermined system ($j > i$) and hence an infinite solution exists with a number of cell phenotypes. To obtain a particular solution, a linear optimization is formulated in which one can find a flux distribution that minimizes or maximizes a particular objective Z. A number of different objective functions have been reviewed in literature such as minimize energy, minimize nutrient uptake, minimize redox production, minimize the Euclidean norm and maximize metabolite production [181, 182]. The most commonly used objective function is maximizing biomass [183]. The mathematical formulation is

$$\text{Maximize } Z = \sum_{j=1}^{j} c_j v_j \text{ subject to } S.v = b \tag{2.2}$$

where, Z is the cellular objective that is represented as a weighted sum of metabolite fluxes $v_j (j = 1, 2, \ldots, j)$ with weights c_j.

The final metabolic flux map shows the estimation of steady-state rate (flux) for all the essential reactions contributing to our objective function. A metabolic flux map contains useful information about the contribution of various pathways towards substrate utilization and product formation. Genetic and environmental perturbations in the system help us to compare specific pathways and reactions in different situations. In addition to quantitative pathway fluxes, MFA provides insights about cell physiological characteristics. Some of them are listed here:

- Identification of branch point control (nodal rigidity)
- Identification of alternate pathways: e.g. transhydrogenase activity in *C. glutamicum* [184]
- Calculation of non-measured extracellular fluxes
- Calculation of maximum theoretical yields.

2.3.1.2 Simulation Tools

Theoretically, MFA is well understood and simple however it is not easy for researchers to manually implement MFA without computational coding and basic

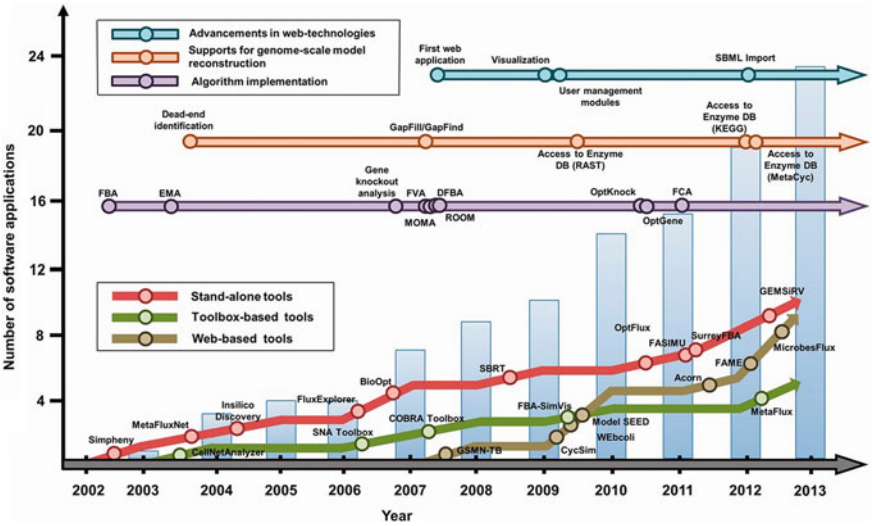

Fig. 2.6 Timeline of FBA software tools developed over a past few years as reported by Lakshmanan et al. [185]

programming skills because of the large number of reactions and metabolites present in an organism. To quantify metabolic fluxes across the pathway, FBA tools have been developed and are freely available online [185]. These tools aid in model development and FBA. They have been divided into three major types. Stand-alone, toolbox-based, and web-based applications as shown in Fig. 2.6 [185]. Some of the most commonly used applications are Simpheny, MetaFluxNet, BioOpt, OptFlux, GEMSiRV, and COBRA Toolbox. Each of these tools is associated with some unique features and limitations.

2.3.1.3 Applications

Genome-scale models are very useful in understanding the interaction of intracellular host functions and the impact of various genetic perturbations on cell behavior. They have been successfully used for fruitful results in many applications. Some examples are (i) Enhanced metabolite production e.g. Butanol production by *Clostridium acetobutylicum* [186], L-lysine production by *Corynebacterium spp.* [187] etc. (ii) Production of new metabolites which are not secreted by microbes such as indigo production by *E. coli* [188], polyhydroxyalkanoate production by *E. coli* [189], etc. (iii) Effect of different media components on cell growth and product formation e.g. effect of various carbon and nitrogen sources on desulfurization activity of *Rhodococcus erythropolis* [190], L-tryptophan production from

sucrose in *E. coli* [191], ethanol production from starch by *Saccharomyces cerevisiae* [192], etc. (iv) Design of new/improved metabolic pathways for degradation of various chemicals e.g. degradation of mixture of xylene, toluene and benzene by *Pseudomonas putida* [193], degradation of chloro-organic compounds by *Dehalococcides spp.* [194] for bioremediation (v) Modification of cell properties to facilitate bioprocessing e.g. better growth of *E. coli* and other microbes under microaerobic conditons [195], slow growth rate and high methane flux under nitrogen gas as the sole nitrogen source [196], ammonia transport without ATP consumption in *Methylophilus methylotrophus* [197], etc. (vi) Understanding the symbiotic relationships e.g. symbiotic relationship of *Rhizobium etli* with plants [198], mutualistic interactions between methanogen *M. maripaludis* and sulfate-reducing bacteria *Desulfovibrio vulgaris* [199] etc.

2.3.2 i*MM518: A Genome-Scale Model*

In recent years, systems biology models have been widely used to understand, analyze, and quantify the extent and impact of complex biological interactions and genetic perturbations [200]. Goyal et al. [201] reported the first constraint-based genome-scale metabolic model (*i*MM518) for *M. maripaludis*. The model includes 570 reactions, 556 metabolites, and 518 genes across 52 pathways. They identified essential and non-essential genes/reactions, and compared the effectiveness of various carbon, hydrogen, and nitrogen sources. Their analyses confirmed that methane production and cell growth compete with each other for available carbon as expected, and methane flux can only be increased at the expense of growth. Sarmiento et al. [202] analyzed gene functions in *M. maripaludis* using whole-genome libraries of Tn5 transposon mutant. While they considered all genes, *i*MM518 focused only on the 30 % of ORFs involved in metabolism. It is interesting that 34 metabolic genes deemed essential for growth by Sarmiento et al. [202] were also deemed essential by *i*MM518. Goyal et al. [201] also identified the best gene combinations whose deletions would maximize methane production rate. Some of their identified targets for single and multiple gene deletions are *adk*A (MMP1031), *acd* (MMP0253), *mdh* (MMP0645), *acd* (MMP0253) and *mdh* (MMP0645), *adk*A (MMP1031) and *mdh* (MMP0645), and *acd* (MMP0253) and *cim*A (MMP1018) and *mdh* (MMP0645). The details of the reactions and enzymes are available in [201].

Using *i*MM518, Goyal et al. showed that N_2 fixation enhances MERs by 7.84 % and reduces growth rate by approx. 50 % compared to NH_3 [201]. Thus, free N_2 is better for methane production than ammonia and in reducing production of waste biomass. We confirmed the same with our ongoing experiments (unpublished). A comparison of *M. maripaludis* S2 with *M. barkeri* and *M. acetivorans* showed *M. maripaludis* to be a better methanogen for producing methane.

2.4 Microbial Electrolysis Cells (MECs)

Recent years have been a turning point for research in microbial bioelectrochemical processes, i.e. whole cell microorganisms are used to catalyze oxidation and/or reduction reactions [203]. Microbial Fuel Cells (MFCs) are one of the examples, which harness electric current from microbes [204]. Another context is MECs, a reverse of MFCs, where applied potential is used to carry out microbial metabolism and biochemical production. This process is known as microbial electrosynthesis [205]. Microbes take external electrons from electrical inputs and reduce carbon source to useful chemicals with the help of hydrogen ions produced during water splitting. Some of the examples are production of acetate from CO_2 [206], fumarate to succinate conversion [207], and increased glutamate yield from glucose fermentation [208].

Electromethanogenesis by archaeon, *Methanobacterium palustre* was demonstrated by Cheng et al. [209]. A recent study on *Sporomusa ovata* by Nevin et al. [206] showed that microbiological catalysts might be a robust alternative for converting CO_2 and water to multi-carbon extracellular compounds, when coupled with photovoltaics. They further extended the work to wider range of microorganisms including two other *Sporomusa* species, *Clostridium ljungdahlii*, *Clostridium aceticum*, and *Moorella thermoacetica* and showed production of organic acids mainly acetate [210]. Some of the major achievements towards microbial electrosynthesis are shown in Fig. 2.7. One of the means of cathodic extracellular electron transfer is through hydrogen [211]. This gas can readily be produced at cathodes and serve as driver for microbial metabolism without affecting microbial integrity. This fact along with range of products formed during metabolism driven by H_2 makes first stepping stone towards electricity driven bio-production of chemicals such as methane.

Lohner et al. [212] demonstrated electromethanogenesis i.e. H_2-independent growth via a hydrogenase-deficient strain of *M. maripaludis* However methane

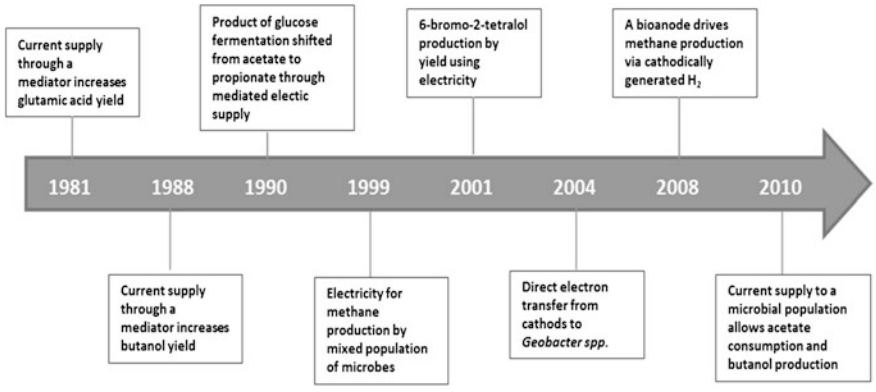

Fig. 2.7 History of major achievements towards microbial electrosynthesis [211]

production rates reduced to 1/10 of that in wild-type cells. They used two chamber (anode and cathode) borosilicate gastight chamber and a Nafion 117 proton exchange membrane separating both the chambers.

Substantial pH gradient between the anode and the cathode contribute to potential losses [213]. Membranes in two chamber setups increases ohmic resistance of the cell result in lower current production for an applied cell potential [31]. In addition, membranes are very expensive. These issues can be avoided with a membraneless reactors [214]. In this thesis, we developed a single-chamber membrane-free MEC for demonstration of electromethanogenesis by a pure culture of wild type *M. maripaludis* S2 and reported preliminary results.

References

1. Saini R, Kapoor R, Kumar R, Siddiqi TO, Kumar A (2011) CO_2 utilizing microbes–a comprehensive review. Biotechnol Adv 29:949–960
2. Wood HG, Werkman C (1940) The fixation of CO_2 by cell suspensions of *Propionibacterium pentosaceum*. Biochem J 34:7–14
3. Werkman CH, Wood HG (2009) Heterotrophic assimilation of carbon dioxide. Adv Enzymol Relat Areas Mol Biol. Part B: Mechanism of Enzyme Action, 74(227):3
4. Thauer RK (2007) A fifth pathway of carbon fixation. Science 318:1732–1733
5. Evans M, Buchanan BB, Arnon DI (1966) A new ferredoxin-dependent carbon reduction cycle in a photosynthetic bacterium. Proc Natl Acad Sci USA 55:928
6. Wood HG (1991) Life with CO or CO_2 and H_2 as a source of carbon and energy. FASEB J 5:156–163
7. Herter S, Fuchs G, Bacher A, Eisenreich W (2002) A bicyclic autotrophic CO_2 fixation pathway in *Chloroflexus aurantiacus*. J Biol Chem 277:20277–20283
8. Berg IA, Kockelkorn D, Buckel W, Fuchs G (2007) A 3-hydroxypropionate/4-hydroxybutyrate autotrophic carbon dioxide assimilation pathway in Archaea. Science 318:1782–1786
9. Huber H, Gallenberger M, Jahn U, Eylert E, Berg IA, Kockelkorn D, Eisenreich W, Fuchs G (2008) A dicarboxylate/4-hydroxybutyrate autotrophic carbon assimilation cycle in the hyperthermophilic Archaeum *Ignicoccus hospitalis*. Proc Natl Acad Sci 105:7851–7856
10. Wang B, Li Y, Wu N, Lan CQ (2008) CO_2 bio-mitigation using microalgae. Appl Microbiol Biotechnol 79:707–718
11. Jones WJ, Paynter MJB, Gupta R (1983) Characterization of *Methanococcus maripaludis sp*. nov., a new methanogen isolated from salt marsh sediment. Arch Microbiol 135:91–97
12. Keswani J, Orkand S, Premachandran U, Mandelco L, Franklin M, Whitman W (1996) Phylogeny and taxonomy of mesophilic *Methanococcus* spp. and comparison of rRNA, DNA hybridization, and phenotypic methods. Int J Syst Bacteriol 46:727–735
13. Whitman WB, Shieh J, Sohn S, Caras DS, Premachandran U (1986) Isolation and characterization of 22 mesophilic methanococci. Syst Appl Microbiol 7:235–240
14. Escalante-Semerena J, Rinehart K, Wolfe R (1984) Tetrahydromethanopterin, a carbon carrier in methanogenesis. J Biol Chem 259:9447–9455
15. Zellner G, Winter J (1987) Secondary alcohols as hydrogen donors for CO_2 reduction by methanogens. FEMS Microbiol Lett 44:323–328
16. Shieh J, Whitman WB (1988) Autotrophic acetyl coenzyme A biosynthesis in *Methanococcus maripaludis*. J Bacteriol 170:3072–3079

17. Costa KC, Yoon SH, Pan M, Burn JA, Baliga NS, Leigh JA (2013) Effects of H_2 and formate on growth yield and regulation of methanogenesis in *Methanococcus maripaludis*. J Bacteriol 195:1456–1462
18. Liu Y (2010) Methanococcales. In: Handbook of hydrocarbon and lipid microbiology. Springer, Berlin, pp 573–581
19. Copeland A, Lucas S, Lapidus A, Barry K, Glavina del Rio T, Dalin E, Tice H, Pitluck S, Chertkov O, Brettin T, Bruce D, Han C, Detter JC, Schmutz J, Larimer F, Land M, Hauser L, Kyrpides N, Mikhailova N, Sieprawska-Lupa M, Whitman WB, Richardson P (2007) Complete genome sequence of *Methanococcus maripaludis*. Unpublished: US DOE Joint Genome Institute
20. Mori K, Tsurumaru H, Harayama S (2010) Iron corrosion activity of anaerobic hydrogen-consuming microorganisms isolated from oil facilities. J Biosci Bioeng 110:426–430
21. Wang X, Greenfield P, Li D, Hendry P, Volk H, Sutherland TD (2011) Complete genome sequence of a nonculturable *Methanococcus maripaludis* strain extracted in a metagenomic survey of petroleum reservoir fluids. J Bacteriol 193:5595
22. Hendrickson EL, Kaul R, Zhou Y, Bovee D, Chapman P, Chung J, Conway de Macario E, Dodsworth JA, Gillett W, Graham DE et al (2004) Complete genome sequence of the genetically tractable hydrogenotrophic methanogen *Methanococcus maripaludis*. J Bacteriol 186:6956–6969
23. Liu Y, Whitman WB (2008) Metabolic, phylogenetic, and ecological diversity of the methanogenic archaea. Ann N Y Acad Sci 1125:171–189
24. Ferry JG (1994) Bioenergetics of methanogenesis. In: Ferry JG (ed) Methanogenesis—ecology, physiology, biochemistry & genetics. Chapman and Hall, New York, p 536
25. Whitman W, Jeanthon C (2006) Methanococcales. In The prokaryotes. Springer, New York, pp 257–273
26. Koga Y, Morii H, Akagawa-Matsushita M, OHGA M (1998) Correlation of polar lipid composition with 16S rRNA phylogeny in methanogens. Further analysis of lipid component parts. Biosci Biotechnol Biochem 62:230–236
27. Dworkin M, Falkow S (2006) The prokaryotes, vol 3. Archaea. bacteria: firmicutes, actinomycetes. Springer, Berlin
28. Akca E, Claus H, Schultz N, Karbach G, Schlott B, Debaerdemaeker T, Declercq JP, Konig H (2002) Genes and derived amino acid sequences of S-layer proteins from mesophilic, thermophilic, and extremely thermophilic methanococci. Extremophiles 6:351–358
29. Jones W, Donnelly M, Wolfe R (1985) Evidence of a common pathway of carbon dioxide reduction to methane in methanogens. J Bacteriol 163:126–131
30. Hedrick DB, Guckert J, White D (1991) Archaebacterial ether lipid diversity analyzed by supercritical fluid chromatography: integration with a bacterial lipid protocol. J Lipid Res 32:659–666
31. Jarrell KF, Koval SF (1989) Ultrastructure and biochemistry of *Methanococcus voltae*. Crit Rev Microbiol 17:53–87
32. Jarrell KF, Jones GM, Kandiba L, Nair DB, Eichler J (2010) S-layer glycoproteins and flagellins: reporters of archaeal posttranslational modifications. Archaea 2010:13
33. Jarrell KF, Stark M, Nair DB, Chong JP (2011) Flagella and pili are both necessary for efficient attachment of *Methanococcus maripaludis* to surfaces. FEMS Microbiol Lett 319:44–50
34. Bardy SL, Jarrell KF (2002) FlaK of the archaeon *Methanococcus maripaludis* possesses preflagellin peptidase activity. FEMS Microbiol Lett 208:53–59
35. Chaban B, Ng SY, Kanbe M, Saltzman I, Nimmo G, Aizawa S, Jarrell KF (2007) Systematic deletion analyses of the *fla* genes in the flagella operon identify several genes essential for proper assembly and function of flagella in the archaeon, *Methanococcus maripaludis*. Mol Microbiol 66:596–609

36. Thomas NA, Mueller S, Klein A, Jarrell KF (2002) Mutants in *fla*I and *fla*J of the archaeon *Methanococcus voltae* are deficient in flagellum assembly. Mol Microbiol 46:879–887
37. VanDyke DJ, Wu J, Ng SY, Kanbe M, Chaban B, Aizawa S, Jarrell KF (2008) Identification of a putative acetyltransferase gene, MMP0350, which affects proper assembly of both flagella and pili in the archaeon *Methanococcus maripaludis*. J Bacteriol 190:5300–5307
38. Kelly J, Logan SM, Jarrell KF, VanDyke DJ, Vinogradov E (2009) A novel N-linked flagellar glycan from *Methanococcus maripaludis*. Carbohydr Res 344:648–653
39. Ng SY, Wu J, Nair DB, Logan SM, Robotham A, Tessier L, Kelly JF, Uchida K, Aizawa S, Jarrell KF (2011) Genetic and mass spectrometry analyses of the unusual type IV-like pili of the archaeon *Methanococcus maripaludis*. J Bacteriol 193:804–814
40. Apolinario EA, Sowers KR (1996) Plate colonization of *Methanococcus maripaludis* and *Methanosarcina thermophila* in a modified canning jar. FEMS Microbiol Lett 145:131–137
41. Costa KC, Lie TJ, Jacobs MA, Leigh JA (2013) H_2-independent growth of the hydrogenotrophic methanogen *Methanococcus maripaludis*. MBio 4:e00062-13
42. Lupa B, Hendrickson EL, Leigh JA, Whitman WB (2008) Formate-dependent H_2 production by the mesophilic methanogen *Methanococcus maripaludis*. Appl Environ Microbiol 74:6584–6590
43. Whitman WB, Sohn S, Kuk S, Xing R (1987) Role of amino acids and vitamins in nutrition of mesophilic *Methanococcus spp*. Appl Environ Microbiol 53:2373–2378
44. Whitman W, Ankwanda E, Wolfe R (1982) Nutrition and carbon metabolism of *Methanococcus voltae*. J Bacteriol 149:852–863
45. Lohner ST, Deutzmann JS, Logan BE, Leigh J, Spormann AM (2014) Hydrogenase-independent uptake and metabolism of electrons by the archaeon *Methanococcus maripaludis*. The ISME journal 8:1673–1681
46. Lie TJ, Costa KC, Lupa B, Korpole S, Whitman WB, Leigh JA (2012) Essential anaplerotic role for the energy-converting hydrogenase Eha in hydrogenotrophic methanogenesis. Proc Natl Acad Sci USA 109:15473–15478
47. Shieh J, Whitman WB (1987) Pathway of acetate assimilation in autotrophic and heterotrophic methanococci. J Bacteriol 169:5327–5329
48. Yang Y-L, Ladapo J, Whitman WB (1992) Pyruvate oxidation by *Methanococcus spp*. Arch Microbiol 158:271–275
49. White RH (1988) Structural diversity among methanofurans from different methanogenic bacteria. J Bacteriol 170:4594–4597
50. Wolfe RS (1985) Unusual coenzymes of methanogenesis. Trends Biochem Sci 10:396–399
51. Noll KM, Rinehart KL, Tanner RS, Wolfe RS (1986) Structure of component B (7-mercaptoheptanoylthreonine phosphate) of the methylcoenzyme M methylreductase system of *Methanobacterium thermoautotrophicum*. Proc Natl Acad Sci 83:4238–4242
52. Taylor CD, Wolfe RS (1974) Structure and methylation of coenzyme M ($HSCH_2CH_2SO_3$). J Biol Chem 249:4879–4885
53. Hendrickson EL, Leigh JA (2008) Roles of coenzyme F420-reducing hydrogenases and hydrogen-and F420-dependent methylenetetrahydromethanopterin dehydrogenases in reduction of F420 and production of hydrogen during methanogenesis. J Bacteriol 190:4818–4821
54. Färber G, Keller W, Kratky C, Jaun B, Pfaltz A, Spinner C, Kobelt A, Eschenmoser A (1991) Coenzyme F430 from methanogenic bacteria: complete assignment of configuration based on an X-Ray analysis of 12, 13-Diepi-F430 pentamethyl ester and on NMR spectroscopy. Helv Chim Acta 74:697–716
55. Thauer RK, Kaster AK, Seedorf H, Buckel W, Hedderich R (2008) Methanogenic archaea: ecologically relevant differences in energy conservation. Nat Rev Microbiol 6:579–591
56. Thauer RK, Kaster A-K, Goenrich M, Schick M, Hiromoto T, Shima S (2010) Hydrogenases from methanogenic archaea, nickel, a novel cofactor, and H2 storage. Annu Rev Biochem 79:507–536
57. Donnelly M, Wolfe R (1986) The role of formylmethanofuran: tetrahydromethanopterin formyltransferase in methanogenesis from carbon dioxide. J Biol Chem 261:16653–16659

58. Mukhopadhyay BSS, Wolfe RS (1998) Purification, regulation, and molecular and biochemical characterization of pyruvate carboxylase from *Methanobacterium thermoautotrophicum* strain ΔH. J Biol Chem 273:5155–5166
59. Kengen SM DP, Duits EF, Keltjens JT, van der Drift C, Vogels GD (1992) Isolation of a 5-hydroxybenzimidazolyl cobamide-containing enzyme involved in the methyltetrahydromethanopterin: coenzyme M methyltransferase reaction in *Methanobacterium thermoautotrophicum*. Biochim Biophys Acta 1118:249–260
60. Kaster A-K, Moll J, Parey K, Thauer RK (2011) Coupling of ferredoxin and heterodisulfide reduction via electron bifurcation in hydrogenotrophic methanogenic archaea. Proc Natl Acad Sci 108:2981–2986
61. Major TA, Liu Y, Whitman WB (2010) Characterization of energy-conserving hydrogenase B in *Methanococcus maripaludis*. J Bacteriol 192:4022–4030
62. Costa KCLT, Xia Q, Leigh JA (2013) VhuD facilitates electron flow from H2 or formate to heterodisulfide reductase in *Methanococcus maripaludis*. J Bacteriol 195:6160–6165
63. Mitchell P (1974) Chemiosmotic coupling in energy transduction: a logical development of biochemical knowledge. Springer, Berlin
64. Kühn W, Fiebig K, Hippe H, Mah RA, Huser BA, Gottschalk G (1983) Distribution of cytochromes in methanogenic bacteria. FEMS Microbiol Lett 20:407–410
65. Muller V, Blaut M, Heise R, Winner C, Gottschalk G (1990) Sodium bioenergetics in methanogens and acetogens. FEMS Microbiol Lett 87:373–376
66. Bull AT, Bunch AW, Robinson GK (1999) Biocatalysts for clean industrial products and processes. Curr Opin Microbiol 2:246–251
67. Park JH, Lee KH, Kim TY, Lee SY (2007) Metabolic engineering of *Escherichia coli* for the production of L-valine based on transcriptome analysis and in silico gene knockout simulation. Proc Natl Acad Sci 104:7797–7802
68. Lewalter K, Müller V (2006) Bioenergetics of archaea: ancient energy conserving mechanisms developed in the early history of life. Biochim Biophys Acta 1757:437–445
69. Yang YL, Glushka JN, Whitman WB (2002) Intracellular pyruvate flux in the methane-producing archaeon *Methanococcus maripaludis*. Arch Microbiol 178:493–498
70. Lin WC, Yang YL, Whitman WB (2003) The anabolic pyruvate oxidoreductase from *Methanococcus maripaludis*. Arch Microbiol 179:444–456
71. Lin W, Whitman WB (2004) The importance of porE and porF in the anabolic pyruvate oxidoreductase of *Methanococcus maripaludis*. Arch Microbiol 181:68–73
72. Moore BC, Leigh JA (2005) Markerless mutagenesis in *Methanococcus maripaludis* demonstrates roles for alanine dehydrogenase, alanine racemase, and alanine permease. J Bacteriol 187:972–979
73. Lie TJ, Leigh JA (2002) Regulatory response of *Methanococcus maripaludis* to alanine, an intermediate nitrogen source. J Bacteriol 184:5301–5306
74. Yu J-P, Ladapo J, Whitman WB (1993) Pathway of glycogen metabolism in *Methanococcus maripaludis*. J Bacteriol 176:325–332
75. Sakuraba H, Yoshioka I, Koga S, Takahashi M, Kitahama Y, Satomura T, Kawakami R, Ohshima T (2002) ADP-dependent glucokinase/phosphofructokinase, a novel bifunctional enzyme from the hyperthermophilic archaeon *Methanococcus jannaschii*. J Biol Chem 277:12495–12498
76. Castro-Fernandez V, Bravo-Moraga F, Herrera-Morande A, Guixe V (2014) Bifunctional ADP-dependent phosphofructokinase/glucokinase activity in the order Methanococcales–biochemical characterization of the mesophilic enzyme from *Methanococcus maripaludis*. FEBS J 281:2017–2029
77. Verhees C, Kengen S, Tuininga J, Schut G, Adams M, de Vos W, Van Der Oost J (2003) The unique features of glycolytic pathways in Archaea. Biochem J 375:231–246
78. Siebers B, Schönheit P (2005) Unusual pathways and enzymes of central carbohydrate metabolism in Archaea. Curr Opin Microbiol 8:695–705

79. Verhees CH, Huynen MA, Ward DE, Schiltz E, de Vos WM, van der Oost J (2001) The phosphoglucose isomerase from the hyperthermophilic archaeon *Pyrococcus furiosus* is a unique glycolytic enzyme that belongs to the cupin superfamily. J Biol Chem 276:40926–40932
80. Graham DE, Xu H, White RH (2002) A divergent archaeal member of the alkaline phosphatase binuclear metalloenzyme superfamily has phosphoglycerate mutase activity. FEBS Lett 517:190–194
81. Berg JM, Tymoczko JL, Stryer L (2002) The glycolytic pathway is tightly controlled. In: Freeman WH (ed) Biochemistry, 5th edn, Section 16.2, New York. Available from: http://www.ncbi.nlm.nih.gov/books/NBK22395/
82. Brunner NA, Siebers B, Hensel R (2001) Role of two different glyceraldehyde-3-phosphate dehydrogenases in controlling the reversible Embden–Meyerhof–Parnas pathway in Thermoproteus tenax: regulation on protein and transcript level. Extremophiles 5:101–109
83. van der Oost J, Schut G, Kengen SM, Hagen WR, Thomm M, de Vos WM (1998) The ferredoxin-dependent conversion of glyceraldehyde-3-phosphate in the hyperthermophilic archaeon *Pyrococcus furiosus* represents a novel site of glycolytic regulation. J Biol Chem 273:28149–28154
84. Ettema TJ, Ahmed H, Geerling AC, van der Oost J, Siebers B (2008) The non-phosphorylating glyceraldehyde-3-phosphate dehydrogenase (GAPN) of Sulfolobus solfataricus: a key-enzyme of the semi-phosphorylative branch of the Entner-Doudoroff pathway. Extremophiles 12:75–88
85. Park MO, Mizutani T, Jones PR (2007) Glyceraldehyde-3-phosphate ferredoxin oxidoreductase from *Methanococcus maripaludis*. J Bacteriol 189:7281–7289
86. Fernie AR, Carrari F, Sweetlove LJ (2004) Respiratory metabolism: glycolysis, the TCA cycle and mitochondrial electron transport. Curr Opin Plant Biol 7:254–261
87. Simpson PG, Whitman WB (1993) Anabolic pathways in methanogens. In Methanogenesis. Springer, Berlin, pp 445–472
88. Ladapo J, Whitman WB (1990) Method for isolation of auxotrophs in the methanogenic archaebacteria: role of the acetyl-CoA pathway of autotrophic CO2 fixation in *Methanococcus maripaludis*. Proc Natl Acad Sci 87:5598–5602
89. Lie TJ, Wood GE, Leigh JA (2005) Regulation of nif expression in *Methanococcus maripaludis*: roles of the euryarchaeal repressor NrpR, 2-oxoglutarate, and two operators. J Biol Chem 280:5236–5241
90. Dodsworth JA, Cady NC, Leigh JA (2005) 2-Oxoglutarate and the PII homologues NifI1 and NifI2 regulate nitrogenase activity in cell extracts of *Methanococcus maripaludis*. Mol Microbiol 56:1527–1538
91. Tumbula DL, Teng Q, Bartlett MG, Whitman WB (1997) Ribose biosynthesis and evidence for an alternative first step in the common aromatic amino acid pathway in *Methanococcus maripaludis*. J Bacteriol 179:6010–6013
92. Porat I, Waters BW, Teng Q, Whitman WB (2004) Two biosynthetic pathways for aromatic amino acids in the archaeon *Methanococcus maripaludis*. J Bacteriol 186:4940–4950
93. Harmen JG, van de Werken, Brouns SJJ, Oost JVD (2002) Pentose metabolism in archaea. In: Blum P (ed) Archaea: new models for prokaryotic biology. Caister Academic Press, Norfolk, pp 71–95
94. Berg JM, Tymoczko JL, Stryer L (2006) Biochemistry: international edition. WH Freeman & Company Limited, London
95. Kessler PS, McLarnan J, Leigh JA (1997) Nitrogenase phylogeny and the molybdenum dependence of nitrogen fixation in *Methanococcus maripaludis*. J Bacteriol 179:541–543
96. Cohen-Kupiec R, CA Marx, Leigh J (1999) Function and regulation of glnA in the methanogenic archaeon *Methanococcus maripaludis*. J Bacteriol 18:256–261
97. Pine MJ, Barker H (1954) Studies of the methane bacteria: XI. Fixation of atmospheric nitrogen by *Methanobacterium omelianskii*1. J Bacteriol 68:589

98. Belay N, Sparling R, Daniels L (1984) Dinitrogen fixation by a thermophilic methanogenic bacterium, vol 312, pp 286–288
99. Belay N, Sparling R, Choi B-S, Roberts M, Roberts J, Daniels L (1988) Physiological and ^{15}N-NMR analysis of molecular nitrogen fixation by *Methanococcus thermolithotrophicus*, *Methanobacterium bryantii* and *Methanospirillum hungatei*. Biochim Biophys Acta 971:233–245
100. Kendall MM, Liu Y, Sieprawska-Lupa M, Stetter KO, Whitman WB, Boone DR (2006) *Methanococcus aeolicus* sp. nov., a mesophilic, methanogenic archaeon from shallow and deep marine sediments. Int J Syst Evol Microbiol 56:1525–1529
101. Takai K, Nealson KH, Horikoshi K (2004) *Methanotorris formicicus* sp. nov., a novel extremely thermophilic, methane-producing archaeon isolated from a black smoker chimney in the Central Indian Ridge. Int J Syst Evol Microbiol 54:1095–1100
102. Blank CE, Kessler PS, Leigh JA (1995) Genetics in methanogens: transposon insertion mutagenesis of a *Methanococcus maripaludis* nifH gene. J Bacteriol 177:5773–5777
103. Kessler PS, Blank C, Leigh JA (1998) The nif gene operon of the methanogenic archaeon *Methanococcus maripaludis*. J Bacteriol 180:1504–1511
104. Huber H, Thomm M, König H, Thies G, Stetter KO (1982) *Methanococcus thermolithotrophicus*, a novel thermophilic lithotrophic methanogen. Arch Microbiol 132:47–50
105. Dodge E (2014) Carbon dioxide can be a resource rather than a waste product. http://www.theenergycollective.com/ed-dodge/341971
106. Kessler PS, Daniel C, Leigh JA (2001) Ammonia switch-off of nitrogen fixation in the methanogenic archaeon Methanococcus maripaludis: mechanistic features and requirement for the novel GlnB homologues, Nif I(1) and NifI(2). J Bacteriol 183:882–889
107. Lie TJ, Leigh JA (2002) A novel repressor of nif and glnA expression in the methanogenic archaeon *Methanococcus maripaludis*. Mol Microbiol 47:235–246
108. Kessler PS, Leigh JA (1999) Genetics of nitrogen regulation in *Methanococcus maripaludis*. Genetics 152:1343–1351
109. Xing R, Whitman WB (1991) Characterization of enzymes of the branched-chain amino acid biosynthetic pathway in *Methanococcus* spp. J Bacteriol 173:2086–2092
110. Smith DR, Doucette-Stamm LA, Deloughery C, Lee H, Dubois J, Aldredge T, Bashirzadeh R, Blakely D, Cook R, Gilbert K (1997) Complete genome sequence of *Methanobacterium thermoautotrophicum* deltaH: functional analysis and comparative genomics. J Bacteriol 179:7135
111. Graupner M, White RH (2001) *Methanococcus jannaschii* generates l-proline by cyclization of L-ornithine. J Bacteriol 183:5203–5205
112. Porat I, Sieprawska-Lupa M, Teng Q, Bohanon FJ, White RH, Whitman WB (2006) Biochemical and genetic characterization of an early step in a novel pathway for the biosynthesis of aromatic amino acids and p-aminobenzoic acid in the archaeon *Methanococcus maripaludis*. Mol Microbiol 62:1117–1131
113. Fondi M, Emiliani G, Lio P, Gribaldo S, Fani R (2009) The evolution of histidine biosynthesis in archaea: insights into the his genes structure and organization in LUCA. J Mol Evol 69:512–526
114. Liu Y (2010) Adaptations of *Methanococcus maripaludis* to its unique lifestyle. The University of Georgia, Georgia
115. Meile L, Leisinger T (1984) Enzymes of arginine biosynthesis in methanogenic bacteria. Experientia 40:899–900
116. Cohen-Kupiec R, Kupiec M, Sandbeck K, Leigh J (1999) Functional conservation between the argininosuccinate lyase of the archaeon *Methanococcus maripaludis* and the corresponding bacterial and eukaryal genes. FEMS Microbiol Lett 173:231–238
117. Kenealy WR, Zeikus J (1982) One-carbon metabolism in methanogens: evidence for synthesis of a two-carbon cellular intermediate and unification of catabolism and anabolism in *Methanosarcina barkeri*. J Bacteriol 151:932–941

118. Stathopoulos C, Kim W, Li T, Anderson I, Deutsch B, Palioura S, Whitman W, Soll D (2001) Cysteinyl-tRNA synthetase is not essential for viability of the archaeon *Methanococcus maripaludis*. Proc Natl Acad Sci USA 98:14292–14297
119. Sauerwald A, Zhu W, Major TA, Roy H, Palioura S, Jahn D, Whitman WB, Yates JR 3rd, Ibba M, Söll D (2005) RNA-dependent cysteine biosynthesis in archaea. Science 307: 1969–1972
120. Zhang C-M, Liu C, Slater S, Hou Y-M (2008) Aminoacylation of tRNA with phosphoserine for synthesis of cysteinyl-tRNA^{Cys}. Nat Struct Mol Biol 15:507–514
121. Turanov AA, Xu X-M, Carlson BA, Yoo M-H, Gladyshev VN, Hatfield DL (2011) Biosynthesis of selenocysteine, the 21st amino acid in the genetic code, and a novel pathway for cysteine biosynthesis. Adv Nutr Intl Rev J 2:122–128
122. Yuan J, Palioura S, Salazar JC, Su D, O'Donoghue P, Hohn MJ, Cardoso AM, Whitman WB, Söll D (2006) RNA-dependent conversion of phosphoserine forms selenocysteine in eukaryotes and archaea. Proc Natl Acad Sci 103:18923–18927
123. Hohn MJ, Palioura S, Su D, Yuan J, Söll D (2011) Genetic analysis of selenocysteine biosynthesis in the archaeon *Methanococcus maripaludis*. Mol Microbiol 81:249–258
124. Stock T, Selzer M, Connery S, Seyhan D, Resch A, Rother M (2011) Disruption and complementation of the selenocysteine biosynthesis pathway reveals a hierarchy of selenoprotein gene expression in the archaeon *Methanococcus maripaludis*. Mol Microbiol 82:734–747
125. Rother M, Mathes I, Lottspeich F, Böck A (2003) Inactivation of the selB gene in *Methanococcus maripaludis*: effect on synthesis of selenoproteins and their sulfur-containing homologs. J Bacteriol 185:107–114
126. Srinivasan G, James CM, Krzycki JA (2002) Pyrrolysine encoded by UAG in archaea: charging of a UAG-decoding specialized tRNA. Science 296:1459–1462
127. Alkalaeva E, Eliseev B, Ambrogelly A, Vlasov P, Kondrashov FA, Gundllapalli S, Frolova L, Söll D, Kisselev L (2009) Translation termination in pyrrolysine-utilizing archaea. FEBS Lett 583:3455–3460
128. Leigh JA, Albers SV, Atomi H, Allers T (2011) Model organisms for genetics in the domain archaea: methanogens, halophiles, thermococcales and sulfolobales. FEMS Microbiol Rev 35:577–608
129. Sarmiento FB, Leigh JA, Whitman WB (2011) Genetic systems for hydrogenotrophic methanogens. Methods Enzymol 494:43–73
130. Argyle JL, Tumbula DL, Leigh JA (1996) Neomycin resistance as a selectable marker in *Methanococcus maripaludis*. Appl Environ Microbiol 62:4233–4237
131. Sandbeck KA, Leigh JA (1991) Recovery of an integration shuttle vector from tandem repeats in *Methanococcus maripaludis*. Appl Environ Microbiol 57:2762–2763
132. Lie TJ, Leigh JA (2007) Genetic screen for regulatory mutations in *Methanococcus maripaludis* and its use in identification of induction-deficient mutants of the euryarchaeal repressor NrpR. Appl Environ Microbiol 73:6595–6600
133. Tumbula DL, Makula RA, Whitman WB (1994) Transformation of *Methanococcus maripaludis* and identification of a Pst I-like restriction system. FEMS Microbiol Lett 121:309–314
134. GIBCO B: Product catalogue and reference guide. Life Technologies Inc.
135. Weisburg WG, Tanner RS (1982) Aminoglycoside sensitivity of archaebacteria. FEMS Microbiol Lett 14:307–310
136. Tumbula DL, Bowen TL, Whitman WB (1997) Characterization of pURB500 from the archaeon *Methanococcus maripaludis* and construction of a shuttle vector. J Bacteriol 179:2976–2986
137. Gardner WL, Whitman W (1999) Expression vectors for *Methanococcus maripaludis* overexpression of acetohydroxyacid synthase and β-galactosidase. Genet Soc Am 152: 1439–1447

138. Walters AD, Smith SE, Chong JP (2011) Shuttle vector system for *Methanococcus maripaludis* with improved transformation efficiency. Appl Environ Microbiol 77: 2549–2551
139. Kim W, Whitman WB (1999) Isolation of acetate auxotrophs of the methane-producing archaeon *Methanococcus maripaludis* by random insertional mutagenesis. Genetics 152:1429–1437
140. Tabatabaei M, Rahim RA, Abdullah N, Wright A-DG, Shirai Y, Sakai K, Sulaiman A, Hassan MA (2010) Importance of the methanogenic archaea populations in anaerobic wastewater treatments. Process Biochem 45:1214–1225
141. Ali Shah F, Mahmood Q, Maroof Shah M, Pervez A, Ahmad Asad S (2014) Microbial ecology of anaerobic digesters: the key players of anaerobiosis. Sci World J 183752:21. doi:10.1155/2014/183752
142. Song C (2003) An overview of new approaches to deep desulfurization for ultra-clean gasoline, diesel fuel and jet fuel. Catal Today 86:211–263
143. Arsova L (2010) Anaerobic digestion of food waste: Current status, problems and an alternative product. Columbia University, New York
144. Morita M, Malvankar NS, Franks AE, Summers ZM, Giloteaux L, Rotaru AE, Rotaru C, Lovley DR (2011) Potential for direct interspecies electron transfer in methanogenic wastewater digester aggregates. MBio 2:e00159–00111
145. Summers ZM, Fogarty HE, Leang C, Franks AE, Malvankar NS, Lovley DR (2010) Direct exchange of electrons within aggregates of an evolved syntrophic coculture of anaerobic bacteria. Science 330:1413–1415
146. Rotaru AE, Mallaá Shrestha P, Liu F, Shrestha M, Shrestha D, Embree M, Zengler K, Wardman C, Nevin KP, Lovley DR (2014) A new model for electron flow during anaerobic digestion: direct interspecies electron transfer to Methanosaeta for the reduction of carbon dioxide to methane. Energy Environ Sci 7:408–415
147. Aaron D, Tsouris C (2005) Separation of CO2 from flue gas: a review. Sep Sci Technol 40:321–348
148. Marshall CW, Ross DE, Fichot EB, Norman RS, May HD (2012) Electrosynthesis of commodity chemicals by an autotrophic microbial community. Appl Environ Microbiol 78:8412–8420
149. Wu K, Birgersson E, Kim B, Kenis PJ, Karimi IA (2015) Modeling and experimental validation of electrochemical reduction of CO_2 to CO in a microfluidic cell. J Electrochem Soc 162:F23–F32
150. Nandi R, Sengupta S (1998) Microbial production of hydrogen: an overview. Crit Rev Microbiol 24:61–84
151. Kuhn M, Steinbüchel A, Schlegel HG (1984) Hydrogen evolution by strictly aerobic hydrogen bacteria under anaerobic conditions. J Bacteriol 159:633–639
152. Yoshida A, Nishimura T, Kawaguchi H, Inui M, Yukawa H (2005) Enhanced hydrogen production from formic acid by formate hydrogen lyase-overexpressing *Escherichia coli* strains. Appl Environ Microbiol 71:6762–6768
153. Valentine DL, Blanton DC, Reeburgh WS (2000) Hydrogen production by methanogens under low-hydrogen conditions. Arch Microbiol 174:415–421
154. Modification of *Methanococcus maripaludis* for production of geraniol. http://2012.igem.org/files/presentation/UGA-Georgia.pdf
155. Boopathy R (1996) Methanogenic transformation of methylfurfural compounds to furfural. Appl Environ Microbiol 62:3483–3485
156. Boopathy R, Kulpa CF (1994) Biotransformation of 2, 4, 6-trinitrotoluene (TNT) by a Methanococcus sp. (strain B) isolated from a lake sediment. Can J Microbiol 40:273–278
157. Moore BC, Leigh JA (2005) Markerless mutagenesis in *Methanococcus maripaludis* demonstrates roles for alanine dehydrogenase, alanine racemase, and alanine permease. J Bacteriol 187:972–979
158. Cohen SN, Chang AC, Boyer HW, Helling RB (1973) Construction of biologically functional bacterial plasmids in vitro. Proc Natl Acad Sci 70:3240–3244

159. Ribaut J, de Vicente M, Delannay X (2010) Molecular breeding in developing countries: challenges and perspectives. Curr Opin Plant Biol 13:213–218
160. Liao JC, Hou SY, Chao YP (1996) Pathway analysis, engineering, and physiological considerations for redirecting central metabolism. Biotechnol Bioeng 52:129–140
161. Stephanopoulos G (1999) Metabolic fluxes and metabolic engineering. Metab Eng 1:1–11
162. Park JH, Lee SY (2008) Towards systems metabolic engineering of microorganisms for amino acid production. Curr Opin Biotechnol 19:454–460
163. Aldor IS, Keasling JD (2003) Process design for microbial plastic factories: metabolic engineering of polyhydroxyalkanoates. Curr Opin Biotechnol 14:475–483
164. Shintani D, DellaPenna D (1998) Elevating the vitamin E content of plants through metabolic engineering. Science 282:2098–2100
165. Singh SP, Zhou X-R, Liu Q, Stymne S, Green AG (2005) Metabolic engineering of new fatty acids in plants. Curr Opin Plant Biol 8:197–203
166. Khosla C, Keasling JD (2003) Metabolic engineering for drug discovery and development. Nat Rev Drug Discovery 2:1019–1025
167. Thomas S, Mooney P, Burrell M, Fell D (1997) Metabolic control analysis of glycolysis in tuber tissue of potato (Solanum tuberosum): explanation for the low control coefficient of phosphofructokinase over respiratory flux. Biochem J 322:119–127
168. Krab K (1995) Kinetic and regulatory aspects of the function of the alternative oxidase in plant respiration. J Bioenerg Biomembr 27:387–396
169. Pettersson G, Ryde-Pettersson U (1988) A mathematical model of the Calvin photosynthesis cycle. Eur J Biochem 175:661–672
170. Luedeking R, Piret EL (1959) A kinetic study of the lactic acid fermentation. Batch process at controlled pH. J Biochem Microbiol Technol Eng 1:393–412
171. Lawrence AW, McCarty PL (1969) Kinetics of methane fermentation in anaerobic treatment. J Water Pollut Control Fed R1–R17
172. Hynne F, Dano S, Sorensen PG (2001) Full-scale model of glycolysis in *Saccharomyces cerevisiae*. Biophys Chem 94:121–163
173. Bakker BM, van Eunen K, Jeneson JA, van Riel NA, Bruggeman FJ, Teusink B (2010) Systems biology from microorganisms to human metabolic diseases-The role of detailed kinetic models. Biochem Soc Trans 38:1294
174. Xu X, Pang KS (1989) Hepatic modeling of metabolite kinetics in sequential and parallel pathways: salicylamide and gentisamide metabolism in perfused rat liver. J Pharmacokinet Biopharm 17:645–671
175. Fleischmann R, Adams M, White O, Clayton R, Tatusov R, Mushegian A, Bork P, Brown N, Hayes W, White O (1995) Whole-genome random sequencing and assembly of Haemophilus. Science 269:496–512
176. Price ND, Papin JA, Schilling CH, Palsson BO (2003) Genome-scale microbial *in silico* models: the constraints-based approach. Trends Biotechnol 21:162–169
177. Terzer M, Maynard ND, Covert MW, Stelling J (2009) Genome-scale metabolic networks. Syst Biol Med 3:285–297 (Wiley Interdisciplinary Reviews)
178. Price ND, Reed JL, Palsson BO (2004) Genome-scale models of microbial cells: evaluating the consequences of constraints. Nat Rev Microbiol 2:886–897
179. Raman K, Chandra N (2009) Flux balance analysis of biological systems: applications and challenges. Brief Bioinform 10:435–449
180. Sherman BT, Huang DW, Tan Q, Guo Y, Bour S, Liu D, Lempicki RA et al (2007) DAVID Knowledgebase: a gene-centered database integrating heterogeneous gene annotation resources to facilitate high-throughput gene functional analysis. BMC bioinformatics 8(1):426
181. Schuetz R, Kuepfer L, Sauer U (2007) Systematic evaluation of objective functions for predicting intracellular fluxes in *Escherichia coli*. Mol Syst Biol 3:119
182. Burgard AP, Maranas CD (2003) Optimization-based framework for inferring and testing hypothesized metabolic objective functions. Biotechnol Bioeng 82:670–677

183. Feist AM, Palsson BO (2010) The biomass objective function. Curr Opin Microbiol 13:344–349
184. Blombach B, Riester T, Wieschalka S, Ziert C, Youn J-W, Wendisch VF, Eikmanns BJ (2011) Corynebacterium glutamicum tailored for efficient isobutanol production. Appl Environ Microbiol 77:3300–3310
185. Lakshmanan M, Koh G, Chung BK, Lee D-Y (2014) Software applications for flux balance analysis. Briefings Bioinform 15:108–122
186. Lee J, Yun H, Feist AM, Palsson BO, Lee SY (2008) Genome-scale reconstruction and in silico analysis of the Clostridium acetobutylicum ATCC 824 metabolic network. Appl Microbiol Biotechnol 80:849–862
187. Vallino JJ, Stephanopoulos G (1994) Carbon flux distributions at the pyruvate branch point in *Corynebacterium glutamicum* during lysine overproduction. Biotechnol Prog 10:320–326
188. Collins D, Briggs D, Morris SC (1983) Expression of naphthalene oxidation genes in *Escherichia coli* results in the biosynthesis of indigo. Science 222:167–69
189. Tong I-T, Liao HH, Cameron D (1991) 1, 3-Propanediol production by *Escherichia coli* expressing genes from the Klebsiella pneumoniae dha regulon. Appl Environ Microbiol 57:3541–3546
190. Aggarwal S, Karimi IA, Lee DY (2011) Reconstruction of a genome-scale metabolic network of *Rhodococcus erythropolis* for desulfurization studies. Mol BioSyst 7:3122–3131
191. Tsunekawa H, Azuma S, Okabe M, Okamoto R, Aiba S (1992) Acquisition of a sucrose utilization system in *Escherichia coli* K-12 derivatives and its application to industry. Appl Environ Microbiol 58:2081–2088
192. Hollenberg CP, Strasser AWM (1990) Improvement of baker's and brewer's yeast by gene technology. J Food Biotechnol 4(1):527–534
193. Lee J-Y, Jung K-H, Choi SH, Kim H-S (1995) Combination of the tod and the tol pathways in redesigning a metabolic route of Pseudomonas putida for the mineralization of a benzene, toluene, and p-xylene mixture. Appl Environ Microbiol 61:2211–2217
194. Islam MA, Edwards EA, Mahadevan R (2010) Characterizing the metabolism of Dehalococcoides with a constraint-based model. PLoS Comput Biol 6:e1000887
195. Kallio PT, Kim D, Tsai PS, Bailey JE (1994) Intracellular expression of Vitreoscilla hemoglobin alters *Escherichia coli* energy metabolism under oxygen-limited conditions. Eur J Biochem 219:201–208
196. Goyal N, Widiastuti H, Karimi IA, Zhou Zhi G (2013) Genome-scale metabolic network reconstruction and in silico analysis of *Methanococcus maripaludis* S2. In: Andrzej K, Ilkka T (eds) Computer aided chemical engineering. Elsevier, Amsterdam, vol 32, pp 181–186
197. Windass J, Worsey M, Pioli E, Pioli D, Barth P, Atherton K, Dart E, Byrom D, Powell K, Senior P (1980) Improved conversion of methanol to single-cell protein by Methylophilus methylotrophus. Nature 287:396–401
198. Resendis-Antonio O, Reed JL, Encarnación S, Collado-Vides J, Palsson BØ (2007) Metabolic reconstruction and modeling of nitrogen fixation in Rhizobium etli. PLoS Comput Biol 3:e192
199. Stolyar S, Van Dien S, Hillesland KL, Pinel N, Lie TJ, Leigh JA, Stahl DA (2007) Metabolic modeling of a mutualistic microbial community. Mol Syst Biol 3:92
200. Henry CS, DeJongh M, Best AA, Frybarger PM, Linsay B, Stevens RL (2010) High-throughput generation, optimization and analysis of genome-scale metabolic models. Nat Biotechnol 28:977–982
201. Goyal N, Widiastuti H, Karimi IA, Zhou Z (2014) Genome-scale metabolic model of *Methanococcus maripaludis* S2 for CO_2 capture and conversion to methane. Mol BioSyst 10:1043–1054
202. Sarmiento F, Mrázek J, Whitman WB (2013) Genome-scale analysis of gene function in the hydrogenotrophic methanogenic archaeon *Methanococcus maripaludis*. Proc Natl Acad Sci 110:4726–4731

203. Rabaey K, Rodriguez J, Blackall LL, Keller J, Gross P, Batstone D, Verstraete W, Nealson KH (2007) Microbial ecology meets electrochemistry: electricity-driven and driving communities. ISME J 1:9–18
204. Logan BE, Hamelers B, Rozendal R, Schröder U, Keller J, Freguia S, Aelterman P, Verstraete W, Rabaey K (2006) Microbial fuel cells: methodology and technology. Environ Sci Technol 40:5181–5192
205. Nie H, Zhang T, Cui M, Lu H, Lovley DR, Russell TP (2013) Improved cathode for high efficient microbial-catalyzed reduction in microbial electrosynthesis cells. Phys Chem Chem Phys 15:14290–14294
206. Nevin KP, Woodard TL, Franks AE, Summers ZM, Lovley DR (2010) Microbial electrosynthesis: feeding microbes electricity to convert carbon dioxide and water to multicarbon extracellular organic compounds. MBio 1:e00103-10.
207. Park D, Laivenieks M, Guettler M, Jain M, Zeikus J (1999) Microbial utilization of electrically reduced neutral red as the sole electron donor for growth and metabolite production. Appl Environ Microbiol 65:2912–2917
208. Hongo M, Iwahara M (1979) Application of electro-energizing method to L-glutamic acid fermentation. Agr Biol Chem 43:2075–2081
209. Cheng S, Xing D, Call DF, Logan BE (2009) Direct biological conversion of electrical current into methane by electromethanogenesis. Environ Sci Technol 43:3953–3958
210. Nevin KP, Hensley SA, Franks AE, Summers ZM, Ou J, Woodard TL, Snoeyenbos-West OL, Lovley DR (2011) Electrosynthesis of organic compounds from carbon dioxide is catalyzed by a diversity of acetogenic microorganisms. Appl Environ Microbiol 77:2882–2886
211. Rabaey K, Rozendal RA (2010) Microbial electrosynthesis—revisiting the electrical route for microbial production. Nat Rev Microbiol 8:706–716
212. Soleimani M, Bassi A, Margaritis A (2007) Biodesulfurization of refractory organic sulfur compounds in fossil fuels. Biotechnol Adv 25:570–596
213. Rozendal RA, Hamelers HV, Molenkamp RJ, Buisman CJ (2007) Performance of single chamber biocatalyzed electrolysis with different types of ion exchange membranes. Water Res 41:1984–1994
214. Clauwaert P, Verstraete W (2009) Methanogenesis in membraneless microbial electrolysis cells. Appl Microbiol Biotechnol 82:829–836
215. Porat I, Kim W, Hendrickson EL, Xia Q, Zhang Y, Wang T, Taub F, Moore BC, Anderson IJ, Hackett M et al (2006) Disruption of the operon encoding Ehb hydrogenase limits anabolic CO_2 assimilation in the archaeon *Methanococcus maripaludis*. J Bacteriol 188:1373–1380

Chapter 3
A Genome-Scale Metabolic Model of *M. maripaludis* S2 for CO_2 Capture and Conversion to Methane

3.1 Introduction

Methane is a major energy source for heating and electricity. Its production by methanogenic bacteria is widely known in nature. *M. maripaludis* S2 is a fully sequenced hydrogenotrophic methanogen and an excellent laboratory strain with robust genetic tools. However, a quantitative systems biology model to complement these tools is absent in the literature.

To understand and enhance its methanogenesis from CO_2, this work presents the first constraint-based genome-scale metabolic model (*i*MM518). It comprises 570 reactions, 556 distinct metabolites, and 518 genes along with gene-protein-reaction (GPR) associations, and covers 30 % of open reading frames (ORFs). The model was validated using biomass growth data and experimental phenotypic studies from the literature. Its comparison with the in silico models of *Methanosarcina barkeri*, *Methanosarcina acetivorans*, and *Sulfolobus solfataricus* P2 shows *M. maripaludis* S2 to be a better organism for producing methane. Using the model, genes essential for growth were identified, and the efficacies of alternative carbon, hydrogen and nitrogen sources were studied. The model can predict the effects of reengineering *M. maripaludis* S2 to guide or expedite experimental efforts.

Some content of this chapter has been reproduced with permission from Nishu Goyal, I A Karimi, and Zhou Zhi. "Genome-scale metabolic model of M. maripaludis S_2 for CO_2 capture and conversion to methane", Molecular BioSystems (2014), Vol.10, 1043–1054

N. Goyal, *In silico Modeling and Experimental Validation for Improving Methanogenesis from CO_2 via M. maripaludis*, Springer Theses,
DOI 10.1007/978-981-10-2510-5_3

3.2 Materials and Methods

3.2.1 Reconstructing Metabolic Network

The process (Fig. 3.1) of metabolic network building has been well reviewed in the literature [1–3]. Genome annotations of *M. maripaludis* were obtained from the sequencing studies performed by Hendrickson et al. [4]. Various biochemical, genetic, and physiological information about *M. maripaludis* was mined from the published literature and public databases such as KEGG [5], METACYC [6], and BRENDA [7]. Reactions from multiple databases were integrated with the help of their EC numbers in KEGG. Spontaneous as well as non-gene associated reactions were included, if their existence was proven by physiological or experimental data. Transport reactions were also added to allow the exchange of metabolites between the cell and its environment. The reaction stoichiometries were checked to verify elemental balances for C, S, P, N, and O. Several ORFs were annotated in the process based on known physiological information and employing comparative genomics and local sequence similarity searches [8] with an e-value of 10^{-5}. Once the reaction set was completed, it was checked for the production of biomass precursors using the FBA in MetaFluxNet [9].

A score of 1–5 reflecting our confidence in the available experimental information was assigned to each reaction. The statistical properties of these scores were then used to evaluate the model reliability. All the reactions in our metabolic model along with their GPR associations, EC numbers, and metabolites with their chemical formulas are available as a supplementary Excel® file (Appendix B). An SBML (Systems Biology Markup Language) file of the model has also been deposited in BioModels database [10] with MODEL1304120000 as its identifier (Appendix A).

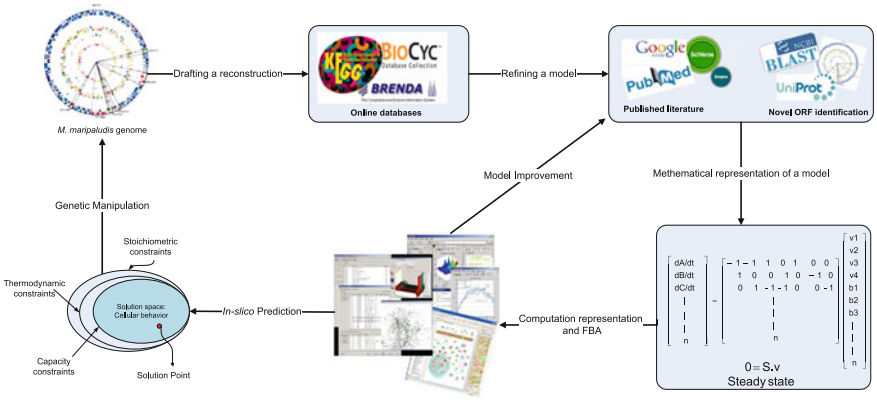

Fig. 3.1 Schematic representation of the procedure used to reconstruct the constraint-based genome-scale metabolic model of *M. maripaludis* S2

3.2.2 Genome-Scale Metabolic Model

The reaction fluxes in a genome-scale model are governed by the following equation. This assumes pseudo-steady state (no accumulation) for all metabolites [1].

$$S \cdot v = b \tag{3.1}$$

where, S is the matrix of stoichiometric coefficients of the reactants and products, v is the vector of reaction fluxes (mmol/gDCW-h) at any given time, and b is the vector of net fluxes into the cell. An external metabolite is treated distinct from its internal form, and both forms are connected via a transport reaction. The b values are zero for the internal metabolites.

Constraint-based FBA models were obtained by adding a suitable cellular objective (such as maximize biomass growth) to Eq. 3.1. In these models, suitable lower and upper bounds were assigned to each reaction flux. For instance, the limits on the flux of an irreversible reaction was set as [0, 1000], while that for a reversible reaction was set as [−1000, 1000]. These optimization models (which are linear programs) were solved using MetaFluxNet version 1.8 [9] to obtain the flux distributions corresponding to various cellular phenotypes.

Specific growth rate (h^{-1}) of biomass is a commonly used a cellular objective for FBA. It quantifies the assembly of various macromolecular precursors into cell biomass. A biomass reaction was formulated to describe this assimilation. Due to the unavailability of an experimental biomass composition for *M. maripaludis*, it was assumed to consist of DNA, RNA, proteins, phospholipids, glycogen, and ATP. DNA and RNA were expressed in terms of five nucleotides (adenine, thymine, guanine, uracil and cytosine) with their compositions estimated following the procedure of Lee et al. [11]. The compositions of proteins and phospholipids for *M. maripaludis* are available in the literature [12–14]. Glycogen synthesis was modeled by the following polymerization reaction of UDP-glucose by glycogen synthase as reported by Yu et al. [15]. For this reaction, glycogen was assumed to consist of UDP-glucose as monomeric entities. ATP quantifies the energy consumption required for cell growth. It is also known as GAM, which is not available for this organism. Therefore, the procedure reported by Verduyn et al. [16] was used to estimate a GAM of 30 mmol ATP/gDCW-h. In addition to GAM, a cell also needs energy for the maintenance of ion gradients, regulatory metabolism, RNA turnover, etc. This is known as NGAM. The NGAM energy usage was modeled as ATP + $H_2O \rightarrow$ ADP + Pi. The NGAM value that best described the experimental data on cell growth was determined during model validation. Detailed description of the biomass composition can be found in supplementary file (Appendix C). Atypical of most bacteria, *M. maripaludis* possesses a fragile proteinaceous S-layer (surface layer) [17, 18] instead of a cell wall. Therefore, the major components of an archaebacterial cell wall such as muramic acid and peptidoglycan were not included in our biomass composition.

During our metabolic pathway reconstructions, we identified several gaps. These included known reactions in *M. maripaludis* S2 with unknown ORFs, and known ORFs with unknown reactions. For the former, we added reactions from closely related methanogens and performed BLASTp searches in the protein database of *M. maripaludis* S2 to identify new ORFs using translated protein queries. For the latter, we performed BLASTx searches in the protein database using translated nucleotide queries. Several other genes exist in *M. maripaludis* S2 that are classified as "conserved hypothetical", "hypothetical", "genes of unknown function", etc. These genes/proteins can be annotated using various methods based on comparative genomics, protein-protein interaction, etc. presented in literature [19, 20] to enhance the ORF coverage of our model.

3.2.3 Experimental Data

M. maripaludis is known to grow on CO_2 as the sole carbon source and hydrogen as the electron donor. However, quantitative data on CO_2 or H_2 utilization profiles vs. growth are missing in the literature. Our genome-scale model was validated using the experimental data from Kral et al. [21] and Lupa et al. [22].

Kral et al. [21] grew a *M. maripaludis* culture in MSH media (MS medium with NaCl, $MgCl_2$, and KCl) with and without organics. A total H_2–CO_2 (75:25 v/v) pressure of 300 kPa and a temperature of 25 °C were maintained in anaerobic pressure tubes. A hydrogen utilization rate of 1.6 ng/μgDCP-min = 28.8 mmol/gDCW-h was measured during cell growth without the organics, and 45 mmol/gDCW-h with the organics. DCP here stands for dry cell protein and is assumed to be 60 % of DCW. The experimental value of hydrogen exchange was used as the lower bound in our model and FBA was used to compute other reaction fluxes.

Lupa et al. [22] performed two experiments with wild-type *M. maripaludis* S2. In the first experiment, cell growth (via absorbance at 600 nm) and MERs (via gas chromatography) at 37 °C were measured over a period of 25 h. The cultures for this experiment were grown at 37 °C in McNA (minimal medium supplemented with acetate) medium [23] under 276 kPa of H_2–CO_2 (80:20 v/v) atmosphere. In the second experiment, sodium formate was used as a source for H_2 under O_2-free N_2 atmosphere. The cultures for this experiment were grown under 138 kPa of N_2:CO_2 (80:20 v/v) atmosphere. To simulate this experiment in our model, the MER values were converted to mmol/gDCW-h and set as upper bounds on methane exchange fluxes. FBA predicted the growth rates corresponding to these MERs.

After validation, model predictions were verified using the phenotypical observations from Haydock et al. [24], Lin and Whitman [25], and Lie and Leigh [26]. Haydock et al. [24] constructed a leucine-auxotrophic mutant for demonstrating the essential role of *leuA* gene in the growth of *M. maripaludis* S2. Lin and Whitman [25] showed the importance of *porE* and *porF* genes on growth and oxidation of pyruvate. Lie and Leigh [26] studied the effect of nitrogen on the regulation of *nif* (N_2-fixation) and *glnA* (glutamine synthetase) operons. Both *nif*

and *glnA* expressions were high under diazotrophic (nitrogen-rich) conditions. Also, both operon expressions were observed in the presence of alanine as a nitrogen source [27].

3.2.4 Gene Essentiality/Flux Variability Analyses

Gene essentiality and flux variability analyses were performed using the Constraint-Based Reconstruction and Analysis (COBRA) toolbox in MATLAB version 7.12.0.635 (R2011a).

Gene/reaction essentiality analyses are useful for strain improvement strategies, as the deletion of an essential gene/reaction may result in a lethal phenotype. To this end, the minimal media identified in our study was used in a series of simulations with CO_2 and H_2 as the sole carbon and hydrogen sources. 10^{-4}/h was taken as the threshold for zero cell growth. For gene essentiality, genes were deleted one at a time by inactivating all the reactions associated with each individual gene. If the deletion of a gene resulted in near-zero biomass, then the gene was classified as essential for growth. Since a reaction catalyzed by multiple genes cannot be inactivated via single gene deletions, single reaction deletion was also performed by inactivating reactions one at a time and solving for growth.

Flux variability analysis (FVA) helps to establish theoretical limits on various fluxes for a given phenotype. While FBA gives one set of flux values, FVA shows the extent by which they may vary for the same phenotype prediction. We performed FVA for cell growth and identified the essential reactions.

3.3 Results and Discussion

3.3.1 Reconstructed Metabolic Network

The genome of *M. maripaludis* S2 is a circular chromosomal DNA with 1722 protein-coding genes (ORFs or Open Reading Frames). Our metabolic model comprises 605 metabolites (556 internal and 49 external) and 570 reactions (521 intracellular and 49 transport) across 52 distinct pathways (Appendix B). It accounts for 518 ORFs out of the 1722 presently known for protein-coding genes (approx. 30 % coverage). 498 ORFs out of the 518 have annotation in different databases while 20 of them were assigned functions by us based on sequence similarity searches. Basic features of *M. maripaludis* S2 genome and in silico reconstructed model are summarized in Table 3.1.

The reactions cover central metabolism, energy metabolism, amino acid metabolism, nucleotide metabolism, vitamin and cofactor metabolism, and production of other secondary metabolites (Table 3.2). The average confidence score for the 570 reactions is 4.67, which indicates that the majority of the reactions added in the model are built on strong evidence.

Table 3.1 Basic features of *M. maripaludis* S2 genome and its in silico reconstructed model

Feature	Number
Genome features	
Genome size (bp)	1,661,137
% GC content	33.1
Open Reading Frames (ORFs) (coverage %)	1722 (88.9 %)
In silico reconstruction	
Total reactions	570
Protein coding genes (ORFs)	518
% ORF coverage	30
Reaction associated with genes	464
Reaction not associated with genes	106
Intracellular/extracellular metabolites	556/49
Transport reactions	49

Table 3.2 Functional classification of the metabolic reactions in a genome-scale model of *M. maripaludis* S2

Central metabolism	40	*Nucleotide metabolism*	82
Glycolysis/Gluconeogenesis	24	Purine	45
Citrate cycle (TCA cycle)	5	Pyrimidine	37
Pentose phosphate pathway	11	*Metabolism of cofactors and vitamins*	127
Energy metabolism	*38*	*Others*	152
Methane metabolism	28	Selenocompound and glutathione metabolism	9
Nitrogen metabolism	6	Metabolism of terpenoids and polyketides	9
Oxidative phosphorylation	4	Xenobiotics biodegradation and metabolism	6
Amino acid metabolism	131	Pyruvate metabolism	6
Valine, leucine and isoleucine	26	Other carbohydrates metabolism	34
Alanine, aspartate and glutamate	11	Lipid metabolism	7
Glycine, serine and threonine	11	tRNA charging	26
Cysteine and methionine	17	Others (Biomass formulation)	7
Arginine and proline	14	Total	570
Phenylalanine, tyrosine and tryptophan	28		
Histidine	10		
Lysine	12		
Asparagine and glutamine	2		

The transport reactions were based on the available genome annotations and known physiological information for various metabolites such as formate, acetate, cobalt, molybdenum, iron, bicarbonates, and sulfates [4–6, 28]. Acetate was

included in this list based on the work by Shieh and Whitman [29], who demonstrated a pathway for acetate assimilation in *M. maripaludis*.

Our initial network (draft model) included 397 unique reactions from KEGG [5]. It lacked reactions essential for the synthesis of several biomass precursors (e.g. proline, methionine, glycine, histidine, and cysteine), cofactors [coenzyme B, coenzyme M, flavin adenine dinucleotide, tetrahydromethanopterin (THMPT)], and vitamins (folic acid, riboflavin, cobalamin) required for enzymatic activities and growth. Therefore, 124 more reactions were added from METACYC [6] and published literature [15, 29–38] to fill these gaps for achieving in silico growth. This gap-filling process was based on a thorough biological understanding of the various intracellular functions in methanogenic species. For instance, the genome annotation studies by Hendrickson et al. [4] report that only one ORF (*metE*, MMP0401) is present in *M. maripaludis* for methionine biosynthesis, but the other literature [32] mentions that cystathionine ß-lyase (*metC*, 4.4.1.8) also plays a key role. Our BLASTp similarity search (e-value = 10^{-17}) showed that an ORF (MMP1072) in *M. maripaludis* S2 matches the sequence of cystathionine ß-lyase present in *Methanobacterium sp.* AL-21. Thus, the reactions corresponding to MMP1072 were also added to complete the synthesis of methionine. Similarly, the synthesis of proline from ornithine was completed by adding the pathway reactions from a closely related methanogen [31]. No ortholog is known to code for histidinol-phosphatase (*his*J, 3.1.3.15) required for histidine synthesis. However, the reactions catalyzed by histidinol-phosphatase were also added to the model, because all other genes (*hisA*, *B*, *C*, *D*, *E*, *F*, *G*, *H*, *I*) involved in the pathway are already reported [5, 6] and hence the presence of *hisJ* locus is also expected. All such reactions based on assumptions were assigned low confidence scores in the model.

M. maripaludis S2 (mmp) uses the modified Wood-Ljungdahl pathway for synthesizing acetyl coenzyme A (acetyl-CoA) from two molecules of CO_2 [39]. As shown in Fig. 3.2, the methyl carbon of acetyl-CoA comes from methylTHMPT, an intermediate produced by formaldehyde and THMPT. The carboxyl carbon of acetyl-CoA comes from the reduction of CO_2 to carbon monoxide (CO) via carbon monoxide dehydrogenase/acetyl-CoA synthase (CODH/ACS), a key enzyme in

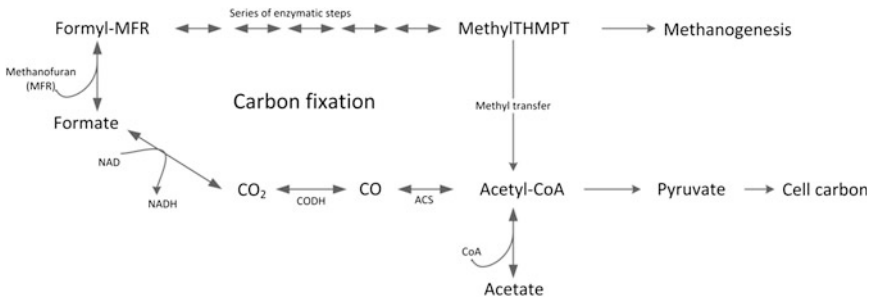

Fig. 3.2 Wood-Ljungdahl pathway for CO_2 fixation occurring in *M. maripaludis*

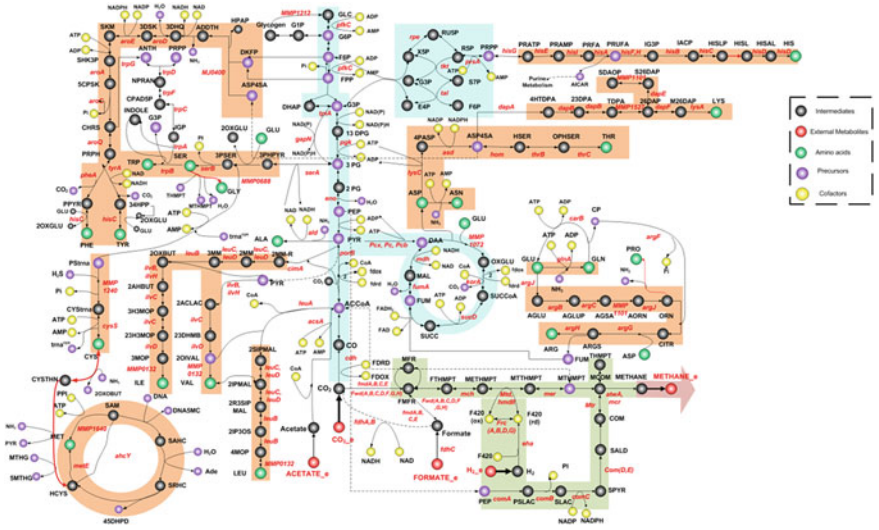

Fig. 3.3 Central metabolism, amino acid metabolism, and methane metabolism shown in different shades along with GPR associations for *M. maripaludis* S2. The figure shows how CO_2 can act as the sole carbon substrate for growth and energy production (see Appendix B for abbreviations and reactions detail)

methanogenesis. CODH catalyzes the reduction of CO_2 to CO and ACS helps in the condensation of CO, methyl group, and coenzyme A to acetyl-CoA. Based on the work by Shieh and Whitman [29], acetyl-CoA can also be synthesized from acetate by acetyl-CoA synthetase, which then participates in the synthesis of biomass precursors for growth and methanogenesis.

Figure 3.3 shows the major metabolic pathways in our model along with their GPR associations. They include glycolysis, citrate cycle, amino acid biosynthesis, pentose phosphate pathway, and methane metabolism. The map also contains useful information about the roles of various pathways in substrate utilization and product formation. For instance, it confirms that CO_2 can indeed be the sole carbon source with H_2 as the reducing agent. In addition to H_2, formate may also act as an electron donor because of the following formate-dependent lyase activity common in methanococci [40].

$$HCO_2^- + H_2O \rightarrow HCO_3^- + H_2 \Delta G = +1.3\,\text{kJ} \tag{3.2}$$

In addition to Eq. 3.2, two potential pathways for formate-dependent hydrogen production in *M. maripaludis* S2 reported by Lupa et al. [22] were also included. Both pathways include the formation of reduced coenzyme F_{420} ($F_{420}H_2$). However, no biochemical or genomic evidence exists for flavin oxidoreductase, the enzyme responsible for formation of $F_{420}H_2$. This, in our judgment, can be explained by the presence of two formate dehydrogenases in *M. maripaludis* S2,

namely *fdhA* and *fdhB*. In the process of oxidizing formate to bicarbonates by these hydrogenses, one electron is donated to NAD or coenzyme F_{420} to generate NADH or $F_{420}H_2$. Alternative way of supplying hydrogen to methanogens is via water splitting, which can be used to generate protons and electrons for reduction of CO_2 to methane. For instance, Cheng et al. [41] reported electromethanogenesis in *Methanobacterium palustre*. Since, no evidence exists so far on ability of *M. maripaludis* to use water as a H_2 source, we did not include this reaction in our metabolic map as well as model. However, we are currently doing experiments to observe if *M. maripaludis* is capable of performing microbial electrosynthesis. Once such an evidence exists, the model can be extended easily to allow microbial electrosynthesis via the following reaction.

$$CO_2 + 8H^+ + 8e^- \rightarrow CH_4 + 2H_2O$$

In total, 20 new ORFs with suggested annotations in Table 3.3 were identified in *M. maripaludis* S2 using BLASTp similarity searches (e-value cutoff 10^{-5}) Table 3.3. These include the loci that have been designated as "unique protein with unknown function" by Hendrickson et al. [4] to allow for the possibility of unknown pathway links. In spite of our best efforts in exhausting the known information and updating the model continuously, the model still has 163 dead-end metabolites. However, it has the highest ORF coverage of the existing models for other organisms.

3.3.2 Model Validation

Experimental conditions of Kral et al. [21] and Lupa et al. [22] were simulated using our model as follows. Unless dictated otherwise by the experimental conditions, fluxes for all metabolites were unrestricted. Growth Associated Maintenance (GAM) was set as 30 mmolATP/gDCW-h, where DCW stands for dry cell weight. For simulating anaerobic experiments, O_2 uptake flux was set as zero. Using the hydrogen uptake rates of *M. maripaludis* reported by Kral et al. [21] as lower bounds in our model, specific growth rates (/h) and MERs with and without organics were predicted. For each of these two predictions, a growth yield (gDCW/molCH_4) was computed. These were then compared with average growth yields computed from the data of Lupa et al. [22] for the two scenarios. As shown in Fig. 3.4, the predictions from our model match closely with the experimentally observed growth yields.

Lupa et al. [22] measured MERs at various times during the growth of *M. maripaludis* S2. These experimentally measured MERs were limited as upper bounds in our model along with an assumed value of Non-Growth Associated Maintenance (NGAM). The NGAM value that gave the closest agreement for the growth values was 0.4 mmolATP/gDCW-h, which was fixed in the model. The resulting match between the experimental and predicted specific growth rates is

Table 3.3 ORFs with suggested annotations for *M. maripaludis* S2

Open reading frame (ORF)	Suggested annotation	E-value (cut-off 10^{-5})	NCBI accession number
MMP0281	ATPase	0	NP_987401
MMP0413	Methyl-accepting chemotaxis sensory transducer	0	NP_987533.1
MMP0487	Methyl-accepting chemotaxis sensory transducer	0	NP_987607.1
MMP0788	Methyl-accepting chemotaxis protein (MCP) signalling domain	0	NP_987908.1
MMP1716	5,10-methenylTHMPT hydrogenase	0.00E+00	NP_988836.1
MMP1493	S-layer protein	0	NP_988613.1
MMP1122	Translation-associated GTPase	2.00E−116	NP_988242.1
MMP0057	FO synthase subunit 2	5.00E−92	NP_987177.1
MMP0814	APHP domain-containing protein	8E−74	NP_987934.1
MMP0883	HEAT domain-containing protein	3E−64	NP_988003.1
MMP1653	HEAT domain containing protein	1E−46	NP_988773.1
MMP1302	Selenium binding protein	2E−40	NP_988422.1
MMP1428	Preprotein translocase subunit SecG	3E−24	NP_988548.1
MMP1300	Nucleic acid binding, OB-fold, tRNA/helicase-type	1E−15	NP_988420.1
MMP0978	Predicted RNA-binding protein	1.6E−14	NP_988098.1
MMP1077	Phosphoglucomutase/phosphomannomutase	2.00E−12	NP_988197.1
MMP1072	Aminotransferase	1.00E−17	NP_988192.1
MMP0542	Phosphoserine phosphatase	3.00E−9	NP_987662.1
MMP1358	Pyruvate formate-lyase	6.00E−07	NP_988478.1
MMP1237	Acetolactate decarboxylase	9.00E−05	NP_988357.1
MMP0339	NUDIX hydrolase	5.00E−06	NP_987459.1

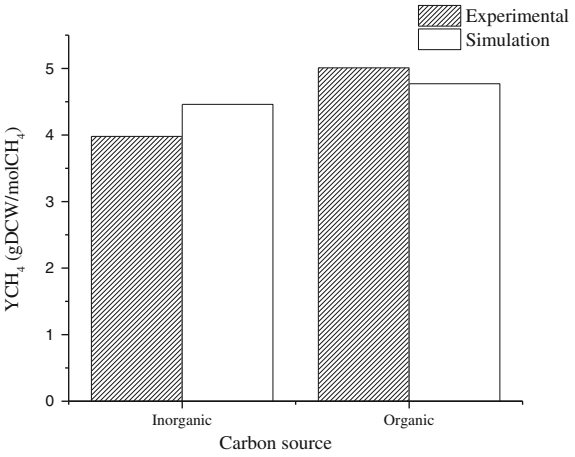

Fig. 3.4 Comparison of experimentally observed and model predicted growth yields of *M. maripaludis* under hydrogen limited condition using data from Kral et al. [21]

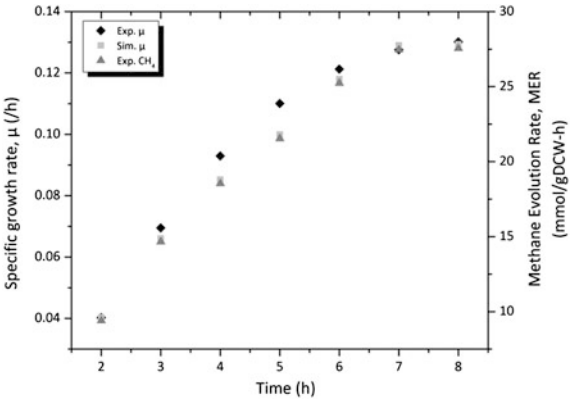

Fig. 3.5 Comparison of the specific growth rates observed in silico and *in vivo* at different time points during the growth of *M. maripaludis* S2 (experimental data from Lupa et al. [22])

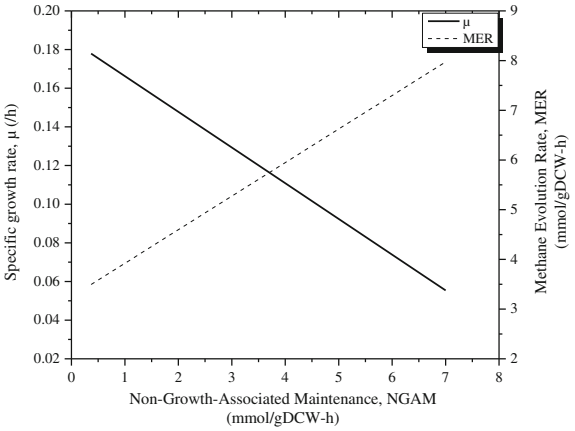

Fig. 3.6 Influence of NGAM on specific growth rates and MER

shown in Fig. 3.5. Experimental values of NGAM vary from 0.2 to 7 mmol/gDCW-h [30, 42, 43] for a microbial cell, thus our fitted estimate of 0.4 mmolATP/gDCW-h is quite acceptable. As seen in Fig. 3.6, NGAM has a significant effect on growth and methanogenesis, thus fitting the best value was necessary.

The predicted yields of methane from CO_2 are 83–85 % mol/mol from our model for the MERs reported by Lupa et al. [22]. While Stolyar et al. [12] reported a yield of 95 % based on one single experimental observation, the details regarding their experiment are insufficient for us to simulate the same in our model. For further verification of our model, gene/reaction knockout experiments performed by Haydock et al. [24], Lin and Whitman [25], and Lie and Leigh [26] were mimicked. Haydock et al. [24] created a leucine auxotroph (S52) by deleting MMP1063 (*leuA*) gene that encodes 2-isopropylmalate synthase (IPMS), the first enzyme in the biosynthesis of leucine from 2-ketoisovalerate. To emulate S52, the reactions associated with IPMS were inactivated in our model. No growth was predicted by the model for S52. However, when leucine was supplied directly to the medium by

adding a transport reaction, full growth was predicted. This validates our model concerning the essentiality of *leuA* gene in leucine production.

Lin and Whitman [25] reported that pyruvate serves as an electron donor in the absence of H_2 and formate, and the deletions of *porE and porF* affect growth and oxidation of pyruvate. To show this, hydrogen and formate uptake was set to zero and pyruvate (10 mmol/gDCW-h) was supplied in the medium. Our model could successfully predict growth rate (0.09321/h) and MER (10.166 mmol/gDCW-h). Furthermore, the reaction catalyzed by pyruvate synthase (EC number: 1.2.7.1), also known as pyruvate:ferredoxin oxidoreductase (PFOR), associated with *porE and porF* was inactivated in our model. Significant reduction in the growth (0.0188/h) and MER (9.77 mmol/gDCW-h) was predicted, which validates our model concerning the essential roles of *por*E and *por*F in maintaining wild-type growth and methanogenesis.

Lie and Leigh [26] mentioned that *nif* and *glnA* expressions depend on nitrogen availability. To simulate this diazotrophic condition, nitrogen was allowed in our model via a transport reaction. Our model correctly predicted the expressions of *nif* and *glnA* and demonstrated the ability of *M. maripaludis* to fix nitrogen, which is unique to hydrogenotrophic methanogens. In the absence of nitrogen and presence of ammonia (non-diazotrophic condition), *nif* did not express, but *glnA* expression was predicted to be high, which is also consistent with the observations of Lie and Leigh [26]. When both ammonia and free nitrogen were supplied, our model showed zero nitrogen uptake. Thus, ammonia seems to be the preferred nitrogen source. This is likely due to the fact that significant amount of energy is required for N_2-fixation as compared to ammonia. This is consistent with the lower growth rate predicted by our model for free nitrogen versus ammonia, as discussed later.

Lastly, our model showed nonzero flux of "hydroxypyruvaldehyde phosphate" during growth, which is the side product of 6-deoxy-5-ketofructose-1-phosphate (DKFP) pathway [44] and responsible for the degradation of methanococcus cells in the presence of oxygen due to the production of hydrogen peroxide (H_2O_2).

3.3.3 Minimal Media

Essential media components were identified by predicting the cell growth for zero uptake of a given extracellular metabolite. Sources for carbon, hydrogen, nitrogen, sulfur, iron salts, sodium ion, cobalt, nickel, and phosphate were found to be essential for growth (see Appendix B for full details). None of the vitamins or amino acids were essential, thus *M. maripaludis* has the ability to synthesize them. However, the presence of some vitamins and/or amino acids enhanced growth in varying extents. While pyruvate, formate, and alanine can be alternate primary carbon sources, acetate, leucine, and isoleucine can only stimulate growth. Among CO_2, pyruvate, and formate, pyruvate seems to be the most efficient carbon source for growth. Free nitrogen, ammonia, and alanine are alternate nitrogen sources. Cysteine can be an alternate sulfur source, as it reduces H_2S intake significantly.

3.3.4 Gene Essentiality and Flux Variability Analyses

The results of these analyses are represented as a gene or locus essentiality matrix indicating the essential proteins or enzymes in supplementary file (Appendix B). Of the 518 genes in our model, 278 proved essential for cell growth, and 241 non-essential. 282 of the 570 reactions proved essential for growth.

FVA showed 476 of 570 reactions (86 %) to have zero variability for maximum growth. Alternate solutions with nonzero fluxes are possible for 67 of the 356 zero fluxes. Most of these belong to citrate cycle and energy metabolism. However, only 9 of the 214 nonzero reaction fluxes can be zero in alternate solutions. This gives an indication of the robustness of our flux predictions.

3.3.5 Formate as Alternate Carbon and Hydrogen Substrate

Literature [45, 46] on *M. maripaludis* S2 mentions that this methanogen is exceptionally equipped with the enzymes for H_2 metabolism and contains genes (*Eha*, *Ehb*, *Fru*, *Frc*, *Vhu*, *Vhc*, and *Hmd*) for seven different hydrogenases. Hydrogenases catalyze the reversible reaction $H_2 \leftrightarrow 2H^+ + 2e^-$ to generate electrons for redox reactions. In another study [47], two sets of formate dehydrogenases were observed *in M. maripaludis* S2 encoded by *fdhA1B1* and *fdhA2B2*. They claimed that *M. maripaludis* S2 growth was superior on CO_2:H_2 than formate. Our model could successfully predict higher growth in the presence of CO_2 than formate irrespective of nitrogen source used (Fig. 3.7).

Hydrogen-independent growth of hydrogenotrophic methanogen *M. maripaludis* S2 in the presence of formate has been demonstrated by Costa et al. [48]. However,

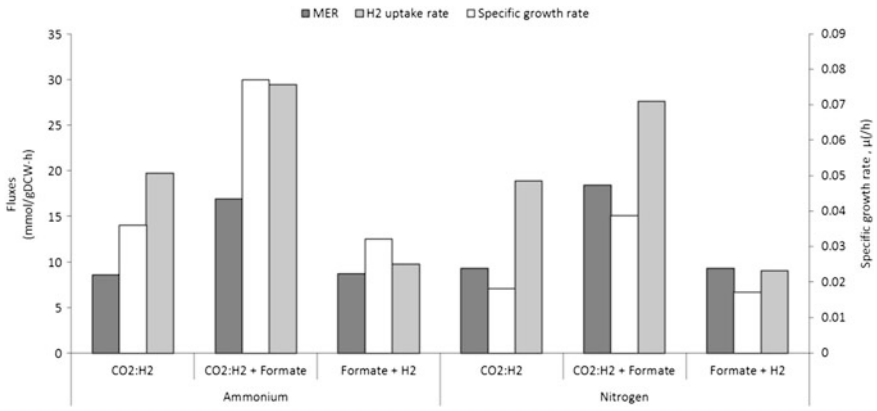

Fig. 3.7 Influence of different nitrogen sources on MERs, hydrogen uptake rates, and specific growth rates at a fixed carbon uptake of 10 mmol/gDCW-h

our model could not predict the growth in absence of hydrogen. This might be due to the existing gaps in the model or the unbalanced hydrogen in our model. However, significant reduction in hydrogen uptake rate was observed in the presence of formate (Fig. 3.7), which clearly shows the presence of formate-hydrogen lyase formate activity and formate-dependent H_2 production in *M. mariapludis* S2 as demonstrated by Lupa et al. [22].

3.3.6 *Effect of Nitrogen Sources*

Nitrogen is essential for the biosynthesis of amino acids, purines, pyrimidines, and polyamines. Nitrogen, ammonium, and alanine are known alternate sole nitrogen sources [27, 49] for *M. maripaludis*. The presence of *nif* cluster was demonstrated [50] earlier for N_2-fixation. Ammonium transporter proteins (*Amt*) encoded by MMP0065 and MMP0068 are responsible for the uptake of NH_3 or NH_4^+ from extracellular medium. Pathways also exist for ATP-dependent glutamine synthesis from NH_4^+ and glutamate via glutamine synthetase. Presence of sodium alanine symporter ensures the uptake of alanine in *M. maripaludis*.

The model could assimilate alanine as a sole nitrogen source for growth and methanogenesis. The presence of alanine dehydrogenase encoded by locus MMP1513, uniquely present in archaea, explains the ability of *M. maripaludis* to catalyze alanine to ammonia and pyruvate. Ammonia then acts as a nitrogen source and pyruvate as an intermediate carbon source. Thus, alanine can act as both carbon and nitrogen source. Our model predicts that the higher the supply of alanine, the higher the growth and MER. However, alanine is not a preferred nitrogen source, as it reduces CO_2 uptake significantly.

The specific growth rates in presence of nitrogen or ammonium as predicted from our model are shown in Fig. 3.7. Ammonium seems significantly better than free nitrogen for growth. This could be due to the additional ATP required by nitrogenases for fixing nitrogen to ammonia. This prediction also agrees with the experimental observations of Belay et al. [51] and Fardeau et al. [52] for other archaebacteria. Interestingly, methanogenesis is higher in the presence of nitrogen than ammonium as shown in Fig. 3.7. The possible reason could be changes in flux distribution due to the activation of *nif* genes, which requires the presence of an electron donor [reduced ferredoxin or fd(rd)] for reducing free nitrogen to ammonia. In addition, lower flux was observed in our model towards CO_2 to acetyl-CoA pathway indicating that reduced supply of electron donor affects growth significantly.

In the presence of ammonium, formate reduces hydrogen uptake significantly from 19.720 mmol/gDCW-h to 9.734 mmol/gDCW-h compared to CO_2:H_2. Replacing ammonium with free nitrogen further decreases the uptake to

8.99 mmol/gDCW-h as shown in Fig. 3.7. A possible explanation for this is the evolution of molecular hydrogen during N_2-fixation:

$$8\mathrm{fd(rd)} + 8\mathrm{H}^+ + \mathrm{N_2} + 16\mathrm{ATP} + 16\mathrm{H_2O} \rightarrow 8\mathrm{fd(ox)} + \mathrm{H_2} + 2\mathrm{NH_3} + 16\mathrm{ADP} + 16\mathrm{pi} \tag{3.3}$$

where, fd(rd) and fd(ox) indicate reduced and oxidized ferredoxin respectively and pi is orthophosphate generated during ATP hydrolysis.

3.3.7 Novel Strains for Enhanced Methanogenesis

Several approaches can be explored for enhancing methanogenesis: best media, enzyme activity regulation, and gene deletions or additions. As seen earlier, free nitrogen is the best source for enhancing MER. Thus, for studying MER enhancements, the carbon uptake was fixed at 10 mmol/gDCW-h in our model with unlimited supply of free nitrogen.

Figure 3.8 shows the relation between MER and growth, which was obtained for the wild type strain by maximizing MER for varying demands on biomass growth. Clearly, MER and growth compete with each other for the available carbon, and MER can only be increased at the expense of growth. With these limits in mind, we now study how the cell metabolism could be manipulated to enhance MER from its base value for the wild type strain.

Enzymes control reaction fluxes, and their activities can be altered via inhibitors, activators, coenzymes, or cofactors. Reaction fluxes were varied in our model to study the effects of enzyme activities on MER. Table 3.4 shows the top 10 reactions with the most impact on MER. All of them are essential reactions and most of them

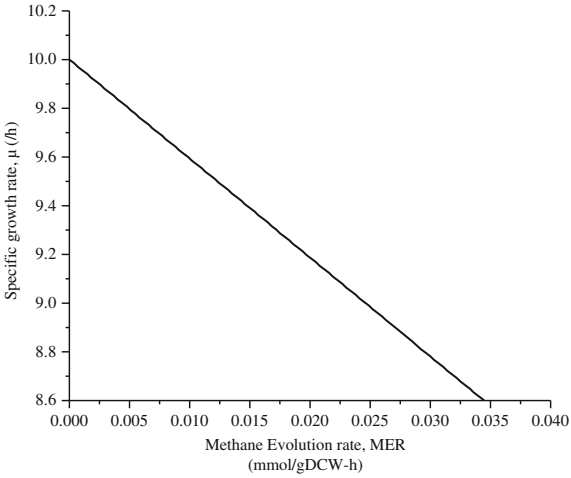

Fig. 3.8 Effect of MER on specific growth rates at a carbon uptake of 10 mmol/gDCW-h

belong to methane metabolism. Two criteria can be used to judge their effectiveness for enhancing MER. One is the ratio of ΔMER to ΔFlux, and the other is the ratio of ΔMER to ΔGrowth. The former weighs the benefits of MER against efforts required to change a reaction flux, while the latter weighs the benefits of MER against the loss of growth. Using the latter as the more desirable metric, R72 catalyzed by nitrogenase seems to be the best reaction for enhancing MER, with R53 catalyzed by 5,10-methyleneTHMPT reductase as the second best. When the flux of R72 increases, the cell uptakes more free nitrogen. It then requires more energy for growth. Since methanogenesis is the only energy-producing pathway in this organism, MER increases to supply the additional energy demand for growth.

The third approach is to increase MER by deleting the genes for one or more nonessential reactions. R53 causes reduction of 5,10-methyleneTHMPT to 5-methylTHMPT with the help of $F_{420}H_2$. Increased flux through R53 requires more F_{420}, which in turn increases the activity of coenzyme F_{420} hydrogenases coupled to the reduction of electron acceptors such as CO_2. Thus, MER increases.

Table 3.5 shows five genes whose individual or combined deletions enhance MER. For combinations of up to three genes, the deletion of *adkA* seems to be the best choice based on the ΔMER to ΔGrowth ratio. *adkA* is involved in the biosynthesis of ATP. Its deletion reduces the supply of ATP, hence MER increases to make up for the shortfall in energy. The deletion of *acd* and *mdh* together seems to be the next best option. Acetate CoA ligase encoded by *acd* plays a key role in propanoate metabolism. Since propanoate metabolism generates energy by phosphorylation of AMP, the deletion of *acd* creates a shortfall in energy supply. Thus, MER increases to supply the shortage of energy. Malate dehydrogenase encoded by *mdh* catalyzes the conversion of malate and oxaloacetate with simultaneous reduction of NAD. In the absence of *mdh*, NAD specific malic enzymes decarboxylate to form pyruvate. Pyruvate oxidation requires more energy and hence MER goes up. The third approach is to increase MER by deleting the genes for one or more nonessential reactions. R53 causes reduction of 5,10-methyleneTHMPT to 5-methylTHMPT with the help of $F_{420}H_2$. Increased flux through R53 requires more F_{420}, which in turn increases the activity of coenzyme F420 hydrogenases coupled to the reduction of electron acceptors such as CO_2. Thus, MER increases.

Table 3.5 also shows that the deletion of *ac*d and *adk*A together may lead to zero growth. Compared to flux variations, impact of gene deletions seems low. But, these can also be used in tandem to further increase methanogenesis.

3.3.8 Comparison with Other Methanogens

Table 3.6 shows a comparison of our genome-scale metabolic model for *M. maripaludis* S2 with the existing genome-scale models for three archaea, viz. *M. barkeri* [30], *M. acetivorans* [53], and *S. solfataricus* [54]. Our model has the

Table 3.4 Top 10 reactions for which MER changes with reaction flux

Reaction	Enzyme	E.C. number	Flux range	ΔFlux ($\times 10^{-2}$)	ΔMER ($\times 10^{-2}$)	ΔGrowth ($\times 10^{-3}$)	ΔMER/ΔFlux	ΔMER/ΔGrowth
R72	Nitrogenase	1.18.6.1	0.095−0.182	0.87	7.24	−1.78	8.34	−40.69
R53	5,10 methyleneTHMPT reductase	1.5.99.11	9.537−9.921	3.84	6.12	−1.51	1.59	−40.53
R360	F420-non-reducing hydrogenase	1.12.98.3	9.262−9.988	7.26	7.25	−1.79	0.99	−40.53
R55	THMPT S-methyltransferase	2.1.1.86	9.262−9.988	7.26	7.25	−1.79	0.99	−40.53
R56	Coenzyme-B sulfoethylthiotransferase	2.8.4.1	9.262−9.988	7.26	7.25	−1.79	0.99	−40.53
R57	CoB CoM heterodisulfide reductase	1.8.98.1	9.262−9.988	7.26	7.25	−1.79	0.99	−40.53
R46	F420-dependent methylene THMPT dehydrogenase	1.5.99.9	9.921−9.561	3.99	6.15	−1.52	1.54	−40.51
R45	MethenylTHMPT cyclohydrolase	3.5.4.27	9.921−9.561	3.99	6.15	−1.52	1.54	−40.51
R43	FormylmethanofuranTHMPT N-formyltransferase	1.2.99.5	9.921−9.561	3.99	6.15	−1.52	1.54	−40.51
R76	H^+-transporting two-sector ATPase	3.6.3.14	2.962−3.327	3.65	6.14	1.68	1.68	−36.58

ΔMER, ΔFlux, and ΔGrowth are the changes in methane evolution rate, reaction flux, and specific growth rate respectively from their base values for the wild type strain. The base values for the wild type strain are an MER of 9.2619 mmol/gDCW-h and growth rate of 0.01817/h for a CO_2 uptake of 10 mmol/gDCW-h. ΔFlux is the 10 % of the range over which a reaction flux can change to effect methanogenesis

Table 3.5 Effects of in silico gene knockouts on MER and cell growth

Gene deletions	Reactions	ΔMER ($\times 10^{-2}$)	ΔGrowth ($\times 10^{-3}$)	ΔMER/ΔGrowth
adkA	R243	0.59	−0.14	−59.0
acd, *mdh*	R495, R26	1.74	−0.43	−43.5
adkA, *mdh*	R243, R26	0.84	−0.21	−42.0
acd	R495	1.50	−0.37	−37.5
acd, *cimA*, *mdh*	R495, R103, R26	1.84	−0.63	−30.7
acd, *cimA*	R495, R103	1.78	−0.61	−29.7
acd, *leuB*, *cimA*	R495, R95, R103	1.78	−0.61	−29.7
mdh	R26	0.24	−0.06	−24.0
adkA, *cimA*, *mdh*	R243, R103, R26	0.95	−0.41	−23.8
adkA, *leuB*	R243, R95	0.89	−0.39	−22.3
adkA, *cimA*	R243, R103	0.89	−0.39	−22.3
adkA, *leuB*, *cimA*	R243, R95, R103	0.89	−0.04	−22.3
leuB, *mdh*	R95, R26	0.37	−0.27	−12.3
cimA, *mdh*	R103, R26	0.37	−0.27	−12.3
leuB, *cimA*, *mdh*	R95, R103, R26	0.37	−0.27	−12.3
leuB	R95	0.31	−0.25	−10.3
cimA	R103	0.31	−0.25	−10.3
leuB, *cimA*	R95, R103	0.31	−0.25	−10.3
acd, *adkA*	R495, R243	N.A.	0.00	N.A.
acd, *adkA*, *leuB*	R495, R243, R95	N.A.	0.00	N.A.
acd, *mdh*, *adkA*	R495, R26, R243	N.A.	0.00	N.A.

highest ORF coverage among the four. Clearly, large amount of annotated information is available for *M. maripaludis* genome. Among the hydrogenotrophic methanogens, methane metabolism is better studied and characterized in *M. maripaludis* [4] compared to the others. The information helped us to compare reactions/genes involved in the methanogenesis pathways of several methanogens.

The proven higher specific growth rate is a clear advantage for *M. maripaludis* compared to the other three methanogens. The model (*i*AF692) of *M. barkeri* by Fiest et al. [30] reported a specific growth of 0.071/h and MER of 8.824 mmol/gDCW-h, when hydrogen uptake was limited to 41 mmol/gDCW-h with CO_2 as the sole carbon source and cysteine as the sulfur source. Under the same conditions, our model (*i*MM518) predicted a growth of 0.0847/h and MER 18.40 mmol/gDCW-h. This highlights the extraordinary capability of *M. maripaludis* for methane

Table 3.6 Comparative analysis of *M. maripaludis* S2 model with previously modeled archaea

Features	*Methanococcus maripaludis* S2 "*mmp*"	*Methanosarcina barkeri* "*mba*"	*Methanosarcina acetivorans* "*mac*"	*Sulfolobus Solfataricus* "*sso*"
Reference	*i*MM518, this study 2013	*i*AF692, [30]	*i*MB745, [57]	*i*TU515, [54] 2012
Genome size (bp)	1,661,137	4,873,766	5,751,492	2,992,245
ORFs in the organism/ORFs in the model	1722/518	5072/692	4540/745	2978/515
ORF coverage in the model (%)	30.1	13.6	16.4	17.3
Number of reactions/metabolites in the model	570/558	619/558	756/715	718/706
Number of reactions/genes associated with methanogenesis	28/141	30/138	26/145	7/52
Known growth rate (μ/h)	0.301	0.0231	0.0288	0.0577

production. The reason could be the presence of H(2)-dependent methyleneTHMPT dehydrogenase associated with *hmd*, which the other three methanogens do not have. This enzyme helps in the reversible oxidation of molecular hydrogen to hydron. It contains neither Ni nor Fe-S cluster, but a Fe-containing cofactor, as recently characterized by Shima et al. [55]. *M. acetivorans* is incapable to grow under H_2 and CO_2. Also, no MER data are available for *M. acetivorans*, and *S. solfataricus* lacks most of the enzymes required for methanogenesis. *S. solfataricus* can utilize and assimilate C1 compounds via 3-hydroxypropionate/4-hydroxybutyrate cycle only in the presence of hydrogen and oxygen [56].

3.4 Conclusions

The first genome-scale metabolic model of *M. maripaludis* S2, a methanogen capable of consuming CO_2 as the sole carbon source for biomass and methane production using Wood-Ljunghdahl pathway, was constructed, validated, and analyzed in this work. The model allows us to study methanogenesis, N_2-fixation, and other metabolic pathways in *M. maripaludis* S2. The developed model is robust, and successfully predicted various observed phenotypes such as substrate uptake rates, MERs, and specific growth rate under different experimental conditions. The model enabled the identification of essential genes/reactions for growth and mutant strains capable of enhanced methanogenesis. A model-based comparison with three other methanogens showed the superiority of *M. maripaludis* in growth and methanogenesis.

References

1. Terzer M, ND Maynard, Covert MW, Jörg Stelling (2009) Genome-scale metabolic networks. Wiley Interdisc Rev: Syst Biol Med 3:285–297
2. Senger RS, Papoutsakis ET (2008) Genome-scale model for Clostridium acetobutylicum: Part I. Metabolic network resolution and analysis. Biotechnol Bioeng 101:1036–1052
3. Zou W, Liu L, Zhang J, Yang H, Zhou M, Hua Q, Chen J (2012) Reconstruction and analysis of a genome-scale metabolic model of the vitamin C producing industrial strain Ketogulonicigenium vulgare WSH-001. J Biotechnol 161:42–48
4. Hendrickson EL, Kaul R, Zhou Y, Bovee D, Chapman P, Chung J, Conway de Macario E, Dodsworth JA, Gillett W, Graham DE, et al (2004) Complete genome sequence of the genetically tractable hydrogenotrophic methanogen *Methanococcus maripaludis*. J Bacteriol 186:6956–6969
5. Kanehisa M, Goto S, Sato Y, Furumichi M, Tanabe M (2012) KEGG for integration and interpretation of large-scale molecular data sets. Nucleic Acids Res 40:D109–D114
6. Caspi R, Foerster H, Fulcher CA, Kaipa P, Krummenacker M, Latendresse M, Paley S, Rhee SY, Shearer AG, Tissier C et al (2008) The MetaCyc database of metabolic pathways and enzymes and the BioCyc collection of pathway/genome Databases. Nucleic Acids Res 36: D623–D631
7. Scheer M, Grote A, Chang A, Schomburg I, Munaretto C, Rother M, Sohngen C, Stelzer M, Thiele J, Schomburg D (2011) BRENDA, the enzyme information system in 2011. Nucleic Acids Res 39:D670–D676
8. Altschul SF, Gish W, Miller W, Myers EW, Lipman DJ (1990) Basic local alignment search tool. J Mol Biol 215:403–410
9. Lee D-Y, Yun H, Park S, Lee SY (2003) MetaFluxNet: the management of metabolic reaction information and quantitative metabolic flux analysis. Bioinformatics 19:2144–2146
10. Li C, Courtot M, Le Novère N, Laibe C (2010) BioModels.net Web Services, a free and integrated toolkit for computational modelling software. Briefings in bioinformatics 11:270–277
11. Lee J, Yun H, Feist AM, Palsson BO, Lee SY (2008) Genome-scale reconstruction and in silico analysis of the Clostridium acetobutylicum ATCC 824 metabolic network. Appl Microbiol Biotechnol 80:849–862
12. Stolyar S, Van Dien S, Hillesland KL, Pinel N, Lie TJ, Leigh JA, Stahl DA (2007) Metabolic modeling of a mutualistic microbial community. Mol Syst Biol 3:92
13. Lombard J, Lopez-Garcia P, Moreira D (2012) Phylogenomic investigation of phospholipid synthesis in archaea. Archaea 2012:630910
14. Tenchov B, Vescio EM, Sprott GD, Zeidel ML, Mathai JC (2006) Salt tolerance of archaeal extremely halophilic lipid membranes. J Biol Chem 281:10016–10023
15. Yu J-P, Ladapo J, Whitman WB (1993) Pathway of glycogen metabolism in *Methanococcus maripaludis*. J Bacteriol 176:325–332
16. Verduyn C, Stouthamer AH, Scheffers WA, Dijken JP (1991) A theoretical evaluation of growth yields of yeasts. Antonie Van Leeuwenhoek 59:49–63
17. Jones WJ, Paynter MJB, Gupta R (1983) Characterization of *Methanococcus maripaludis* sp. nov., a new methanogen isolated from salt marsh sediment. Arch Microbiol 135:91–97
18. Xia Q, Wang T, Hendrickson EL, Lie TJ, Hackett M, Leigh JA (2009) Quantitative proteomics of nutrient limitation in the hydrogenotrophic methanogen *Methanococcus maripaludis*. BMC Microbiol 9:149
19. Reed JL, Famili I, Thiele I, Palsson BO (2006) Towards multidimensional genome annotation. Nat Rev Genet 7:130–141
20. Sivashankari S, Shanmughavel P (2006) Functional annotation of hypothetical proteins–A review. Bioinformation 1:335
21. Kral TA, Brink KM, Miller SL, McKay CP (1998) Hydrogen consumption by methanogens on the early earth. Orig Life Evol Biosph 28:311–319

22. Lupa B, Hendrickson EL, Leigh JA, Whitman WB (2008) Formate-dependent H_2 production by the mesophilic methanogen *Methanococcus maripaludis*. Appl Environ Microbiol 74:6584–6590
23. Whitman WB, Shieh J, Sohn S, Caras DS, Premachandran U (1986) Isolation and characterization of 22 mesophilic methanococci. Syst Appl Microbiol 7:235–240
24. Haydock AK, Porat I, Whitman WB, Leigh JA (2004) Continuous culture of *Methanococcus maripaludis* under defined nutrient conditions. FEMS Microbiol Lett 238:85–91
25. Lin W, Whitman WB (2004) The importance of porE and porF in the anabolic pyruvate oxidoreductase of *Methanococcus maripaludis*. Arch Microbiol 181:68–73
26. Lie TJ, Leigh JA (2003) A novel repressor of nif and glnA expression in the methanogenic archaeon *Methanococcus maripaludis*. Mol Microbiol 47:235–246
27. Lie TJ, Leigh JA (2002) Regulatory response of *Methanococcus maripaludis* to Alanine, an intermediate Nitrogen Source. J Bacteriol 184:5301–5306
28. Costa KC, Yoon SH, Pan M, Burn JA, Baliga NS, Leigh JA (2013) Effects of H_2 and formate on growth yield and regulation of methanogenesis in *Methanococcus maripaludis*. J Bacteriol 195:1456–1462
29. Shieh J, Whitman WB (1987) Pathway of acetate assimilation in autotrophic and heterotrophic methanococci. J Bacteriol 169:5327–5329
30. Feist AM, Scholten JCM, Palsson BØ, Brockman FJ, Ideker T (2006) Modeling methanogenesis with a genome-scale metabolic reconstruction of *Methanosarcina barkeri*. Mol Syst Biol 2
31. Graupner M, White RH (2001) Methanococcus jannaschii Generates L-Proline by Cyclization of L-Ornithine. J Bacteriol 183:5203–5205
32. Liu Y (2010) **A**daptations of *Methanococcus maripaludis* to its unique lifestyle. The University of Georgia
33. Hausinger RP, Orme-Johnson WH, Walsh C (1985) Factor 390 chromophores: phosphodiester between AMP or GMP and methanogenic factor 420. Biochemistry 24:1629–1633
34. Namboori SC, Graham DE (2008) Acetamido sugar biosynthesis in the Euryarchaea. J Bacteriol 190:2987–2996
35. White RH (2004) L-Aspartate semialdehyde and a 6-deoxy-5-ketohexose 1-phosphate are the precursors to the aromatic amino acids in Methanocaldococcus jannaschii. Biochemistry 43:7618–7627
36. Worrell V, Nagle D Jr (1988) Folic acid and pteroylpolyglutamate contents of archaebacteria. J Bacteriol 170:4420–4423
37. Ragsdale SW (2002) Biocatalytic One-Carbon Conversion. Encyclopedia Catal (Wiley Inc.)
38. Strassman M, Ceci LN (1964) Enzymatic formation of homocitric acid, an intermediate in lysine biosynthesis. Biochem Biophys Res Commun 14:262
39. Ladapo J, Whitman WB (1990) Method for isolation of auxotrophs in the methanogenic archaebacteria: role of the acetyl-CoA pathway of autotrophic CO2 fixation in *Methanococcus maripaludis*. Proc Natl Acad Sci 87:5598–5602
40. Belay N, Sparling R, Daniels L (1986) Relationship of formate to growth and methanogenesis by *Methanococcus thermolithotrophicus*. Appl Environ Microbiol 52:1080–1085
41. Cheng S, Xing D, Call DF, Logan BE (2009) Direct biological conversion of electrical current into methane by electromethanogenesis. Environ Sci Technol 43:3953–3958
42. Feist AM, Scholten JC, Palsson BØ, Brockman FJ, Ideker T (2006) Modeling methanogenesis with a genome-scale metabolic reconstruction of *Methanosarcina barkeri*. Mol Syst Biol 2
43. Mahadevan R, Bond D, Butler J, Esteve-Nunez A, Coppi M, Palsson B, Schilling C, Lovley D (2006) Characterization of metabolism in the Fe (III)-reducing organism Geobacter sulfurreducens by constraint-based modeling. Appl Environ Microbiol 72:1558–1568
44. Porat I, Sieprawska-Lupa M, Teng Q, Bohanon FJ, White RH, Whitman WB (2006) Biochemical and genetic characterization of an early step in a novel pathway for the biosynthesis of aromatic amino acids and p-aminobenzoic acid in the archaeon *Methanococcus maripaludis*. Mol Microbiol 62:1117–1131

45. Lie TJ, Costa KC, Lupa B, Korpole S, Whitman WB, Leigh JA (2012) Essential anaplerotic role for the energy-converting hydrogenase Eha in hydrogenotrophic methanogenesis. Proc Natl Acad Sci U S A 109:15473–15478
46. Major TA, Liu Y, Whitman WB (2010) Characterization of energy-conserving hydrogenase B in *Methanococcus maripaludis*. J Bacteriol 192:4022–4030
47. Wood GE, Haydock AK, Leigh JA (2003) Function and regulation of the formate dehydrogenase genes of the methanogenic archaeon *methanococcus maripaludis*. J Bacteriol 185:2548–2554
48. Costa KC, Lie TJ, Jacobs MA, Leigh JA (2013) H_2-independent growth of the hydrogenotrophic methanogen *Methanococcus maripaludis*. MBio 4
49. Kessler PS, Daniel C, Leigh JA (2001) Ammonia switch-off of nitrogen fixation in the methanogenic archaeon *Methanococcus maripaludis*: mechanistic features and requirement for the novel GlnB homologues, Nif I(1) and NifI(2). J Bacteriol 183:882–889
50. Lie TJ, Leigh JA (2002) A novel repressor of nif and glnA expression in the methanogenic archaeon *Methanococcus maripaludis*. Mol Microbiol 47:235–246
51. Belay N, Sparling R, Choi B-S, Roberts M, Roberts J, Daniels L (1988) Physiological and ^{15}N-NMR analysis of molecular nitrogen fixation by *Methanococcus thermolithotrophicus*, *Methanobacterium bryantii* and *Methanospirillum hungatei*. Biochimica et Biophysica Acta (BBA)-Bioenergetics 971:233–245
52. Fardeau M-L, Peillex J-P, Belaich J-P (1987) Energetics of the growth of Methanobacterium thermoautotrophicum and Methanococcus thermolithotrophicus on ammonium chloride and dinitrogen. Arch Microbiol 148:128–131
53. Satish Kumar V, Ferry JG, Maranas CD (2011) Metabolic reconstruction of the archaeon methanogen *Methanosarcina acetivorans*. BMC Syst Biol 5:28
54. Ulas T, Riemer SA, Zaparty M, Siebers B, Schomburg D (2012) Genome-scale reconstruction and analysis of the metabolic network in the hyperthermophilic archaeon *Sulfolobus solfataricus*. PLoS ONE 7:e43401
55. Shima S, Pilak O, Vogt S, Schick M, Stagni MS, Meyer-Klaucke W, Warkentin E, Thauer RK, Ermler U (2008) The crystal structure of [Fe]-hydrogenase reveals the geometry of the active site. Science 321:572–575
56. Berg IA, Kockelkorn D, Buckel W, Fuchs G (2007) A 3-hydroxypropionate/4-hydroxybutyrate autotrophic carbon dioxide assimilation pathway in Archaea. Science 318:1782–1786
57. Benedict MN, Gonnerman MC, Metcalf WW, Price ND (2012) Genome-scale metabolic reconstruction and hypothesis testing in the Methanogenic Archaeon *Methanosarcina acetivorans* C2A. J Bacteriol 194:855–865

Chapter 4
Flux Measurements and Maintenance Energy for CO_2 Utilization by *M. maripaludis*

4.1 Introduction

Genome-scale models are very useful for quantifying extracellular and intracellular fluxes, analyzing cultivation data, designing media and processes, and engineering microbial strains for enhanced production [1, 2]. However, these models need to be validated with experimental flux measurements to accurately predict intracellular metabolic fluxes [3]. While extracellular fluxes can be measured by estimating changes in external metabolite concentrations, intracellular flux measurements are difficult because ^{13}C NMR labeling is usually required [4]. We developed a genome-scale metabolic model (*i*MM518) for *M. maripaludis* S2 [5], but the model had not been fully validated due to inadequate quantitative data on uptake and production rates.

In this study, we performed batch culture experiments and quantified three key extracellular fluxes (CO_2, H_2, and CH_4) and specific growth rates of *M. maripaludis*. To the best of our knowledge, this is the first experimental study to report CO_2, H_2 consumption and CH_4 production rates with CO_2 as the sole carbon substrate. In addition, this study presents novel approaches to quantify extracellular fluxes and determine maintenance energy parameters using experimentally measured extracellular fluxes along with a genome-scale model. Using the model, we analyzed the effects of amino acids on growth rates, CO_2 utilization rates, and CH_4 production rates, and studied the distribution of carbon flux between biomass synthesis and methanogenesis.

Some content of this chapter has been reproduced with permission from Nishu Goyal, Zhou Zhi, and I A Karimi. "Flux measurements and maintenance energy for CO2 Utilization by *M. maripaludis*", Microbial Cell Factories (2015), Vol. 14, 146

N. Goyal, *In silico Modeling and Experimental Validation for Improving Methanogenesis from CO_2 via M. maripaludis*, Springer Theses,
DOI 10.1007/978-981-10-2510-5_4

4.2 Materials and Methods

4.2.1 Chemicals and Gases

All chemicals used in this study were American Chemical Society (ACS) analytical reagents purchased from Sigma-Aldrich. Pure gases (N_2, Ar) and 80/20 v/v H_2/CO_2 mixture were purchased from AIR Liquide, Singapore.

4.2.2 Strain and Medium

M. maripaludis S2 (DSM 14266) was purchased from DSMZ-German Collection of Microorganisms and Cell Cultures. Methanococcus culture medium 141 was used to cultivate the culture at 37 °C with a headspace pressure of 200 kPa under 80/20 H_2/CO_2 and constantly stirred at 180 rpm [6]. The minimal medium for the growth experiments comprised 0.34 g of KCl, 4 g of $MgCl_2{\cdot}6H_2O$, 3.45 g of $MgSO_4{\cdot}7H_2O$, 0.25 g of NH_4Cl, 0.14 g of $CaCl_2{\cdot}2H_2O$, 0.14 g of K_2HPO_4, 18 g of NaCl, 10 ml of trace elements, and 2 mg of $Fe(NH_4)_2(SO_4)_2{\cdot}7H_2O$ per liter. The trace element solution comprised 3 g $MgSO_4{\cdot}7H_2O$, 0.5 g $MnSO_4{\cdot}H_2O$, 1 g NaCl, 0.10 g $FeSO_4{\cdot}7H_2O$, 0.18 g $CoSO_4{\cdot}7H_2O$, 0.10 g $CaCl_2{\cdot}2H_2O$, 0.18 g $ZnSO_4{\cdot}7H_2O$, 0.01 g $CuSO_4{\cdot}5H_2O$, 0.02 g $KAl(SO_4)_2{\cdot}12H_2O$, 0.01 g H_3BO_3, 0.01 g $Na_2MoO_4{\cdot}2H_2O$, 0.03 g $NiCl_2{\cdot}6H_2O$, 0.30 mg $Na_2SeO_3{\cdot}5H_2O$, and 990 ml DI H_2O. Soluble carbon source and cysteine were removed and CO_2 was the only carbon source. Vitamins were also omitted [7].

4.2.3 Batch Cultivation

230 ml of medium was dispensed into 600 ml serum bottles, and sparged with 80/20 v/v H_2/CO_2 to remove dissolved oxygen and create an anaerobic atmosphere. After autoclaving at 121 °C for 20 min, the bottles were cooled to room temperature and 0.5 mg/ml of $Na_2S{\cdot}7H_2O$ was injected. To initiate the growth in minimal medium, 20 ml of inoculum (pre-cultured cells in late exponential phase) was injected into each bottle. The bottles were then pressurized with 250 kPa 80/20 v/v H_2/CO_2 and incubated at 37 °C under constant stirring at 180 rpm. Cell density and concentrations of CO_2, H_2, and CH_4 in the headspace were measured. The growth experiments were discontinued when the headspace pressure fell below 100 kPa to avoid the inflow of air into the reactor. All growth experiments were performed in duplicates accompanied by a control experiment with no inoculum.

4.2.4 Analytical Procedures

Cellular growth was monitored by measuring optical density (OD) of 1 ml culture samples during the experiments. OD was recorded at 600 nm using a double-beam UV/Vis Spectrophotometer (Hitachi Model U-2800, High Technologies America, Inc.). Our OD measurements had a standard deviation of 3.35×10^{-3}. Bottle pressure was measured using a M1 digital pressure gauge (Cole Parmer, USA) with sensitivity of 10^{-4} bar. Headspace gases were analyzed with an Agilent 7890A series SRI Instrument GC equipped with three columns (a Porapak Q 80/100 SS packed column of size 6 ft L × 1/8″ OD × 2 mm ID, a Molecular Sieve 5A 80/100 SS packed column of size 3 ft L 1/8″ OD 2 mm ID, and a Hayesep T 80/100 UM column of size 0.5 m L 1/8″ OD 2 mm ID) and a thermal conductivity detector with electronic pneumatic control (EPC). The carrier gas (Ar) was continuously supplied at 100 psig. N_2 was supplied at 30 psig to act as the actuation gas to compensate for the pressure and volume differences between the injected sample and required standard. The GC oven was maintained at 60 °C and front detector at 150 °C. 1 ml of gas samples were drawn from the bottles using gas airtight microsyringes (Hamilton Samplelock syringe), and analyzed immediately in GC. The GC was calibrated for dry gas compositions (% v/v) using the series of gas standards.

4.2.5 Cell Growth Measurements

To estimate specific growth rate (μ), OD was measured at various time points. Lupa et al. [8] have reported an experimentally measured value ($1\mathrm{OD}_{600\,\mathrm{nm}} = 0.34\ \mathrm{g\ DCW}/L$) for converting OD to dry cell biomass specifically for *M. maripaludis* S2. Using this, the measured OD values were converted to biomass given by X (gDCW) = OD × 0.34 g/L × culture volume and specific growth rate (dX/dt)/X was computed by curve-fitting and differentiating the time profile.

4.2.6 Calculation of Extracellular Fluxes

Estimating extracellular fluxes from a cell culture study is not straightforward as gases are distributed into both aqueous media and headspace. The fraction of gases in the aqueous medium depends on bottle temperature, pressure, mixing speed, and the solubility and dissociation properties of the gases in water. In order to estimate fluxes precisely, we simulated the dynamics of a 600 ml reactor using Aspen HYSYS V8.2 [9] for the entire experiment. The block flow diagram for this simulation is shown in Fig. 4.1. This method can be also used for all hydrogenotrophic methanogens that can grow on CO_2 as the sole carbon substrate.

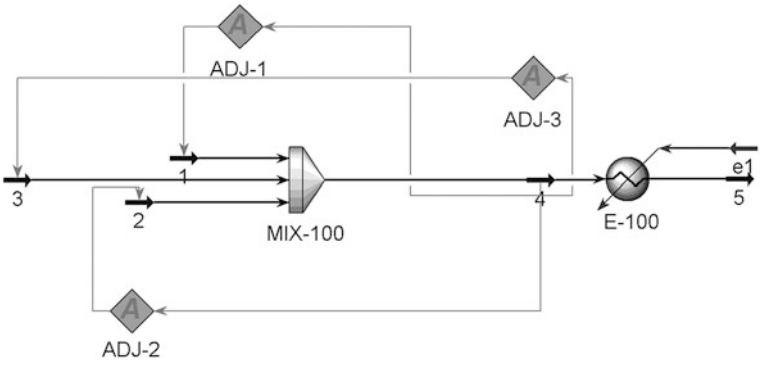

Fig. 4.1 Block flow diagram in Aspen Hysys for simulating the dynamics of a batch reactor

We simulated this initial state of the bottle by mixing sufficient amounts of pure water (stream 2), 80/20 H_2/CO_2 (stream 1), and pure CO_2 (stream 3). The flows of streams 1 and 2 were adjusted to achieve 350 ml headspace and 250 ml liquid medium, while the flow of stream 3 was adjusted to make the amount of CO_2 in the headspace exactly equal to that supplied in stream 1. We measured culture OD, bottle pressure, bottle temperature, and headspace gas compositions. At each time point, we set stream 1 composition to be the same as the headspace composition (dry basis), the temperatures of streams 1, 2, and 3 as 37 °C, and the pressures of streams 1, 2, and 3 using the measured pressure. Then, we computed the total moles of H_2 and CH_4 in the bottle at each time point as the sum of moles of H_2 (CH_4) in the headspace from Hysys and moles of H_2 (CH_4) in the aqueous medium from Hysys. For computing the total moles of CO_2 in the bottle, we also accounted for the high solubility (1.05 g/L) and dissociation of CO_2 into bicarbonates (HCO_3^-) and carbonates (CO_3^{2-}). The initial pH of the growth culture was measured as 5.6, and it remained constant throughout the experiment. Therefore, $[H^+]$ was fixed at $10^{-5.6}$ for the above calculations. Then, $[H_2CO_3]$ obtained from Aspen Hysys was used to compute other ionic concentrations. The total amount of CO_2 at time t was computed as the sum of $n(CO_2)$ from Aspen Hysys, HCO_3^-, and CO_3^{2-}. The fluxes $v_i = 1/X(t) \cdot dn(i)/dt$ for CO_2 and H_2 consumption and CH_4 production were computed by plotting the time profiles of total moles of CO_2, H_2, and CH_4, where $n(i)$ is the moles of species i (CO_2, H_2, or CH_4) in the bottle and $X(t)$ is the dry cell mass (gDCW) at time t.

4.2.7 Parameter Estimation for iMM518

*i*MM518 is a genome-scale in silico metabolic model developed for *M. maripaludis* and is available in BioModel database as MODEL1304120000 [5]. It comprises 570 reactions and 556 distinct metabolites, and covers 518 (∼30 %) of the known

1722 open reading frames (ORFs). We implemented *i*MM518 in GAMS (build 38380/38394) and used CPLEX and BARON respectively as the solvers for various linear and nonlinear optimization problems. *i*MM518 uses two energy parameters: GAM and NGAM. We showed how the experimental data on fluxes and growth can be integrated with an in silico model (*i*MM518 in this case) to estimate GAM and NGAM. First, we used the time profiles of extracellular fluxes and specific growth rates to obtain a regression for each flux with growth rate, and estimated experimental growth rates for various CO_2 uptake rates.

For flux balance analysis, we assumed the cellular objective to be maximum biomass. Then, to predict cell growth rate for a given CO_2 uptake rate, we solved the following LP (Linear Programming) using *i*MM518.

$$\text{Maximize } Z = \sum_{j=1}^{J} c_j v_j \text{ subject to } S \cdot v = b \tag{4.1}$$

where, Z is the cellular objective that is represented as a weighted sum of metabolite fluxes $v_j (j = 1, 2, \ldots, J)$ with weights c_j, S is an $I \times J$ matrix of stoichiometric coefficients of the metabolic reactions, I is the number of metabolites, J is the number of metabolic reactions, v is a $J \times 1$ vector of reaction fluxes, and b is a $I \times 1$ vector of net metabolite fluxes.

The linear CO_2 flux versus growth rate relationship estimated in earlier experiments showed that cell growth was zero for a CO_2 uptake rate below 23.51 mmol/gDCW-h, and we computed NGAM as the amount of energy spent for maintenance without growth. For estimating GAM, we selected twelve CO_2 uptake rates $v^k_{CO_2} = b^k_{CO_2}, k = 1, 2, \ldots, 12$. Using the CO_2 flux versus growth rate expression, we computed respective experimental growth rates ($b^k_G, k = 1, 2, \ldots, 12$). We estimated the experimental fluxes ($b^k_{CH_4}$ and $b^k_{H_2}, k = 1, 2, \ldots, 12$) for CH_4 and H_2 at these b^k_G using the linear expressions for CH_4 and H_2 fluxes versus growth rates. Further, we fixed the CO_2 uptake rates inside *i*MM518 to predict cell growth rates ($v^k_G, k = 1, 2, \ldots, 12$) and fluxes for CH_4 ($v^k_{CH_4}$) and H_2 ($v^k_{H_2}$) for varying values of GAM. For each GAM value, we used these model predictions to compute a weighted sum of squares of errors (SSE) as follows:

$$\text{SSE(GAM)} = \sum_{k=1}^{12} [\gamma^2_G (v^k_G - b^k_G)^2 + \gamma^2_{CH_4} (v^k_{CH_4} - b^k_{CH_4})^2 + \gamma^2_{H_2} (v^k_{H_2} - b^k_{H_2})^2] \tag{4.2}$$

where, γ_G = 3 gDCW/gDCW, $\gamma_{CH_4} = 0.016$ g/mmol, and $\gamma_{H_2} = 0.002$ g/mmol. The GAM value with the minimum SSE was our best estimation for the growth energy required by *M. maripaludis*.

4.3 Results and Discussion

4.3.1 Cell Growth

M. maripaludis grew extremely well on CO_2 without any complex substrates, such as acetate and yeast extract. The measured cell growth profile for *M. maripaludis* is shown in Fig. 4.2. The dry cell biomass increased by 15.49 mg in 7 h. The doubling time was about 2 h, which is consistent with the literature [10].

The lag phase duration varied with the state of inoculum, and found to be the shortest for an inoculum from the late exponential phase. Figure 4.2 also shows the concentration profiles (% v/v) of CO_2, H_2, and CH_4 in the headspace of the reactor over a period of about 7 h. The headspace pressure dropped from 250 to 100 kPa. The headspace contained 80/20 v/v H_2/CO_2 at time zero. The metabolic/biocatalytic action of *M. maripaludis* increased methane concentration in the headspace to approximately 30 % v/v at the end of 7 h.

As the headspace pressure decreased with time, both growth rates and extracellular fluxes decreased (Fig. 4.3). The maximum growth rate was estimated to be 0.50 ± 0.05/h for a CO_2 uptake of 132.13 ± 15.13 mmol/gDCW-h, H_2 uptake of 423.06 ± 44.94 mmol/gDCW-h, and CH_4 production of 105.61 ± 17.75 mmol/gDCW-h. Kral et al. [11] reported a H_2 uptake of 28.8 mmol/gDCW-h in inorganic media. However, they did not state the growth phase for this rate. Our observed H_2 uptake was 423.06 ± 44.94 mmol/gDCW-h in the early exponential phase, and 107.5 ± 44.94 mmol/gDCW-h at the end of 7 h, suggesting that the rate reported by Kral et al. [11] might be measured for a late exponential phase. Lupa et al. [8] reported MERs ranging from 9.40 to 27.55 mmol/gDCW-h for cell growth rates of 0.04 to 0.13/h, which is close to our MER of 27.19 ± 17.75 mmol/gDCW-h for a growth rate of 0.064 ± 0.049/h in the late exponential phase. Apart from these two studies, no other data have been reported in the literature for the uptake and production rates of *M. maripaludis*. Thus, our study is the first to give a full range of comprehensive growth and flux data for *M. maripaludis*. In fact, we could not find

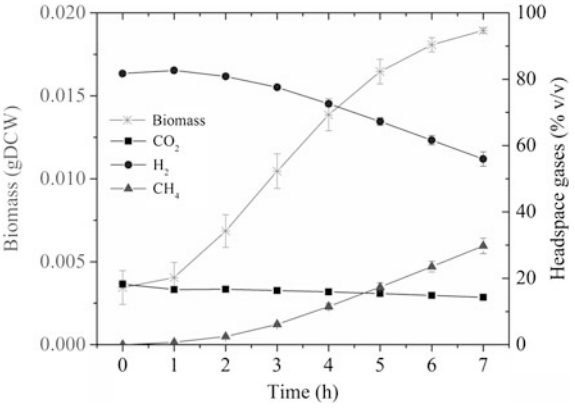

Fig. 4.2 Profiles of headspace gas compositions and biomass of *M. maripaludis* S2 in batch cultures under minimal media conditions using CO_2 as the sole carbon substrate

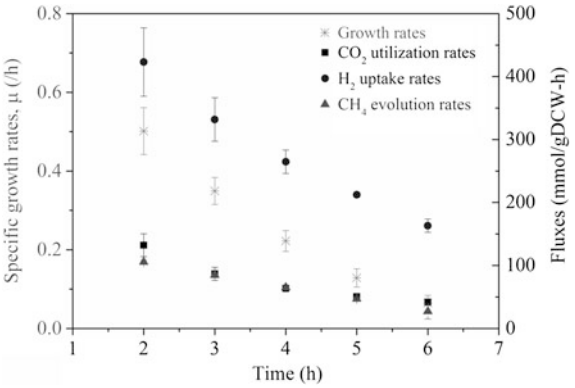

Fig. 4.3 The time profiles of specific growth rates and corresponding extracellular fluxes (CO_2, H_2, and CH_4)

similar data for any other methanogen except for one study [12] on *M. barkeri*, which reported a maximum H_2 uptake rate of 41 mmol/gDCW-h with a corresponding CO_2 uptake rate of 11.61 mmol/gDCW-h and CH_4 production rate of 8.82 mmol/gDCW-h. Our observed fluxes are one order of magnitude higher than those reported for *M. barkeri*, which could be attributed to the doubling time of *M. maripaludis* ($\sim$2 h) being much shorter than that of *M. barkeri* ($\sim$30 h).

From the plot of dry cell weight (g) versus methane produced over time, we obtained a growth yield of 3.549 $\pm$ 0.149 gDCW/molCH_4 for *M. maripaludis* during the exponential phase. Table 4.1 shows a comparison of growth yield and specific growth rate for different methanogens. The yield of *M. maripaludis* matches well with the yield reported for other hydrogenotrophic methanogens growing on H_2/CO_2 in batch cultures [13, 14]. Although a much higher yield on H_2/CO_2 (8.7 $\pm$ 0.8 gDCW/mol CH_4) was reported in *M. barkeri* [15], the specific growth

Table 4.1 Quantitative comparison of growth yields and specific growth rates for some methanogens

Organism	Substrate	Yield, Y_{CH_4} (gDCW/molCH_4)	Specific growth rate, μ (/h)	Reference
M. thermoautotrophicum	H_2, CO_2	1.6–3	0.690	[13]
M. bryantii	H_2, CO_2, organic supplements	2.4	0.031	[16]
M. str AZ	H_2, CO_2	2.32	0.110	[17]
M. barkeri	H_2, CO_2	8.7	0.058	[15]
M. formicicum	H_2, CO_2, organic supplements	3.5	0.060	[18]
M. maripaludis	H_2, CO_2	3.54	0.346	This study

rate of *M. maripaludis* observed in this study (0.346/h) was 5.97-fold higher than that in *M. barkeri* (0.058/h) [15]. A high specific growth rate suggests that *M. maripaludis* can grow rapidly and have good potentials for industrial and environmental applications.

4.3.2 Extracellular Fluxes

Using the data from Fig. 4.3, the extracellular fluxes (CO_2, H_2, and CH_4) are correlated linearly with specific growth rates in Fig. 4.4. Using these linear correlations, we obtained the following relations among the extracellular fluxes:

$$v_{H_2}/v_{CO_2} = 2.858 + 64.759/v_{CO_2} \tag{4.3}$$

$$v_{CH_4}/v_{CO_2} = 0.854 + 1.855/v_{CO_2} \tag{4.4}$$

Equation 4.4 suggests that the fraction of CO_2 conversion to CH_4 decreases with increase in CO_2 uptake rate (or equivalently cell growth). This is consistent with the fact that cell growth competes with methanogenesis for carbon utilization [5]. When cell growth is low, most of the carbon is diverted to produce energy for maintenance via methanogenesis, resulting in a higher CH_4 yield, and vice versa. Our observed conversion rate for maximum growth rate is 0.868, which is higher than 0.810 reported for *M. barkeri* in a chemostat culture grown on H_2/CO_2 [19].

Gas-to-liquid mass transfer of O_2, CO_2, H_2, N_2 etc. plays an important role in the cultivation of microbes [20]. Various factors such as gas-liquid interfacial area, mixing, temperature, and pressure affect this mass transfer. Thus, we expected higher uptake rates of CO_2 and H_2 in *M. maripaludis* with enhanced mass transfer. To confirm this, we tested the effect of mixing and gas-liquid interfacial area on the

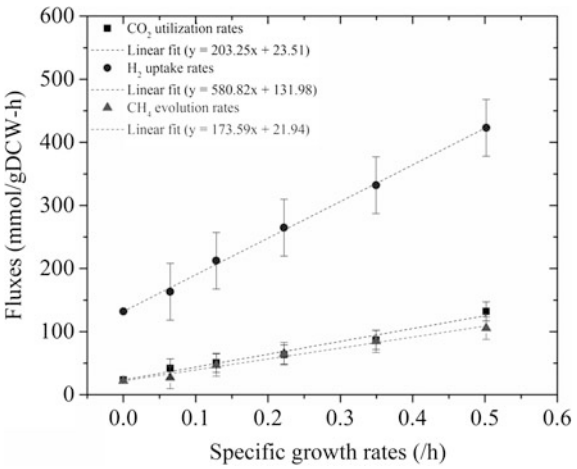

Fig. 4.4 Linear correlations between extracellular fluxes and specific growth rates

growth and metabolism of *M. maripaludis* S2 at 37 °C. Increasing the gas-liquid interfacial area by positioning the bottle reactor from vertical to horizontal roughly doubled MER, while shaking the reactor increased it multiple folds (data not shown).

4.3.3 GAM, NGAM, and ATP Gain

Microorganisms carry out catabolic oxidation-reduction reactions to obtain energy for growth and cell maintenance. These energy usages are captured in a genome-scale model in the form of two parameters, Growth Associated Maintenance (GAM mmol ATP/gDCW) and Non-Growth Associated Maintenance (NGAM mmol ATP/gDCW-h). GAM represents the energy required for the polymerization of macromolecules, such as DNA, RNA, proteins, and glycogen, during growth. It appears as the stoichiometric coefficient of ATP in the reaction representing biomass formation (cell growth) in *i*MM518. In contrast, NGAM represents the energy (mmol ATP/gDCW-h) required for cell repair, motility, maintenance of ion gradients etc., which the cell uses in addition to GAM [21, 22].

While it is possible to theoretically estimate GAM, it is not possible to estimate NGAM. Using a literature procedure [23], we estimated GAM as 30.0 mmol ATP/gDCW for *M. maripaludis*. Although literature did not report any values for GAM and NGAM for *M. maripaludis*, we were able to estimate them using *i*MM518 and with our comprehensive experimental data in this study. Our earlier validation of *i*MM518 was based on limited biomass growth data and phenotypic observations on gene knock-outs due to the unavailability of experimentally measured fluxes [5]. In this study, we are presenting a novel procedure to estimate GAM and NGAM precisely for *M. maripaludis*, and validating our model predictions for extracellular fluxes.

Our experiments indicated that cell growth rate was zero at a CO_2 uptake of 23.51 mmol/gDCW-h, and the non-growth maintenance energy that gave zero growth prediction from *i*MM518 was 7.836 mmol ATP/gDCW-h. Thus, NGAM was calculated as 7.836 mmol ATP/gDCW-h. NGAM was then fixed in the model and total SSE (TSSE) was calculated for a range of GAM values. Figure 4.5 shows how TSSE varied with GAM. TSSE was minimum at GAM = 27.14 mmol ATP/gDCW, which is the best estimate of GAM from our experiments. The deviations in H_2 uptake predictions contributed the most (67.4 %) to the minimum TSSE = 0.044, followed by those in CH_4 evolution rates (31.7 %). The prediction of biomass growth from the model matched almost exactly with the experimental values. Our estimated GAM of 27.14 mmol ATP/gDCW-h agrees very well with the theoretical estimate of 30.0 mmol ATP/gDCW-h) [5] for *M. maripaludis*. Table 4.2 lists GAM and NGAM reported for selected microorganisms in the literature.

A common method for estimating GAM and NGAM is to measure substrate uptake fluxes (mmol substrate/gDCW-h) at different growth rates and use an estimated ATP gain (mol ATP/mol substrate). However, the difficulty with this

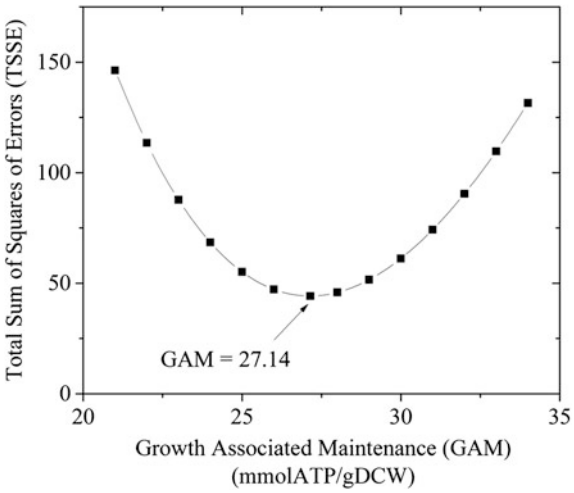

Fig. 4.5 The variation of TSSE with GAM with the minimum at GAM = 27.14 mmol/gDCW for NGAM = 7.836 mmol/gDCW-h

Table 4.2 Comparison of our estimated GAM and NGAM for *M. maripaludis* with those reported for other model organisms

Organism	Substrate	GAM (mmol/gDCW)	NGAM (mmol/gDCW.h)	Ref.
Escherichia coli	Glucose	59.81	8.39	[24]
Lactococcus lactis	Different sugar substrates e.g. mannose, galactose, sucrose, lactose, etc.	18.15	1	[25]
Methanosarcina barkeri	Methanol or acetate or H_2/CO_2 or pyruvate	70	1.75	[12]
Methanosarcina acetivorans	CO or methanol	65	2.5	[26]
Methanococcus maripaludis	H_2/CO_2	27.14	7.836	This study

approach is that precise values for ATP gains are unavailable for most microbes including *M. maripaludis*, as it is difficult to assess the amount of ATP generation per mole of substrate or product. In contrast, our approach combines experimentally measured values along with a genome-scale model to estimate NGAM and GAM without requiring an ATP gain. In fact, we estimated ATP gains from our NGAM as 0.33 mol ATP/mol CO_2, 0.35 mol ATP/mol CH_4, and 0.238 mol ATP/mol H_2. While the ATP gains from CO_2 and CH_4 are similar, the ATP gain from H_2 is much lower. This could be due to the deviations observed in our flux predictions for H_2 in TSSE. The value of 0.35 mol ATP/molCH_4 is in the acceptable range of 0.3–0.7 mol ATP/molCH_4 reported for microbes with autotrophic growth on

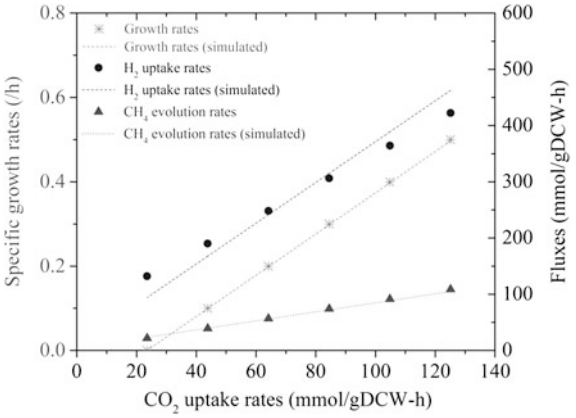

Fig. 4.6 Comparison of model predicted growth rates, H_2 uptake rates, and CH_4 evolution rates with experimentally measured values

H_2/CO_2 [27]. Kaster et al. [28] suggested an ATP gain of less than 1 mol ATP/mol CH_4 for methanogens without cytochromes (e.g. *M. maripaludis*) and more than 1 mol ATP/mol CH_4 for methanogens with cytochromes (e.g. *M. barkeri*). Thus, our estimate of 0.35 mol ATP/mol CH_4 is in agreement with the literature.

With GAM = 27.14 mmol/gDCW and NGAM = 7.836 mmol/gDCW-h in *i*MM518, we fixed CO_2 uptake rate at various values and predicted cell growth, MER, and H_2 uptake rate for the maximum biomass growth. Figure 4.6 compares experimental results with our model predictions. As we can see, our model predictions and experimental results match very well.

4.3.4 Intracellular Fluxes

Genetic and/or environmental perturbations can change extracellular or intracellular fluxes in an organism. If a genome-scale model can be used to simulate these perturbations, then it can help us study phenotypes under various culture conditions, improve microbial strains in bioprocesses, analyze multispecies relationships, etc. Therefore, we further applied *i*MM518 to study the impacts of various experimentally studied or hypothetical scenarios on the distribution of intracellular fluxes in *M. maripaludis* S2.

4.3.5 Effects of Amino Acids and Vitamins from **i***MM518*

The amino acids are known to stimulate the growth of autotrophic methanococci [7, 29], but the precise mechanisms behind these stimulations and the effects of amino acids on methanogenesis are unknown. To study these, we first modeled a culture with all amino acids. We fixed CO_2 uptake at 60 mmol/gDCW-h in

*i*MM518, and allowed unlimited uptakes for all amino acids. As compared to the scenario with no amino acids in the culture, the cell growth increased by 44.4 %, and MER increased by 11.2 %. The former is consistent with previous experimental observations [7, 29], while the latter has not been measured in the literature. *M maripaludis* prefers alanine overwhelmingly over all other amino acids, as the uptake distribution was alanine 34.6 mol%, aspartate 14.4 mol%, serine 13.7 mol%, leucine 5.8 mol%, valine 4.6 mol%, and the rest <5.0 mol%. *M. maripaludis* avoids the uptake of glycine, tyrosine, glutamate, and glutamine. These in silico observations are already confirmed experimentally on autotrophic methanococci [7].

In order to study the effects of amino acids individually, we performed 20 culture simulations with single amino acid each in *i*MM518. Interestingly, the uptakes and effects were quite different from what we observed with all amino acids in one culture simulation (Fig. 4.7). This is primarily because the microbe may prefer some amino acids over others for energetic reasons. Table 4.3 lists the changes in cell growth and MER due to each amino acid. Alanine proved the most effective for growth and MER, as it increased growth by 11.37 % and MER by 10.3 %. In contrast to the earlier scenario with all amino acids, the microbe consumed aspartate, and growth increased by 11.46 % and MER by 3.0 %. All other amino acids individually increased growth rate by less than 7 %. To evaluate the differences in the increments of growth and MER between alanine and aspartate, we examined the distribution of intracellular fluxes in both cases. Alanine served as the sole nitrogen source which has been confirmed by previous experiments [7]. On the other hand, aspartate could not supply the entire nitrogen demands of the cell, but acted as a supplement to reduce ammonium uptake by 25.9 %. Alanine increased growth primarily by supplying additional pyruvate via the reaction Alanine + NAD + H_2O ↔ pyruvate + NH_3 + NADH + H, which in turn increased the biosynthesis of cell growth precursors such as amino acids. Most of the CO_2 was diverted to methane production to provide the energy for the additional growth, and hence MER also increased. The model also predicted that the autotrophic formation of acetyl-CoA drastically reduced (approx. 65.4 %) with alanine in medium. This is consistent with previous experimental results that alanine is an efficient means of labeling pyruvate,

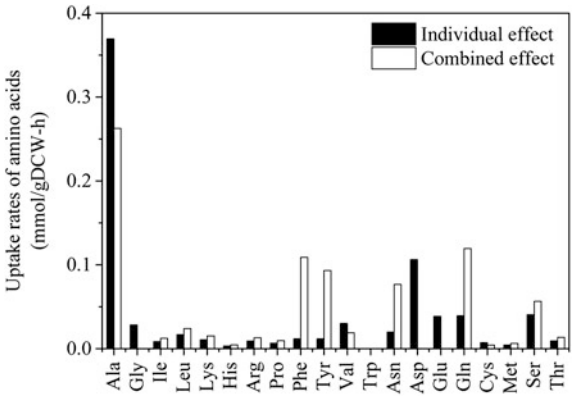

Fig. 4.7 In silico uptake rates of amino acids when supplied individually versus all-together in the culture medium

Table 4.3 Individual and combined effects of amino acids on growth rates, H_2 uptake rates, and CH_4 evolution rates as predicted by *i*MM518

Amino acids	% increment in specific growth rates	% increment in H_2 uptake rates	% increment in CH_4 evolution rates
Alanine	11.370	1.788	3.349
Glycine	2.205	0.084	0.100
Isoleucine	0.787	0.059	0.144
Leucine	1.543	0.114	0.280
Lysine	1.984	0.055	0.135
Histidine	1.512	0.006	−0.001
Arginine	2.268	−0.036	−0.070
Proline	0.315	−0.018	−0.013
Phenylalanine	6.520	0.102	0.199
Tyrosine	6.520	0.112	0.199
Valine	2.331	0.178	0.421
Tryptophan	0.157	0.002	0.003
Asparagine	3.055	0.108	0.140
Aspartate	11.465	0.691	0.966
Glutamate	0.000	0.000	0.000
Glutamine	1.827	−0.041	−0.081
Cysteine	0.567	0.033	0.051
Methionine	0.472	0.022	0.039
Serine	3.748	0.174	0.255
Threonine	1.890	0.026	0.047
Combined	45.730	2.000	4.890

as only 3–5 % of the carbon in acetyl-CoA was from CO_2 [30]. On the other hand, aspartate did not contribute significantly towards the formation of pyruvate and only 10 % drop in the flux was observed for the formation of acetyl-CoA from CO_2.

Interestingly, several amino acids such as arginine, histidine, proline and glutamine showed marginally reduced (<0.1 %) MERs. This is because the cell saved the energy for making these amino acids. Methanogenesis, being the only energy producing pathway in *M. maripaludis*, reduced MER accordingly. None of the vitamins including water-soluble riboflavin, biotin, and vitamin B12 affected growth at all. This is again validated by a previous experimental study [7], and needs no repeat experimentation.

4.4 Conclusions

Our experimental measurements of extracellular fluxes were in excellent agreement with in silico predictions of *i*MM518 at GAM = 27.14 mmol/gDCW and NGAM = 7.836 mmol/gDCW-h, thus allowed us to elucidate the physiological and

metabolic states of the cells during batch culture. With *M. maripaludis*, an instantaneous conversion efficiency of 70–95 % from CO_2 to CH_4 was observed at an optimum temperature of 37 °C, while the conversion efficiency using metal catalyst did not go beyond 70 % even at 800 °C [31]. Understanding biofuel production from methanogens will help scientists develop an immobilized enzymes based bioreactor instead of a whole cell bioreactor. It is also possible to perform methanogenesis from CO_2 at a very fast rate and avoids wasteful microbial biomass without the need for extraction of biofuels.

Biochemical conversion of CO_2 to biofuels using such strategies provides a promising route for more efficient renewable energy production. It should be noted that the cellular objective could be different depending on environmental or physiological conditions, with considerable implication on the final cellular phenotype [32]. For example, maximizing the growth rate during stationary phase may not be cellular objective. In that case it is important to identify the most plausible cellular objectives, such as minimization of ATP production, maximization of metabolite production, and minimization of nutrient uptake, and the predictive power a genomic-scale model can be greatly improved.

References

1. Price ND, Reed JL, Palsson BO (2004) Genome-scale models of microbial cells: evaluating the consequences of constraints. Nat Rev Microbiol 2:886–897
2. Pires J, Alvim-Ferraz M, Martins F, Simões M (2012) Carbon dioxide capture from flue gases using microalgae: engineering aspects and biorefinery concept. Renew Sustain Energy Rev 16:3043–3053
3. Zupke C, Stephanopoulos G (1995) Intracellular flux analysis in hybridomas using mass balances and in vitro ^{13}C NMR. Biotechnol Bioeng 45:292–303
4. Wiechert W (1996) Metabolic flux determination by stationary ^{13}C tracer experiments: Analysis of sensitivity, identifiability and redundancy. In: Doležal J, Fidler J (eds) System modelling and optimization. Springer, USA, pp 128–135. [IFIP—The International Federation for Information Processing]
5. Goyal N, Widiastuti H, Karimi IA, Zhou Z (2014) Genome-scale metabolic model of *Methanococcus maripaludis* S2 for CO_2 capture and conversion to methane. Mol BioSyst 10:1043–1054
6. Whitman WB, Shieh J, Sohn S, Caras DS, Premachandran U (1986) Isolation and characterization of 22 mesophilic methanococci. Syst Appl Microbiol 7:235–240
7. Whitman WB, Sohn S, Kuk S, Xing R (1987) Role of amino acids and vitamins in nutrition of mesophilic *Methanococcus spp*. Appl Environ Microbiol 53:2373–2378
8. Lupa B, Hendrickson EL, Leigh JA, Whitman WB (2008) Formate-dependent H_2 production by the mesophilic methanogen *Methanococcus maripaludis*. Appl Environ Microbiol 74:6584–6590
9. Hamid MKA (2007) HYSYS: an introduction to chemical engineering simulation for UTM Degree++ program
10. Jones WJ, Paynter MJB, Gupta R (1983) Characterization of *Methanococcus maripaludis sp*. nov., a new methanogen isolated from salt marsh sediment. Arch Microbiol 135:91–97
11. Kral TA, Brink KM, Miller SL, McKay CP (1998) Hydrogen consumption by methanogens on the early earth. Orig Life Evol Biosph 28:311–319

12. Feist AM, Scholten JCM, Palsson BØ, Brockman FJ, Ideker T (2006) Modeling methanogenesis with a genome-scale metabolic reconstruction of *Methanosarcina barkeri*. Mol Syst Biol 2
13. Taylor GT, Pirt SJ (1977) Nutrition and factors limiting the growth of a methanogenic bacterium (*Methanobacterium thermoautotrophicum*). Arch Microbiol 113:17–22
14. Woese CR, Magrum LJ, Fox GE (1978) Archaebacteria. J Mol Evol 11:29–30
15. Smith MR, Mah RA (1978) Growth and methanogenesis by *Methanosarcina* strain 227 on acetate and methanol. Appl Environ Microbiol 36:870–879
16. Roberton A, Wolfe R (1970) Adenosine triphosphate pools in *Methanobacterium*. J Bacteriol 102:43–51
17. Zehnder AJB, Wuhrmann K (1977) Physiology of a *Methanobacterium* strain Az. Arch Microbiol 111:199–205
18. Schauer NL, Ferry JG (1980) Metabolism of formate in *Methanobacterium formicicum*. J Bacteriol 142:800–807
19. Weimer P, Zeikus J (1978) One carbon metabolism in methanogenic bacteria. Arch Microbiol 119:49–57
20. Pauss A, Andre G, Perrier M, Guiot SR (1990) Liquid-to-gas mass transfer in anaerobic processes: inevitable transfer limitations of methane and hydrogen in the biomethanation process. Appl Environ Microbiol 56:1636–1644
21. Rozendal RA, Hamelers HV, Molenkamp RJ, Buisman CJ (2007) Performance of single chamber biocatalyzed electrolysis with different types of ion exchange membranes. Water Res 41:1984–1994
22. Rozendal RA, Hamelers HV, Buisman CJ (2006) Effects of membrane cation transport on pH and microbial fuel cell performance. Environ Sci Technol 40:5206–5211
23. Verduyn C, Stouthamer AH, Scheffers WA, Dijken JP (1991) A theoretical evaluation of growth yields of yeasts. Antonie van Leeuwenhoek 59:49–63
24. Feist AM, Henry CS, Reed JL, Krummenacker M, Joyce AR, Karp PD, Broadbelt LJ, Hatzimanikatis V, Palsson BØ (2007) A genome-scale metabolic reconstruction for *Escherichia coli* K-12 MG1655 that accounts for 1260 ORFs and thermodynamic information. Mol Syst Biol 3
25. Oliveira AP, Nielsen J, Förster J (2005) Modeling *Lactococcus lactis* using a genome-scale flux model. BMC Microbiol 5:39
26. Benedict MN, Gonnerman MC, Metcalf WW, Price ND (2012) Genome-scale metabolic reconstruction and hypothesis testing in the methanogenic archaeon *Methanosarcina acetivorans* C2A. J Bacteriol 194:855–865
27. Kates M, Kushner DJ, Matheson A (1993) The biochemistry of archaea *(archaebacteria).* Elsevier
28. Kaster A-K, Moll J, Parey K, Thauer RK (2011) Coupling of ferredoxin and heterodisulfide reduction via electron bifurcation in hydrogenotrophic methanogenic archaea. Proc Natl Acad Sci 108:2981–2986
29. Wang B, Li Y, Wu N, Lan CQ (2008) CO_2 bio-mitigation using microalgae. Appl Microbiol Biotechnol 79:707–718
30. Yang YL, Glushka JN, Whitman WB (2002) Intracellular pyruvate flux in the methane-producing archaeon *Methanococcus maripaludis*. Arch Microbiol 178:493–498
31. Wei W, Jinlong G (2011) Methanation of carbon dioxide: an overview. Front Chem Sci Eng 5:2–10
32. Leigh JA (2000) Nitrogen fixation in methanogens: the archaeal perspective. Curr Issues Mol Biol 2:125–131

Chapter 5
Diazotrophy Enhances CO_2 to Methane Conversion in *M. maripaludis*

5.1 Introduction

Flue gases from the combustion of fossil fuels in transport and industrial sectors are a major source of CO_2 emissions, and it's estimated that exhaust flue gases account for about 59.9 % of the CO_2 emissions worldwide [1]. Microbes with the ability to capture CO_2 from these sources, such as microalgae, cyanobacteria, and methanogens, are of particular interest to researchers in the field of renewable energy [2–4]. Methanogens have several advantages over other microorganism, as they can convert CO_2 to a cleaner fuel such as biogas, and separation of gaseous products do not need costly equipment. Compared with algae and cyanobacteria, methanogens do not produce excess cell biomass, i.e., methanogens serve as efficient whole cell biocatalysts.

M. maripaludis is a fast growing, mesophilic, hydrogenotrophic methanogen with some unique characteristics and advantages [5–7]. It reduces CO_2 (an electron acceptor) with H_2 (an electron donor) for growth and methanogenesis. Since nitrogen gas (N_2) is a major component of flue gases, N_2-fixation (diazotrophy) by *M. maripaludis* is of much interest and has been demonstrated in the literature [8–11]. *M. maripaludis* has been shown to switch to N_2-fixation in the absence of ammonia and alanine [10]. However, the major focus of existing literature was genetics and regulation of diazotrophy rather than its impact on methanogenesis. Furthermore, the growth rates of methanogens during N_2-fixation are usually slow. We developed a genome-scale model (*i*MM518) and predicted significant MER enhancement during N_2-fixation in *M. maripaludis* [6]. However, this has not been proven experimentally, and no study has been reported in the literature on MERs during N_2-fixation by *M. maripaludis*.

The objective of this study was to evaluate the impacts of nitrogen sources on methane production in *M. maripaludis*. The growth rates and MERs on N_2 and NH_4^+ for *M. maripaludis* were measured and compared.

N. Goyal, *In silico Modeling and Experimental Validation for Improving Methanogenesis from CO_2 via M. maripaludis*, Springer Theses,
DOI 10.1007/978-981-10-2510-5_5

5.2 Materials and Methods

5.2.1 Chemicals and Gases

All chemicals in this study were American Chemical Society (ACS) analytical reagents from Sigma-Aldrich. Pure gases (N_2, Ar) and 80/20 v/v H_2/CO_2 mixtures were purchased from AIR Liquide, Singapore.

5.2.2 Strain and Media

A pure culture of *M. maripaludis* S2 (DSMZ-German Collection of Microorganisms and Cell Cultures with accession number DSM14266) was grown on carbon-free minimal medium at 37 °C with a headspace pressure of 200 kPa 80/20 H_2/CO_2 and constant stirring at 180 rpm. The minimal growth medium comprised 0.34 g KCl, 4 g $MgCl_2{\cdot}6H_2O$, 3.45 g $MgSO_4{\cdot}7H_2O$, 0.25 g NH_4Cl, 0.14 g $CaCl_2{\cdot}2H_2O$, 0.14 g·K_2HPO_4, 18 g NaCl, 10 ml of trace elements, and 2 mg $Fe(NH_4)_2(SO_4)_2{\cdot}7H_2O$ per liter. The trace element solution was prepared by adding 3 g $MgSO_4{\cdot}7H_2O$, 0.5 g $MnSO_4{\cdot}H_2O$, 1 g NaCl, 0.10 g $FeSO_4.7H_2O$, 0.18 g $CoSO_4{\cdot}7H_2O$, 0.10 g $CaCl_2{\cdot}2H_2O$, 0.18 g $ZnSO_4{\cdot}7H_2O$, 0.01 g $CuSO_4{\cdot}5H_2O$, 0.02 g $KAl(SO_4)_2{\cdot}12H_2O$, 0.01 g H_3BO_3, 0.01 g $Na_2MoO_4{\cdot}2H_2O$, 0.03 g $NiCl_2{\cdot}6H_2O$, 0.30 mg $Na_2SeO_3{\cdot}5H_2O$ to 990 ml distilled water. Cysteine and any other carbon source were removed from the media so carbon flux can be accurately quantified. Vitamins were also omitted, as they do not affect the growth of *M. maripaludis* [12]. For N_2-fixation experiments, NH_4Cl was omitted from the growth medium, Fe $(NH_4)_2(SO_4)_2{\cdot}7H_2O$ was replace by $Fe(SO_4)_2$, and N_2 was supplied to the headspace. For N_2-free experiments, all possible sources of nitrogen were eliminated from the media and headspace.

5.2.3 Reactor Setup

A total of 230 ml of medium in 600 ml serum bottles was outgassed with 80/20 v/v H_2/CO_2 to remove dissolved oxygen, sealed with butyl-rubber stopper and aluminum crimp, autoclaved at 121 °C for 20 min, and injected with 1 ml of 125 mg/ml $Na_2S{\cdot}7H_2O$, which was prepared anaerobically and autoclaved separately. The growth experiments were initiated by injecting 20 ml of the inoculum, which was pre-cultured in minimal medium during late exponential phase, and pressurized with 250 kPa 80/20 v/v H_2/CO_2, and incubated at 37 °C under constant stirring at 180 rpm.

Three growth experiments were performed: (1) N-free medium and no N_2 in the headspace, (2) N-free medium but with N_2 in the headspace, and (3) NH_4^+ in the

medium with no N_2 in the headspace. Cell density and CO_2, H_2, and CH_4 concentrations in the headspace were measured every hour in a day, until the headspace pressure fell below 100 kPa. The headspace was outgassed the next day, and replenished with 250 kPa 80/20 v/v H_2/CO_2. The procedure was repeated for several days.

5.2.4 Analytical Procedures

Cellular growth was monitored by measuring optical density (OD) of 1 ml culture samples every hour during the experiments. OD was recorded at 600 nm using a double-beam UV/Vis Spectrophotometer (Hitachi Model U-2800). Bottle pressure was measured using a digital gauge (Cole Parmer, USA, 68873-44) with sensitivity of 10^{-4} bar. Headspace gases were analyzed via an Agilent 7890A series SRI Instrument GC equipped with three columns (a Porapak Q 80/100 SS packed column of size 6 ft L × 1/8″ OD × 2 mm ID, a Molecular Sieve 5A 80/100 SS packed column of size 3 ft L 1/8″ OD 2 mm ID, and a Hayesep T 80/100 UM column of size 0.5 m L 1/8″ OD 2 mm ID), and a thermal conductivity detector with electronic pneumatic control (EPC). The carrier gas (Ar) was continuously supplied at 100 psig. The GC oven was maintained at 60 °C and its front detector at 150 °C. 1 ml headspace gas samples were drawn in using airtight microsyringes (Hamilton Samplelock), and analyzed immediately in GC.

5.2.5 Extracellular Fluxes and Maintenance Energy Estimation

For calculating growth rates and extracellular fluxes from experimental data, we followed the same approach as described in Sects. 4.2.5 and 4.2.6 of this thesis. The nitrogen source NH_4^+ is replaced by free N_2 for N_2-fixation experiments and therefore we simulated the initial state of the bottle by mixing sufficient amounts of pure water (stream 2), 60/20/20 $H_2/CO_2/N_2$ (stream 1), and pure CO_2 (stream 3). The fluxes $v_i = 1/X(t) \cdot dn(i)/dt$ for CO_2 and H_2 consumption and CH_4 production were computed by plotting the time profiles of total moles of CO_2, H_2, and CH_4, where $n(i)$ is the moles of species i (CO_2, H_2, or CH_4) in the bottle and $X(t)$ is the dry cell mass (g DCW) at time t.

The procedure described in Sect. 4.2.7 of this thesis was used to estimate energy parameters during N_2-fixation. However, it is to be noted that growth during N_2-fixation is extremely low. The linear CO_2 flux vs growth rate relationship showed that cell growth was zero for a CO_2 uptake rate below 39.62 mmol/gDCW-h, and we computed NGAM as the amount of energy spent for maintenance without growth. For estimating GAM, we selected twenty two CO_2 uptake rates

($v^k_{CO_2} = b^k_{CO_2}, k = 1, 2, \ldots, 22$). Using the CO_2 flux versus growth rate expression, we computed respective experimental growth rates ($b^k_G, k = 1, 2, \ldots, 22$). We estimated the experimental fluxes ($b^k_{CH_4}$ and $b^k_{H_2}, k = 1, 2, \ldots, 22$) for CH_4 and H_2 at these b^k_G using the linear expressions for CH_4 and H_2 fluxes vs growth rates. Further, we fixed the CO_2 uptake rates inside *i*MM518 to predict cell growth rates ($v^k_G, k = 1, 2, \ldots, 22$) and fluxes for CH_4 ($v^k_{CH_4}$) and H_2 ($v^k_{H_2}$). For varying values of GAM. For each GAM value, we used these model predictions to compute a weighted sum of squares of errors (SSE) as follows:

$$SSE(GAM) = \sum_{k=1}^{12} \left[\gamma_G^2 \left(v^k_G - b^k_G\right)^2 + \gamma^2_{CH_4} \left(v^k_{CH_4} - b^k_{CH_4}\right)^2 + \gamma^2_{H_2} \left(v^k_{H_2} - b^k_{H_2}\right)^2 \right] \tag{5.1}$$

where, γ_G = 3 gDCW/g DCW, γ_{CH_4} = 0.016 g/mmol, and γ_{CH_2} = 0.002 g/mmol. The GAM value with the minimum SSE was our best estimation for the growth energy required by *M. maripaludis* during N_2 fixation.

5.3 Results and Discussion

5.3.1 Growth Under Different Nitrogen Sources

The growth profiles of *M. maripaludis* at various times on day 1, 2 and 5 for the three experiments are shown in Fig. 5.1. The cells enter the stationary phase on depletion of CO_2 and H_2 in the headspace, and then re-entered the exponential

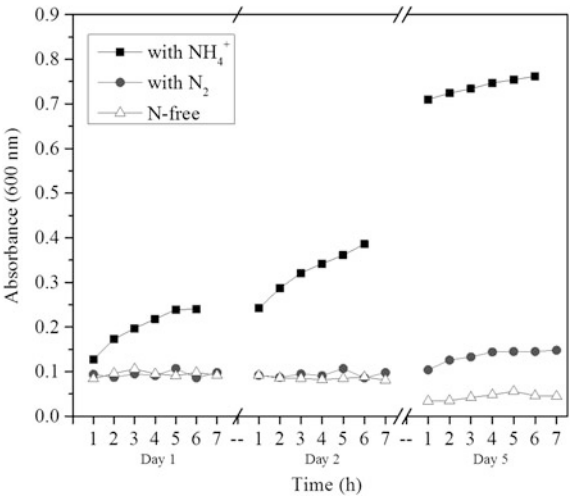

Fig. 5.1 OD profiles of *M. maripaludis* in the presence of NH_4^+, N_2, and N-free medium on day 1, 2, and 5. The cultures were inoculated from an NH_4^+ grown medium. Breaks on x-axis indicate the outgassing of headspace and re-pressurization with CO_2/H_2 or $CO_2/H_2/N_2$ depending on the nitrogen source required. The reactors were pressurized every day

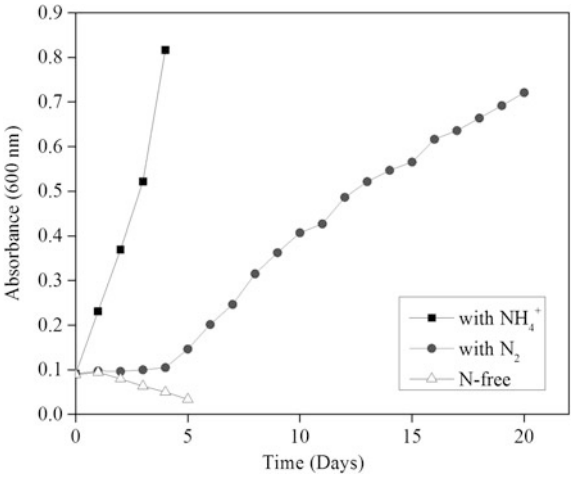

Fig. 5.2 Daily OD measurements during the experiments

phase on the replenishment of headspace (shown by breaks). The daily OD measurements along on each day are shown in Fig. 5.2.

For NH_4^+-medium, the OD increased from 0.089 ± 0.007 at time zero to 0.817 ± 0.007 on day 4. However, the growth slowed every day, and OD began decreasing after day 5. For N_2-medium, the OD increased from 0.095 ± 0.007 at time zero to 0.104 ± 0.007 on day 4. However, from day 5 onwards, OD value showed noticeable increase on each day for more than 20 days, and reached 0.721 ± 0.007 on day 20. The cells seemed reaching the stationary phase for the first four days, and in the exponential phase thereafter. However, the daily OD increments were far below those observed for NH_4^+-medium during days 1–4. For N-free experiment, the OD remained constant on day 1, but decreased continuously thereafter. The cells survived on day 1 in the stationary phase possibly on some residual nitrogen from the inoculum. After the residual nitrogen source was exhausted, cells entered death phase. These results confirmed the growth of *M. maripaludis* on N_2 and CO_2, which are two main components of flue gases.

The MERs at various times on days 1, 2, and 5 were shown in Fig. 5.3. For NH_4^+-medium, the MERs were the highest on day 1 and showed significant decrease each day. Cell biomass increased with time, but methane production rate remained constant, which resulted in decreasing MERs. Particularly on days 1 and 2, the MERs dropped sharply during the first few hours, as the cells were in mid-exponential phase. On day 5, the MER dropped slowly, as the cells reached late exponential phase. MERs continued to decrease every day, and reached nearly zero on day 9. The MER curves remained convex on all days.

The MERs on N_2 were much higher than those with NH_4^+ as nitrogen sources. Interestingly, the MER curves were concave on days 1 and 2, but became convex on day 5. These shapes suggest that the cells were in stationary phases on days 1 and 2, and entered exponential phases on day 5 and beyond. The difference between the convexities of the exponential phases for N_2-growth on day 5 and NH_4^+-growth

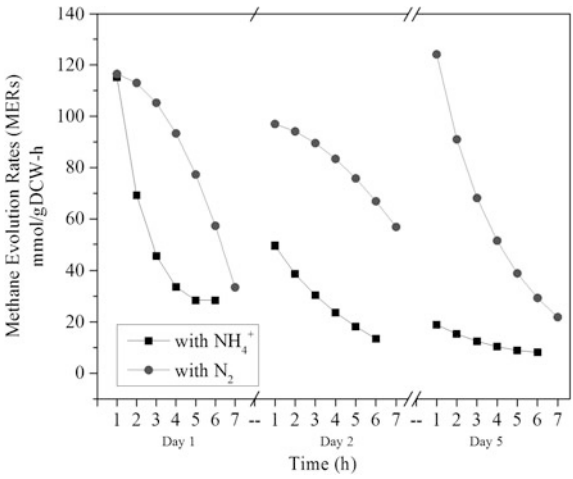

Fig. 5.3 MERs measured at various time points on day 1, 2, and 5

on day 1 confirmed the slower nature of cell growth with the former than the latter. Once the cells entered into exponential phase, the MERs continued to decrease every day at a very slow pace and did not become zero even after 20 days. No growth on N-free medium was observed, and hence the corresponding MERs were not reported. The foregoing discussion suggests interesting applications of diazotrophy in carbon utilization. The much lower growth of *M. maripaludis* during N_2-fixation had little effect on methane evolution. Given the same amounts of nutrients other than CO_2 and H_2, the cells produced methane for more than 20 days on N_2, while only 8 days on NH_4^+. During diazotrophy, *M. maripaludis* can capture and convert much higher CO_2 per gDCW to methane at the expense of less nutrients. This is an ideal scenario for carbon utilization from flue gases, which contain both N_2 and CO_2.

5.3.2 *Comparison with Other Diazotrophic Methanococci*

Diazotrophy is critical for methanogens in high-carbon low-nitrogen environments such as landfills. Previous studies on methanococci have indicated that *Methanotorris formicicus*, *Methanococcus aeolicus*, *Methanothermococcus thermolithotrophicus*, and *Methanococcus maripaludis* are known to fix N_2 [13], and therefore it is be interesting to compare the diazotrophic abilities of other strains with *M. maripaludis*. No growth yield and MER data have been reported for *Methanotorris formicicus* and *Methanococcus aeolicus.* On the other hand, the thermophilic *M. thermolithotrophicus* showed a cell yield of 0.94 g dry cell weight/mol CH_4 and a methanogenesis flux of 20.2 μmol/min-mg protein using NH_4^+ as the nitrogen source [14], which was possibly due to its short doubling time (∼0.6 h) and high growth temperature (65 °C). During N_2-fixation, the cell yield

and methanogenesis flux of *M. thermolithotrophicus* decreased by 61.7 and 43.1 %, respectively. In our study, *M. maripaludis* showed a cell yield of 2.82 g dry cell weight/mol CH_4 and a methanogenesis flux of 1.55 μmol/min-mg protein using NH_4^+ as the nitrogen source. During N_2-fixation, the cell yield of *M. maripaludis* decreased by 69.9–0.85 g dry cell weight/mol CH_4, but its methanogenesis flux surprisingly increased by 27.1–1.97 μmol/min-mg protein. The results of diazotrophy enhancing CO_2 to methane conversion in *M. maripaludis* have great potentials for industrial application on carbon capture and utilization. The low cell growth yield and increased methanogenesis flux of *M. maripaludis* enabled it as an ideal whole cell biocatalyst, and its low growth temperature (35 °C) is also beneficial as less energy is needed to heat up the conversion system as required for *M. thermolithotrophicus.*

5.3.3 *Growth, Extracellular Fluxes During N_2-Fixation and Maintenance Energy Estimation Using* iMM518

As the headspace pressure decreased with time, both growth rates and extracellular fluxes decreased. Figure 5.4 shows the time profiles of specific growth rates and extracellular fluxes during N_2-fixation. On a particular day, an increase in OD was observed during first few hours but no noticeable increase was seen after 3 h and hence could not be quantified. As shown, growth rates for all those time point are zero. As discussed previously, zero growth rates during N_2-fixation did not affect CO_2 and H_2 utilization rates and CH_4 evolution continued to occur. It suggests that the cell is producing energy continuously even when the growth is zero. Now the question arises: is the surplus energy used for only cell maintenance and survival? OR is there any other energy consuming mechanism during zero growth?

To understand this, we correlated CO_2 utilization fluxes with H_2 uptake rates and CH_4 evolution fluxes during growth phase and stationary phase. Fraction of the

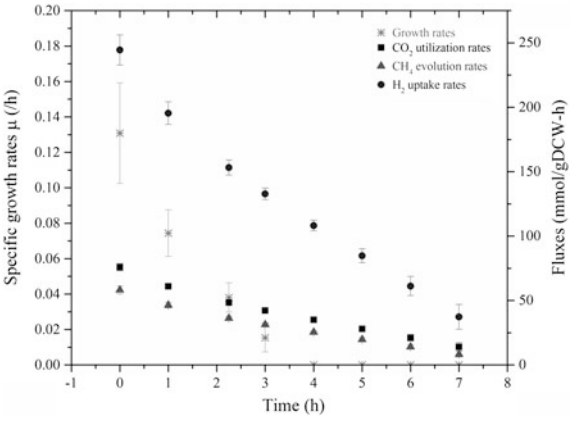

Fig. 5.4 The time profiles of specific growth rates and corresponding extracellular fluxes (CO_2, H_2, and CH_4) during N_2 fixation

carbon flux diverted towards methane production is observed to be 0.759 during growth phase while fraction of the carbon flux diverted towards methane production is 0.701 during stationary phase. Energy generated via methanogenesis during growth phase is utilized for growth associated maintenance, non-growth associated maintenance, N_2-fixation, biomass growth, etc. However energy generated during stationary phase possibly constitutes a major fraction for non-growth associated maintenance as cell growth is zero. Assuming that all the energy generated during stationary phase is used for cell maintenance and cell survival, it remains unclear where the remaining fraction of carbon flux i.e. 0.299 is getting diverted and needs to be investigated. Keeping this in mind, *i*MM518, a genome-scale metabolic model of *M. maripaludis*, was utilized to estimate maintenance energy during N_2-fixation and to study the flux distributions.

In order to estimate the maintenance energy during N_2-fixation, we used our novel approach reported earlier in Sect. 4.2.7. Our experiments indicated that cell growth rate was zero at a CO_2 uptake of 39.62 mmol/gDCW-h (Fig. 5.5), and the non-growth maintenance energy that gave zero growth prediction from *i*MM518 was 13.2 mmol ATP/gDCW-h. Thus, NGAM was estimated as 13.2 mmolATP/gDCW-h. The high value of NGAM during N_2-fixation is expected because cell growth is extremely low on N_2 and most of the energy is possibly used for non-growth associated maintenance. NGAM was then fixed in the model and TSSE was calculated for a range of GAM values. TSSE was minimum at a GAM value of nearly 0.001 mmol ATP/gDCW, which is the best estimate of GAM from our experiments. With GAM = 0.001 mmol/g DCW and NGAM = 13.2 mmol/gDCW-h in *i*MM518, we fixed CO_2 uptake rate at various values and predicted cell growth, MER, and H_2 uptake rate for the maximum biomass growth. Figure 5.6 compares experimental results with our model predictions.

The deviations in CH_4 evolution rates contributed the most (76.1 %) to the minimum TSSE = 1.071, followed by those in H_2 uptake rates (15.9 %).

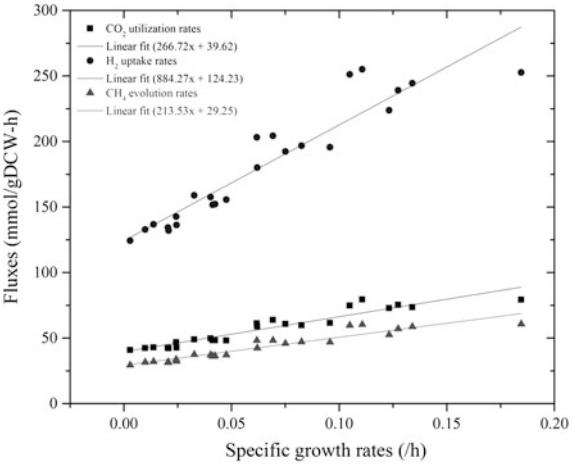

Fig. 5.5 Linear correlations between extracellular fluxes and specific growth rates during N_2-fixation

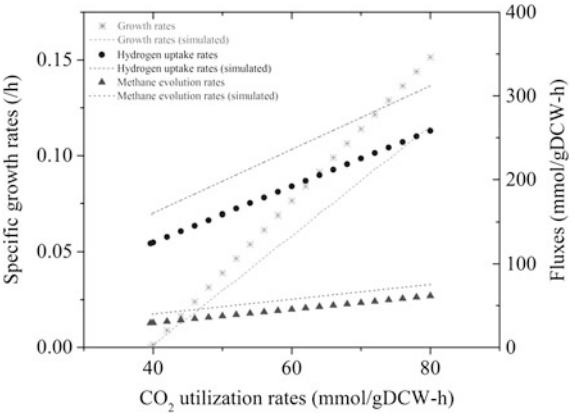

Fig. 5.6 Comparison of model predicted growth rates, H_2 uptake rates, and CH_4 evolution rates with experimentally measured values during N_2 fixation

The prediction of biomass growth from the model contributed least (7.8 %) to the minimum TSSE. Our estimated GAM value (nearly 0.001 mmol ATP/gDCW) for *M. maripaludis* during N_2-fixation is extremely low compared to that predicted with growth on NH_4^+ (27.14 mmolATP/gDCW-h). In addition, unlike excellent model predictions for growth on NH_4^+, *i*MM518 was unable to predict the accurate fluxes during N_2-fixation which could be due to reasons such as absence of certain regulatory mechanism/reactions taking place during N_2-fixation, a different objective function of the cell, specificity of a model for substrates, etc. and hence require further understanding.

5.4 Conclusions

The necessity for diazotrophy in methanogens to survive in nitrogen-poor environment can be exploited to fix carbon and nitrogen simultaneously from flue gases. This study has demonstrated that *M. maripaludis* can produce methane for at least 20 days in N_2–CO_2–H_2 environment and fix 250 % more carbon compared with NH_4^+–CO_2–H_2 environment. No such data exist for any other methanogens in the literature. Although N_2-fixation is energy demanding, this study shows that slow growth and high methanogenesis flux under diazotrophy is in fact beneficial for carbon capture and utilization in flue gases, as it enhances methane yield significantly. We further observed that NGAM is higher during N_2-fixation compared to growth on NH_4^+ and GAM value is very low due to extremely slow growth. However, the comparison of experimental and simulation fluxes at estimated NGAM and GAM raises a doubt on model predictions during N_2-fixation and needs further improvement.

References

1. Eliasson B, Riemer P, Wokaun (1999) A: greenhouse gas control technologies. Elsevier Science
2. Zhang ZY, Maekawa T (1993) Kinetic study on fermentation from CO_2 and H_2 using the acclimated-methanogen in batch culture. Biomass Bioenergy 4:439–446
3. Brilman W, Alba LG, Veneman R (2013) Capturing atmospheric CO_2 using supported amine sorbents for microalgae cultivation. Biomass Bioenergy 53:39–47
4. Kumar K, Dasgupta CN, Nayak B, Lindblad P, Das D (2011) Development of suitable photobioreactors for CO_2 sequestration addressing global warming using green algae and cyanobacteria. Bioresour Technol 102:4945–4953
5. Jones WJ, Paynter MJB, Gupta R (1983) Characterization of *Methanococcus maripaludis sp*. nov., a new methanogen isolated from salt marsh sediment. Arch Microbiol 135:91–97
6. Goyal N, Widiastuti H, Karimi IA, Zhou Z (2014) Genome-scale metabolic model of *Methanococcus maripaludis* S2 for CO_2 capture and conversion to methane. Mol BioSyst 10:1043–1054
7. Costa KC, Lie TJ, Jacobs MA, Leigh JA (2013) H_2-independent growth of the hydrogenotrophic methanogen *Methanococcus maripaludis*. MBio 4
8. Blank CE, Kessler PS, Leigh JA (1995) Genetics in methanogens: transposon insertion mutagenesis of a *Methanococcus maripaludis* nifH gene. J Bacteriol 177:5773–5777
9. Kessler PS, McLarnan J, Leigh JA (1997) Nitrogenase phylogeny and the molybdenum dependence of nitrogen fixation in *Methanococcus maripaludis*. J Bacteriol 179:541–543
10. Kessler PS, Daniel C, Leigh JA (2001) Ammonia switch-off of nitrogen fixation in the methanogenic archaeon *Methanococcus maripaludis*: mechanistic features and requirement for the novel GlnB homologues, NifI(1) and NifI(2). J Bacteriol 183:882–889
11. Kessler PS, Leigh JA (1999) Genetics of nitrogen regulation in *Methanococcus maripaludis*. Genetics 152:1343–1351
12. Whitman WB, Sohn S, Kuk S, Xing R (1987) Role of amino acids and vitamins in nutrition of mesophilic *Methanococcus spp*. Appl Environ Microbiol 53:2373–2378
13. Liu Y (2010) Methanococcales. In Handbook of hydrocarbon and lipid microbiology (pp. 573–581). Springer Berlin Heidelberg
14. Belay N, Sparling R, Daniels L (1984) Dinitrogen fixation by a thermophilic methanogenic bacterium. 312:286–288

Chapter 6
Contributions and Future Recommendations

6.1 Contributions

Rapid depletion of fossil fuel-based resources has caused energy and environmental concerns and encourages production of renewable chemicals and fuels from CO_2 consuming microorganisms. Attempts have been made in the past to capture CO_2 from flue gases using algae and cyanobacteria. However space, harvesting and sunlight remains to be a challenging problem. Thus, it is important to explore other CO_2 fixing microbes. In this work, we used a modeling approach to understand methanogenesis from CO_2 from a methanogenic archaea, *M. maripaludis* S2. In addition to CO_2, *M. maripaludis* also possesses a unique capability to fix N_2 and hence provides an ideal scenario to capture two major components of a flue gas. The following section presents some of the key contributions from this work.

6.1.1 Consolidated Review of M. maripaludis *Metabolism*

In spite of more than 100 publications on the biochemistry of *M. maripaludis*, a consolidated review was missing in the literature. This work reviewed existing literature on *M. maripaludis*, and explored its potential industrial and environmental applications. Our review of its metabolic processes, energy production, and genome-scale models suggested that more efforts are required towards metabolic cycle regulations, acetate biosynthesis, value-added chemicals/fuels production, metabolism under stress, carbon capture and utilization applications, and systems biology models. Recent tools such as next generation sequencing, omics, and systems biology technologies can facilitate our understanding at the molecular level and promote further research into this interesting microbe.

N. Goyal, *In silico Modeling and Experimental Validation for Improving Methanogenesis from CO_2 via M. maripaludis*, Springer Theses,
DOI 10.1007/978-981-10-2510-5_6

6.1.2 i*MM518, Development of First Constraint-Based Genome-Scale Metabolic Model of* M. maripaludis *S2*

*i*MM518, the first genome-scale metabolic model of *M. maripaludis* S2 was constructed, validated, and analyzed in this work. The model allowed us to study methanogenesis, N_2-fixation, and other metabolic pathways at genome-scale in *M. maripaludis* S2. The developed model is robust, and successfully predicted various observed phenotypes under different experimental conditions. The model enabled the identification of essential genes/reactions for growth and mutant strains capable of enhancing methanogenesis. Its comparison with the in silico models of *Methanosarcina barkeri*, *Methanosarcina acetivorans*, and *Sulfolobus solfataricus* P2 showed *M. maripaludis* S2 to be a better organism for producing methane.

6.1.3 *Experimental Measurement of Fluxes and Estimation of Maintenance Energy Parameters*

In this study, we performed batch culture experiments on *M. maripaludis* S2 using CO_2 as the sole carbon substrate to quantify three key extracellular fluxes (CO_2, H_2, and CH_4) along with specific growth rates. This is the first study to report experimental gas consumption and production rates for the growth of *M. maripaludis* on CO_2 and H_2 in minimal media. A systematic process simulation and optimization procedure was successfully developed to precisely quantify extracellular fluxes along with cell growth and maintenance energy parameters. Our growth yields, ATP gain, and energy parameters fall within acceptable ranges known in the literature for hydrogenotrophic methanogens.

6.1.4 *Effect of Diazotrophy on Methanogenesis by* M. maripaludis

Few methanogens demonstrate metabolic capabilities of N_2-fixation (diazotrophy) along with CO_2 capture in the absence of external nitrogen sources, however the growth rates during N_2-fixation are usually slow. In this study, the impacts of nitrogen sources on methane production in *M. maripaludis* were evaluated with batch reactors. Our results indicated that diazotrophy in *M. maripaludis* with reduced growth rates is in fact beneficial for CO_2 conversion, suggesting that diazotrophic methanogens are ideal biocatalysts to efficiently capture both carbon and nitrogen in flue gases to produce renewable energy. However, the comparison of experimental and simulation fluxes at estimated NGAM and GAM raised a doubt on model predictions during N_2-fixation and needs further improvement.

6.2 Future Recommendations

6.2.1 *Electromethanogenesis*

Electromethanogenesis is the bio-catalyzed reduction of CO_2 to CH_4 where, instead of H_2, electricity is supplied as the source of electrons. Direct extracellular electron transfer is represented as follows:

$$CO_2 + 8H^+ + 8e^- \rightarrow CH_4 + 2H_2O \; (E_{cathode} = -0.24 \text{ V vs. NHE})$$

$$4H_2O \rightarrow 2O_2 + 8H^+ + 8e^- \; (E_{anode} = 0.81 \text{ V vs. NHE})$$

$$CO_2 + 2H_2O \rightarrow CH_4 + 2O_2 \; (E_{cell} = -1.05 \text{ vs. NHE})$$

Literature reported an efficiency up to 96 % [1] on a biocathode where electrons can be captured by methanogen to form methane and thus, allows storage of electrical energy in a stable form as carbon-neutral methane. In order to study the direct uptake of electrons by *M. maripaludis*, two-chamber electromethanogenesis was demonstrated in *M. maripaludis* by Lohner et al. [2]. They demonstrated H_2-independent electromethanogenesis from CO_2 in both wild-type *M. maripaludis* strain MM901 and hydrogenase mutant strain MM1284. However, as discussed earlier, two-chamber electromethanogenesis require membranes such as Nafion. The membranes are expensive, increase the pH gradient across two chambers and contribute to potential losses. In addition, maintaining pressure is very difficult in a two-chamber set-up. The single-chamber membraneless MEC decreases the internal resistance and hence increases energy recovery.

It is interesting to study single-chamber membrane-free electrosynthesis for direct uptake of electrons by *M. maripaludis* and to compare the results with two-chamber MECs. As a preliminary work, we designed single-chamber membrane-free MECs to study the electromethanogenesis by a pure culture of *M. maripaludis* S2 and investigated methane production at varying voltages.

Single-Chamber MEC set-up

A membraneless MEC set-up (Fig. 6.1) used to study electromethanogenesis in *M. maripaludis* S2 consists of a 600 ml serum bottle that contained 250 ml of anaerobic growth medium and 350 ml of headspace. It is easy to maintain anaerobic environment in serum bottles as they can be easily sealed and autoclaved. Two graphite electrodes (5 cm × 1 cm × 0.3 cm) acted as anode and cathode and spaced approx. 2 cm apart using rubber fixture. Titanium wires were used to connect the electrodes to the circuit and a power supply (HM7042-5, RS Singapore) is used to provide an overall potential ranging from 1.0 to 1.6 V.

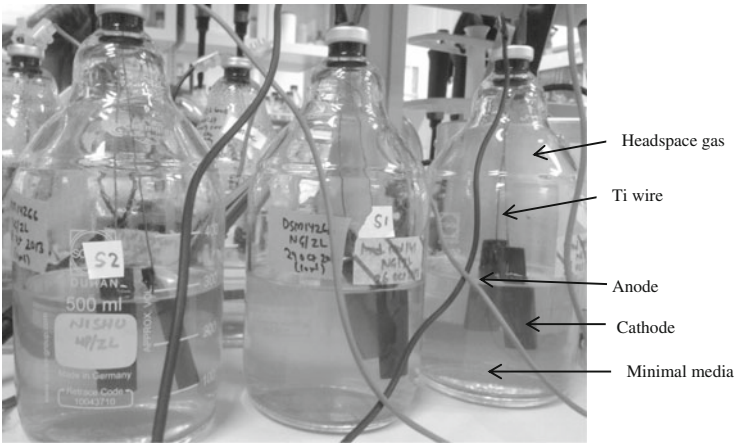

Fig. 6.1 Single-Chamber Membrane-Free MEC set-up

Growth conditions

The minimal growth medium was prepared as described in Sect. 4.2.2 of this thesis. 20 ml inoculum (cells in late exponential phase) was added to 230 ml of growth media and anaerobic conditions were maintained by flushing the reactor with 80/20 v/v N_2/CO_2 and to remove dissolved oxygen. The MECs were pressurized with 80/20 v/v N_2/CO_2 usually up to 2.0 bars and incubated at 37 °C. Each experiment was performed in duplicates.

Analytical Procedures

Bottle pressure was measured periodically using a digital gauge (Cole Parmer, USA, 68873-44) with a sensitivity of 10^{-4} bar. Headspace gas samples were taken at regular intervals and analyzed immediately using GC as described in Sect. 4.2.4.

Cellular growth was monitored by measuring optical density (OD) of 1 ml culture samples. OD was recorded at 600 nm using a double-beam UV/Vis Spectrophotometer (Hitachi Model U-2800).

Coulombic efficiency was determined using the method described by Eerten-Jansen et al. [3]. Cumulative electric charge i.e. the amount of electrons consumed, was calculated by integrating the current profile logged by the potentiostat and efficiencies were then determined as the ratio of the electrons theoretically needed to form the measured product ($8e^-$ for CH_4 and $2e^-$ for H_2) and the cumulative electric charge measured as the current by the potentiostat.

Preliminary results and future work

Four MECs were setup each with a different E_{cat} (−0.10, −0.20, −0.35, and −0.49 V) versus Ag/AgCl. As shown in Fig. 6.2, methane production at −0.49 V is highest compared to −0.20 and −0.35 V. Almost negligible methane was seen in MEC operated at E_{cat} = −0.10 V. High voltage produced more H_2 during water splitting

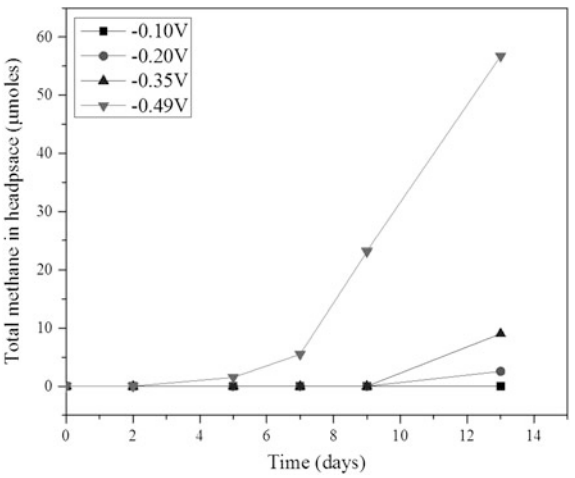

Fig. 6.2 Effect of different voltages (E_{cat} vs. Ag/AgCl) on methane production during single-chamber electrosynthesis

which is then used by *M. maripaludis* for CH_4 production. However the coulombic efficiencies from these MECs were less than 1 %. The reason for low coulombic efficiencies could be deposition of salts on the cathode surface, causing a significant voltage drop. Shaking the reactors at low rpm would increase the mass transfer, reduce the rate of salt deposition and may lead to increase in coulombic efficiency. Thus, more work is required to comment on the direct or indirect uptake of electrons by *M. maripaludis* in a single-chamber MEC.

We need to optimize single-chamber MECs for CH_4/H_2 production at varying voltages, temperature, shaking speed, etc. Once optimized, a comparison with two-chamber MECs can be made. To study direct electron transfer we also need further investigation by employing a hydrogenase mutant strain.

6.2.2 Model-Driven Approaches for Production of Desired Fuels/Chemicals

A systematic model-driven approach is required to evaluate the production potential of *M. maripaludis* for other fuels such as methanol, butanol, etc. and value-added products such as isoprenoids, terpenes, etc. from CO_2 through coupling metabolite production to growth rate. Specific metabolic interventions i.e. strain designs for production strains that can be experimentally implemented, characterizes the potential of *M. maripaludis* and its other strains, to produce novel compounds is needed. *i*MM518 will enable the genome-scale study of *M. maripaludis* as a useful biocatalyst. In addition, the predictability of the model can be improved by adding the regulatory information. In order to account for the impact of gene expression and regulation on metabolism, a genome-scale model should integrate some regulatory mechanisms such as activity of RNA polymerase, transcription factors and

its binding sites, promoters, sigma factors, etc. The approach that includes regulatory information with the cellular metabolism will significantly improve our understanding of metabolism in *M. maripaludis.*

6.2.3 Co-culture Modeling/Experimentation

Stolyar et al. [4] developed a first multispecies stoichiometric metabolic model of *M. maripaludis* and *D. vulgaris* to study methane production during mutualistic interactions. The model could successfully predict metabolic fluxes and growth phenotypes. In a similar manner, other co-culture models of *M. maripaludis* can be developed to study CO_2 conversion to a useful fuel such as acetate, methanol, butanol, etc. For instance, during microbial conversion of CO_2 to methanol, we need to identify the similar growth conditions of a methanogen and methanotroph to grow them in co-cultures. Quantifying the products using GC/HPLC and comparing the results among different pairs of methanogens and methanotrophs can helps us identify the best co-culture for production of methanol. The experimental data can then be integrated with modeling to further enhance its production.

References

1. Cheng S, Xing D, Call DF, Logan BE (2009) Direct biological conversion of electrical current into methane by electromethanogenesis. Environ Sci Technol 43:3953–3958
2. Lohner ST, Deutzmann JS, Logan BE, Leigh J, Spormann AM (2014) Hydrogenase-independent uptake and metabolism of electrons by the archaeon *Methanococcus maripaludis*. ISME J 8:1673–1681
3. Eerten-Jansen V, Mieke C, Heijne AT, Buisman CJ, Hamelers HV (2012) Microbial electrolysis cells for production of methane from CO2: long-term performance and perspectives. Int J Energy Res 36:809–819
4. Stolyar S, Van Dien S, Hillesland KL, Pinel N, Lie TJ, Leigh JA, Stahl DA (2007) Metabolic modeling of a mutualistic microbial community. Mol Syst Biol 3:92

Summary

Exhaust flue gas generated during combustion of fossil fuels such as coal accounts for about 59.69 % of the CO_2 emissions worldwide [1]. To capture the CO_2 from flue gas and convert it into a relatively cleaner and sustainable fuel such as methane cost-effective, clean and efficient approaches are needed. One such approach is biochemical conversion of CO_2 which drew numerous attentions over the past few years. Methanogens play a key role in the biochemical conversion of CO_2 by not only capturing it but simultaneously converting it to a relatively cleaner fuel, methane.

M. maripaludis is a fast growing, mesophilic, hydrogenotrophic methanogen with some unique characteristics and advantages [2–4]. It reduces CO_2 (an electron acceptor) with the help of H_2 (an electron donor) for growth and methanogenesis. Despite several decade of research on *M. maripaludis*, a consolidated review on its metabolic processes and applications was lacking in the literature. In addition, efforts to generate a systems biology model for *M. maripaludis* have not been successful. In this thesis, we fill these gaps and experimentally measure specific growth rates and extracellular fluxes (CO_2, H_2 uptake and CH_4 evolution) during growth in a batch reactor. To minimize errors in the flux measurements, we propose a novel process simulation approach. Furthermore, we show that how flux data from experiments and genome-scale model can be integrated to estimate the maintenance energy parameters i.e. Growth Associated Maintenance (GAM) and Non-Growth Associated Maintenance (NGAM) for a cell. We further explore the N_2-fixing ability of *M. maripaludis* and demonstrate an ideal scenario for CO_2 capture from flue gas, which has both N_2 and CO_2.

Briefly, the thesis has four major parts. The first part reviews the biochemistry and genetics of *M. maripaludis* S2 and describes the approach for constraint-based genome-scale metabolic modeling. Second, to initiate the system level analysis we successfully reconstruct the first genome-scale metabolic model (*i*MM518, [3]) of *M. maripaludis* based on the available genomics and biochemical data. Notably, this model comprises 570 reactions, 556 distinct metabolites, and 518 genes along with Gene-Protein-Reaction (GPR) associations, and covers 30 % of Open Reading Frames (ORFs). *i*MM518 was validated using biomass growth data and gene knockout studies from the literature. The model successfully predicts all the known metabolic phenotypes and shows the superiority of *M. maripaludis* compared to

N. Goyal, *In silico Modeling and Experimental Validation for Improving Methanogenesis from CO_2 via M. maripaludis*, Springer Theses,
DOI 10.1007/978-981-10-2510-5

three other modeled archaea. Using *i*MM518, we identify the essential/non-essential genes for growth and study the efficacy of alternate carbon, hydrogen and nitrogen sources.

Third, although *i*MM518 was validated using available biomass growth data, the validation was inadequate due to unavailability of quantitative data on uptake and production rates. Therefore, we perform batch culture experiments and quantify three key extracellular fluxes (CO_2, H_2, and CH_4) along with specific growth rates of *M. maripaludis*. A novel process simulation approach was developed to accurately estimate such fluxes. Consumption and production rates were reported for *M. maripaludis* with a growth yield of 3.549 ± 0.149 gDCW/mol CH_4. The experimental results indicated that *M. maripaludis* was capable of reducing 70–95 % of CO_2 to CH_4 during the exponential phase. We estimated maintenance energy parameters to be NGAM = 7.836 mmol/gDCW-h and GAM = 27.14 mmol/gDCW for *M. maripaludis* using a genome-scale in silico metabolic model (*i*MM518) and experimentally measured compositional data. A thoroughly validated *i*MM518 was then used to study the effect of amino acids on microbial growth and CH_4 production rates by investigating the intracellular flux distributions.

Fourth, *i*MM518 has predicted significant MER enhancement during N_2-fixation in *M. maripaludis*. However, this required an experimental proof. Thus, we perform batch culture studies on *M. maripaludis* to compare the effect of NH_4^+ or N_2 on methane production. Our results show that with the same amount of nutrients in both the reactors, N_2-fixation allows methane production up to 20 days while it stops after 8 days in the presence of NH_4^+. Clearly, the amount of carbon fixed to methane in N_2-fixing reactor is approx. 250 % higher compared to NH_4^+ and hence provide an ideal scenario for dual capture of carbon and nitrogen from flue gas. Furthermore, we used the experimental data for growth and extracellular fluxes to study the effect of N_2-fixation on maintenance energy.

Overall, this work provides a systematic computational framework to study metabolism in *M. maripaludis* at genome-scale by combining constraints-based metabolic modeling and flux data under different culture conditions. With the ever increasing genomics and biochemical data, the developed framework can be applied to any other CO_2 fixing methanogen for analyzing its metabolism in a systematic way.

References

1. Eliasson B, Riemer P, Wokaun A (1999) Greenhouse gas control technologies. Elsevier Science
2. Jones WJ, Paynter MJB, Gupta R (1983) Characterization of *Methanococcus maripaludis sp*. nov., a new methanogen isolated from salt marsh sediment. Arch Microbiol 135:91–97
3. Goyal N, Widiastuti H, Karimi IA, Zhou Z (2014) Genome-scale metabolic model of *Methanococcus maripaludis* S2 for CO_2 capture and conversion to methane. Mol BioSyst 10:1043–1054
4. Costa KC, Lie TJ, Jacobs MA, Leigh JA (2013) H_2-independent growth of the hydrogenotrophic methanogen *Methanococcus maripaludis*. MBio 4

Appendices

A. SBML File of a Genome-Scale Metabolic Model of *M. maripaludis* (*i*MM518) Available in BioModels Database

http://www.ebi.ac.uk/compneur-srv/biomodels-main/MODEL1304120000

B. List of Metabolic Reactions Used for *i*MM518

http://www.rsc.org/suppdata/mb/c3/c3mb70421a/c3mb70421a1.xls

C. Biomass Composition of *M. maripaludis* Used in *i*MM518

http://www.rsc.org/suppdata/mb/c3/c3mb70421a/c3mb70421a2.pdf

N. Goyal, *In silico Modeling and Experimental Validation for Improving Methanogenesis from CO_2 via M. maripaludis*, Springer Theses,
DOI 10.1007/978-981-10-2510-5

D. Implementation Code of *i*MM518 in GAMS Build 38380/38394

```
$Title
$Ontext
Source:
$Offtext
Set i all metabolites /
$include "metabolites.txt"
/;

Set e(i) external metabolites /
$include "externals.txt"
/;

Set j reactions / Rxn1*Rxn572 / ;

Set r(j) reversible reactions /
$include "reversibles.txt"
/;

Set t time /t1, t2, t3, t4, t5, t6, t7, t8, t9, t10, t11, t12 /;
Set tf(t) /t1, t2, t3, t4, t5, t6, t7, t8, t9, t10, t11, t12/;

Parameter S(i,j) stoichiometric coefficient of metabolite i in reaction j /
$include "coefficients1.txt"
/;

*Select Objective function
Parameter mw(e) / CO2 0.044, h2 0.002, ch4 0.016, biomass 3.0/
Parameter bexp(t,e), ss(e), tss;
Parameter bco2(t) /t1 -30, t2 -40, t3 -50, t4 -60, t5 -70, t6 -80, t7 -90,
t8 -100, t9 -110, t10 -120, t11 -130, t12 -23.5106 /;

Variables
      v(t,j)    Flux of reaction j in network
      b(t,i)    Net flux of metabolite i
      obj       Objective function;

Parameter
      ngam      non growth substrate flux / 7.836 /
      gam       growth substrate flux / 27.14/;

v.lo(t,j) = -1000.0 $r(j);
v.up(t,j) = 1000.0;
```

```
bexp(t,"co2") = bco2(t);
bexp(t,"biomass") = (bco2(t)+23.5106)/(-203.2507);
bexp(t,"h2") = -580.8699*bexp(t,"biomass")-131.95;
bexp(t,"ch4") = 173.5926*bexp(t,"biomass")+21.9355;

b.lo(t,i) = -1000.0 $e(i);
b.up(t,i) = 1000.0 $e(i);
b.lo(t,"n2") = 0.0;
b.lo(t,"biomass") = 0.0;
b.lo(t,"btn_e") = 0.0;
b.fx(t,"hco3_e") = 0.0;
b.fx(t,"h_e") = 0.0;
b.lo(t,"cys_e") = 0.0;
b.lo(t,"lys") = 0.0;
b.fx(t,"cd2_e") = 0.0;
b.lo(t,"formate") = 0.0;
b.lo(t,"acetate_e") = 0.0;
b.fx(t,"selt") = 0.0;
b.fx(t,"oxygen") = 0.0;
b.lo(t,"ala_e") = 0.0;
b.lo(t,"pro_e") = 0.0;
b.lo(t,"csn_e") = 0.0;
*reactions that were forming the loop
v.fx(t,"Rxn26") = 0.0;
v.fx(t,"Rxn27") = 0.0;
v.fx(t,"Rxn59") = 0.0;
v.fx(t,"Rxn81") = 0.0;
v.fx(t,"Rxn82") = 0.0;
v.fx(t,"Rxn140") = 0.0;
v.fx(t,"Rxn243") = 0.0;
v.fx(t,"Rxn252") = 0.0;
v.fx(t,"Rxn266") = 0.0;
v.fx(t,"Rxn283") = 0.0;
v.fx(t,"Rxn317") = 0.0;
v.fx(t,"Rxn359") = 0.0;
v.fx(t,"Rxn360") = 0.0;
v.fx(t,"Rxn463") = 0.0;
v.fx(t,"Rxn475") = 0.0;
v.fx(t,"Rxn555") = 0.0;
v.fx(t,"Rxn493") = 0.0;
v.fx(t,"Rxn494") = 0.0;
```

```
*reactions that have been used as transport
v.fx(t,"Rxn135") = 0.0;
v.fx(t,"Rxn145") = 0.0;
v.fx(t,"Rxn235") = 0.0;
v.fx(t,"Rxn258") = 0.0;
v.fx(t,"Rxn259") = 0.0;
v.fx(t,"Rxn268") = 0.0;
v.fx(t,"Rxn282") = 0.0;
v.fx(t,"Rxn316") = 0.0;
v.fx(t,"Rxn439") = 0.0;
v.fx(t,"Rxn450") = 0.0;
v.fx(t,"Rxn458") = 0.0;
v.fx(t,"Rxn462") = 0.0;
v.fx(t,"Rxn487") = 0.0;
v.fx(t,"Rxn501") = 0.0;
v.fx(t,"Rxn513") = 0.0;
v.fx(t,"Rxn521") = 0.0;
v.fx(t,"Rxn523") = 0.0;
v.fx(t,"Rxn525") = 0.0;
v.fx(t,"Rxn536") = 0.0;
v.fx(t,"Rxn556") = 0.0;
v.fx(t,"Rxn559") = 0.0;
v.fx(t,"Rxn569") = 0.0;
v.fx(t,"Rxn572") = 0.0;
v.fx(t,"Rxn561") = 0.0;

b.fx(t,"co2") = bexp(t,"co2");


Equations
        Flux(t,i)     Flux for metabolite i
        atp(t)        atp consumption
        Objfun        Desired physiological property (objective function);

        Flux(t,i) $tf(t) .. sum(j,S(i,j)*v(t,j)) =e= b(t,i) $e(i);
        Objfun.. obj =e= sum( t $tf(t),v(t,"Rxn136"));
        atp(t) $tf(t).. v(t,"Rxn459") =g= ngam + gam*v(t,"Rxn136");

Model FBA /Flux, atp, Objfun /;
option nlp = baron;
option optcr = 0.000001;
solve FBA using lp maximizing obj;
mw("biomass") = 3.0;
```

```
ss(e) = 1000*sum( t $tf(t), sqr(mw(e)*(b.l(t,e)-bexp(t,e))));
tss = sum(e, ss(e));
display obj.l, ngam, gam, b.l, ss, tss;

file res /mbio1.txt/;
put res;
put /'Objective Funcion:', obj.l:10:5 / ;
put /'Overall Reaction:'/
loop( (t,e), put e.tl, @15, b.l(t,e):10:5 /);
put /'Flux Distribution:'/
loop( (t,j), put j.tl, @15, v.l(t,j):10:5 /);
```

Results-Display

```
----  2740 VARIABLE obj.L              =        3.040  Objective function
      PARAMETER ngam                   =        7.836  non growth substrate flux
      PARAMETER gam                    =       27.140  growth substrate flux

----  2740 VARIABLE b.L  Net flux of metabolite i
```

	biomass	h2o	dasn	h2s	pim	urea	a_2plac	a_1hydtc	amob	mtr1p	ch4	h2
t1	0.032	59.585	1.70E-05	−0.007	−3.47E-06	1.40E-05	−5.02E-06	−2.62E-06	3.47E-06	8.49E-06	28.71	−117.336
t2	0.081	78.947	4.31E-05	−0.018	−8.82E-06	3.55E-05	−1.27E-05	−6.66E-06	8.82E-06	2.16E-05	36.723	−153.232
t3	0.13	98.308	6.93E-05	−0.029	−1.42E-05	5.70E-05	−2.05E-05	−1.07E-05	1.42E-05	3.46E-05	44.736	−189.128
t4	0.178	117.67	9.54E-05	−0.04	−1.95E-05	7.85E-05	−2.82E-05	−1.47E-05	1.95E-05	4.77E-05	52.748	−225.025
t5	0.227	137.031	1.22E-04	−0.051	−2.49E-05	1.00E-04	−3.59E-05	−1.88E-05	2.49E-05	6.08E-05	60.761	−260.921
t6	0.276	156.393	1.48E-04	−0.063	−3.02E-05	1.22E-04	−4.36E-05	−2.28E-05	3.02E-05	7.39E-05	68.774	−296.817
t7	0.325	175.754	1.74E-04	−0.074	−3.56E-05	1.43E-04	−5.14E-05	−2.69E-05	3.56E-05	8.69E-05	76.787	−332.713
t8	0.374	195.116	2.00E-04	−0.085	−4.09E-05	1.65E-04	−5.91E-05	−3.09E-05	4.09E-05	1.00E-04	84.8	−368.61
t9	0.423	214.477	2.26E-04	−0.096	−4.63E-05	1.86E-04	−6.68E-05	−3.50E-05	4.63E-05	1.13E-04	92.813	−404.506
t10	0.472	233.839	2.52E-04	−0.107	−5.16E-05	2.08E-04	−7.45E-05	−3.90E-05	5.16E-05	1.26E-04	100.825	−440.402
t11	0.521	253.2	2.78E-04	−0.118	−5.70E-05	2.29E-04	−8.23E-05	−4.30E-05	5.70E-05	1.39E-04	108.838	−476.298
t12	1.29E-05	47.021	2.82E-09	−2.92E-06	−1.41E-09	5.67E-09		−1.06E-09	1.41E-09	3.44E-09	23.51	−94.041

	Glycald	nh4	rbz	co2	hpap	a_5mthg	so3_e	co_2_e	pi_e	ni2_e	fe2_e	mthg
t1		−0.301	−5.40E-07	−30	0.011	−0.004	−5.56E-06	−5.40E-07	−0.189	−9.26E-07	−9.26E-07	0.004
t2	1.96E-06	−0.763	−1.37E-06	−40	0.028	−0.011	−1.41E-05	−1.37E-06	−0.481	−2.35E-06	−2.35E-06	0.011
t3	3.15E-06	−1.226	−2.20E-06	−50	0.045	−0.017	−2.27E-05	−2.20E-06	−0.772	−3.78E-06	−3.78E-06	0.017
t4	4.34E-06	−1.689	−3.04E-06	−60	0.062	−0.024	−3.12E-05	−3.04E-06	−1.063	−5.20E-06	−5.20E-06	0.024
t5	5.53E-06	−2.152	−3.87E-06	−70	0.079	−0.031	−3.98E-05	−3.87E-06	−1.355	−6.63E-06	−6.63E-06	0.031
t6	6.71E-06	−2.615	−4.70E-06	−80	0.096	−0.037	−4.83E-05	−4.70E-06	−1.646	−8.06E-06	−8.06E-06	0.037
t7	7.90E-06	−3.078	−5.53E-06	−90	0.113	−0.044	−5.69E-05	−5.53E-06	−1.937	−9.48E-06	−9.48E-06	0.044
t8	9.09E-06	−3.541	−6.36E-06	−100	0.13	−0.05	−6.55E-05	−6.36E-06	−2.229	−1.09E-05	−1.09E-05	0.05
t9	1.03E-05	−4.004	−7.20E-06	−110	0.147	−0.057	−7.40E-05	−7.20E-06	−2.52	−1.23E-05	−1.23E-05	0.057
t10	1.15E-05	−4.466	−8.03E-06	−120	0.164	−0.064	−8.26E-05	−8.03E-06	−2.812	−1.38E-05	−1.38E-05	0.064
t11	1.27E-05	−4.929	−8.86E-06	−130	0.181	−0.07	−9.11E-05	−8.86E-06	−3.103	−1.52E-05	−1.52E-05	0.07
t12		−1.19E-04	−2.19E-10	−23.511	4.48E-06	−1.74E-06	−2.25E-09	−2.19E-10	−7.60E-05	−3.76E-10	−3.76E-10	1.74E-06

---- 2740 PARAMETER ss biomass 0.338, ch4 14.066, h2 29.823

---- 2740 PARAMETER tss = 44.227

E. Raw Experimental Data

Growth on NH_4^+

Sample 1					Headspace composition			Biomass
Time (h)	Temp. (°C)	Pressure (CO_2/H_2)	Volume of culture (ml)	Volume of headspace (ml)	CO_2 (%)	H_2 (%)	CH_4 (%)	OD (600 nm)
1	37	1.3858	248	352	16.343	81.079	7.51E-01	0.059
2	37	1.2214	247	353	16.433	79.353	2.556	0.088
3	37	0.9456	246	354	16.221	77.0162	6.353	0.132
4	37	0.6428	245	355	15.469	70.388	11.882	0.174
5	37	0.4115	244	356	14.852	64.515	17.721	0.209
6	37	0.232	243	357	13.990	57.585	23.415	0.221
7	37	0.0847	242	358	13.405	51.479	29.751	0.23
8	37	−0.312	241	359	12.599	44.912	35.561	0.242
Sample 2					Headspace composition			Biomass
Time (h)	Temp. (°C)	Pressure (CO_2/H_2)	Volume of culture (ml)	Volume of headspace (ml)	CO_2 (%)	H_2 (%)	CH_4 (%)	OD (600 nm)
1	37	1.417	248	352	16.555	82.532	6.59E-01	0.041
2	37	1.2633	247	353	16.374	79.309	2.261	0.072
3	37	0.9963	246	354	16.164	76.932	5.763	0.118
4	37	0.7138	245	355	15.706	72.033	10.691	0.155
5	37	0.486	244	356	15.216	66.867	16.124	0.198
6	37	0.3022	243	357	14.475	60.580	21.640	0.209
7	37	0.1569	242	358	13.735	55.011	26.903	0.232
8	37	0.032	241	359	13.144	48.605	33.172	0.238

Growth on N_2

Sample 1 Day 1					Headspace composition				Biomass
Time (h)	Temp. (°C)	Pressure ($CO_2/H_2/N_2$)	Volume of culture (ml)	Volume of headspace (ml)	CO_2 (%)	H_2 (%)	CH_4 (%)	N_2	OD (600 nm)
1	37	1.419	249	351	11.200	65.387	2.379	11.518	0.214
2	37	1.098	248	352	11.090	60.153	6.628	13.988	0.224
3	37	0.8041	247	353	9.733	52.999	11.440	15.858	0.247
4	37	0.6493	246	354	9.247	49.787	14.770	17.682	0.249
5	37	0.4663	245	355	8.069	43.542	19.287	19.663	0.252
6	37	0.3386	244	356	7.179	38.965	23.405	21.617	0.253
7	37	0.2312	243	357	5.651	29.810	24.673	21.375	0.251
8	37	0.139	242	358	5.169	26.869	29.746	24.201	0.257

(continued)

(continued)

Sample 1 Day 2					Headspace composition				Biomass
Time (h)	Temp. (°C)	Pressure (CO_2/H_2/N_2)	Volume of culture (ml)	Volume of headspace (ml)	CO_2 (%)	H_2 (%)	CH_4 (%)	N_2	OD (600 nm)
1	37	1.5247	240	360	11.778	64.847	4.587	12.414	0.275
2	37	1.2115	239	361	10.871	59.585	8.666	14.166	0.291
3	37	0.9797	238	362	9.541	53.855	11.941	15.200	0.317
4	37	0.7851	237	363	8.880	49.056	16.083	17.334	0.312
5	37	0.609	236	364	7.834	43.753	20.290	19.109	0.317
6	37	0.4723	235	365	6.830	38.431	23.984	20.632	0.315
7	37	0.3557	234	366	5.445	31.994	25.982	20.848	0.319
8	37	0.266	233	367	4.964	28.966	31.027	23.601	0.321

Growth on N_2

Sample 2 Day 1					Headspace composition				Biomass
Time (h)	Temp. (°C)	Pressure (CO_2/H_2/N_2)	Volume of culture (ml)	Volume of headspace (ml)	CO_2 (%)	H_2 (%)	CH_4 (%)	N_2	OD (600 nm)
1	37	1.3585	249	351	11.800	67.293	3.203	13.350	0.206
2	37	1.0402	248	352	10.112	57.833	11.967	15.533	0.218
3	37	0.7571	247	353	9.507	52.159	12.465	17.618	0.241
4	37	0.6041	246	354	8.777	48.225	15.719	19.233	0.243
5	37	0.4346	245	355	7.363	39.444	19.260	20.607	0.254
6	37	0.3149	244	356	6.890	37.927	24.559	23.609	0.25
7	37	0.215	243	357	5.608	30.031	26.583	24.058	0.248
8	37	0.1305	242	358	4.710	24.599	29.504	25.276	0.253
Sample 2 Day 2					Headspace composition				Biomass
Time (h)	Temp. (°C)	Pressure (CO_2/H_2/N_2)	Volume of culture (ml)	Volume of headspace (ml)	CO_2 (%)	H_2 (%)	CH_4 (%)	N_2	OD (600 nm)
1	37	1.3912	240	360	11.136	62.574	6.379	14.405	0.272
2	37	1.085	239	361	10.049	56.633	10.967	16.533	0.301
3	37	0.8568	238	362	8.930	50.479	14.978	18.376	0.315
4	37	0.667	237	363	7.858	44.414	19.165	20.276	0.314
5	37	0.5059	236	364	6.784	39.412	23.872	22.559	0.303
6	37	0.3855	235	365	5.631	33.396	27.097	23.778	0.306
7	37	0.2825	234	366	4.759	28.889	31.718	26.081	0.313
8	37	0.2046	233	367	3.984	24.422	34.685	27.372	0.312

Growth on N_2

Sample 3 Day 1					Headspace composition				Biomass
Time (h)	Temp. (°C)	Pressure (CO_2/H_2/N_2)	Volume of culture (ml)	Volume of headspace (ml)	CO_2 (%)	H_2 (%)	CH_4 (%)	N_2	OD (600 nm)
1	37	1.2786	249	351	11.364	64.081	4.183	14.942	0.211
2	37	0.9824	248	352	10.280	57.193	8.443	17.069	0.222
3	37	0.7193	247	353	10.045	55.803	12.611	18.243	0.249
4	37	0.5688	246	354	8.191	45.430	16.506	21.076	0.244
5	37	0.4062	245	355	7.123	39.562	21.134	23.490	0.241
6	37	0.296	244	356	6.080	34.144	24.355	24.945	0.245
7	37	0.2004	243	357	5.249	29.492	27.946	26.751	0.251
8	37	0.1197	242	358	4.387	24.413	31.360	28.435	0.257
Sample 3 Day 2					Headspace composition				Biomass
Time (h)	Temp. (°C)	Pressure (CO_2/H_2/N_2)	Volume of culture (ml)	Volume of headspace (ml)	CO_2 (%)	H_2 (%)	CH_4 (%)	N_2	OD (600 nm)
1	37	1.3366	240	360	11.164	63.525	6.512	13.840	0.274
2	37	1.0172	239	361	10.004	57.526	11.227	15.974	0.291
3	37	0.802	238	362	8.868	51.172	15.338	17.714	0.303
4	37	0.62	237	363	7.585	44.076	18.994	19.112	0.313
5	37	0.4616	236	364	6.674	39.811	24.251	21.685	0.309
6	37	0.3415	235	365	5.567	34.258	27.946	23.211	0.315
7	37	0.2386	234	366	4.549	28.763	31.883	24.919	0.325
8	37	0.1633	233	367	3.767	24.027	35.053	26.289	0.321